Remote Sensing of Environment 136 (2013) 99–116

Contents lists available at SciVerse ScienceDirect

Remote Sensing of Environment

journal homepage: www.elsevier.com/locate/rse

Intercomparison of satellite dust retrieval products over the west African Sahara during the Fennec campaign in June 2011 ☆

J.R. Banks [a,*], H.E. Brindley [a], C. Flamant [b], M.J. Garay [c], N.C. Hsu [d], O.V. Kalashnikova [c], L. Klüser [e], A.M. Sayer [d,f]

[a] Space and Atmospheric Physics Group, Imperial College, London, UK
[b] Laboratoire Atmosphères, Milieux, Observations Spatiales, CNRS, UMR 8190, Paris, France
[c] Jet Propulsion Laboratory, California Institute of Technology, Pasadena, CA, USA
[d] NASA Goddard Space Flight Center, Greenbelt, MD, USA
[e] German Aerospace Center (DLR), German Remote Sensing Datacenter (DFD), 82334 Wessling, Germany
[f] Goddard Earth Sciences Technology and Research (GESTAR), Universities Space Research Association (USRA), Columbia, MD, USA

ARTICLE INFO

Article history:
Received 21 December 2012
Received in revised form 30 April 2013
Accepted 1 May 2013
Available online 25 May 2013

Keywords:
Remote sensing of dust
Satellite retrieval intercomparisons
Aerosol optical depth
Fennec

ABSTRACT

Four aerosol optical depth retrieval algorithms over the Sahara Desert during June 2011 from the IASI, MISR, MODIS, and SEVIRI satellite instruments are compared against each other in order to understand the strengths and weaknesses of each retrieval approach. Particular attention is paid to the effects of meteorological conditions, land surface properties, and the magnitude of the dust loading. The period of study corresponds to the time of the first Fennec intensive measurement campaign, which provides new ground-based and aircraft measurements of the dust characteristics and loading. Validation using ground-based AERONET sunphotometer data indicates that of the satellite products, the SEVIRI retrieval is most able to retrieve dust during optically thick dust events, whereas IASI and MODIS perform better at low dust loadings. This may significantly affect observations of dust emission and the mean dust climatology. MISR and MODIS are least sensitive to variations in meteorological conditions, while SEVIRI tends to overestimate the aerosol optical depth (AOD) under moist conditions (with a bias against AERONET of 0.31), especially at low dust loadings where the AOD < 1. Further comparisons are made with airborne LIDAR measurements taken during the Fennec campaign, which provide further evidence for the inferences made from the AERONET comparisons. The effect of surface properties on the retrievals is also investigated. Over elevated surfaces IASI retrieves AODs which are most consistent with AERONET observations, while the AODs retrieved by MODIS tend to be biased low. In contrast, over the least emissive surfaces IASI significantly underestimates the AOD (with a bias of −0.41), while MISR and SEVIRI show closest agreement.

1. Introduction

The Sahara is the largest source of mineral dust aerosols in the world (e.g. Washington et al., 2003), and the atmosphere above it has some of the highest dust loadings. Large Saharan dust storms have been observed to increase the reflected shortwave radiation by as much as 100 W m^{-2} and to simultaneously significantly decrease the outgoing longwave radiation (Slingo et al., 2006). Dust may also have effects on ocean biogeochemistry through the transport of iron (e.g. Mahowald et al., 2005) and can affect fertility in the Amazon (Koren et al., 2006). Moreover, dust also interacts with the cloudy atmosphere and can change the occurrence and microphysical properties of clouds (e.g. Mahowald & Kiehl, 2003; Lee & Penner, 2010). Dust loading over the Sahara peaks during the summer months when the Sahara has one of the deepest boundary layers on the planet (Cuesta et al., 2009).

Recent measurement campaigns have sought to deepen our understanding of climate and of dust activity in and near the Sahara. Such campaigns have included the African Monsoon Multidisciplinary Analyses (AMMA) project in 2006 (Redelsperger et al., 2006), which sought chiefly to understand the west African monsoon; Dust Outflow and Deposition (DODO) in 2006 (McConnell et al., 2008), which sought to quantify dust deposition into the ocean; the Saharan Mineral Dust Experiment (SAMUM) in 2006 and 2008 (Ansmann et al., 2011; Heintzenberg, 2009), which sought to measure dust composition and optical properties; Geostationary Earth Radiation Budget experiment Intercomparison of Longwave and Shortwave radiation (GERBILS) in June 2007 (Haywood et al., 2011), which sought to understand dust properties and the atmospheric radiation balance over the western Sahara; and most recently Fennec in June 2011 and June 2012 (Washington et al., 2012), which aims to understand the climate system

* Corresponding author at: Space and Atmospheric Physics Group, The Blackett Laboratory, Imperial College London, Prince Consort Road, London, SW7 2BW, UK. Tel.: +44 207 5947677; fax: +44 207 7594 7772.
E-mail address: j.banks@imperial.ac.uk (J.R. Banks).

0034-4257/$ – see front matter © 2013 The Authors. Published by Elsevier Inc. All rights reserved.
http://dx.doi.org/10.1016/j.rse.2013.05.003

of the western Sahara in summer. The Fennec approach has used ground (Marsham et al., in press; Todd et al., in press), aircraft (McQuaid et al., 2013; Ryder et al., 2013), and satellite (Banks & Brindley, 2013) observations, alongside numerical modelling.

The high dust loading in the turbulent Saharan summer atmosphere clearly has implications for the local climate. However, it is only relatively recently that multiple satellite retrieval algorithms have been developed which are able to quantify dust loadings over this region. Satellite observations are powerful tools which can also be used to study the distribution and intensity of dust sources (e.g. Schepanski et al., 2007; Ginoux et al., 2012). Depending on the methodology used, satellite retrievals will be variously sensitive to the amount of dust, meteorological conditions, and surface properties (e.g. Shi et al., 2011). Previous studies have sought to quantify the differences between the satellite retrievals over the Sahara, e.g. during a large regional dust storm in March 2006 (Carboni et al., 2012), and during GERBILS in June 2007 (Christopher et al., 2011). These studies briefly investigated the links between the retrievals and surface albedo, but it would be useful to set the dust retrieval algorithms within a wider context, by also considering atmospheric conditions and the surface emissivity, which the infrared retrievals may be more sensitive to. In addition, the information from the AERONET sites and aircraft flights established and undertaken under the auspices of the Fennec project provide valuable extra data to test the quality of the various retrievals from Saharan locations that were not sampled in previous studies. Indeed, the positioning of the Bordj Badji Mokhtar AERONET site is particularly well suited for quantifying aerosol loading associated with large dust events during boreal summer (Marsham et al., in press).

In this paper we present an analysis of co-located satellite aerosol retrieval products over the western half of the Sahara during the Fennec campaign in June 2011. We seek to quantify and understand the differences in the four specific retrievals from the IASI, MISR, MODIS, and SEVIRI satellite instruments with respect to dust loading, meteorological conditions, and surface properties, before evaluating the retrievals using data provided by AERONET (Holben et al., 1998) and aircraft observations made during the Fennec campaign.

2. Satellite, ground, and aircraft instrumentation

2.1. Satellite instruments and their retrieval products

The Spinning Enhanced Visible and InfraRed Imager (SEVIRI) is located onboard the Meteosat Second Generation (MSG) series of satellites (Schmetz et al., 2002), which are in geostationary orbit above 0°N, 0°E, providing excellent coverage over Africa: these observations from SEVIRI have the advantage of a 15 minute temporal resolution, compared with the one or two observations over a given area per day provided by satellites in low Earth orbit. The nadir spatial sampling rate is 3 km (increasing to ~4.5 km at higher SEVIRI viewing zenith angles within the west African field of interest), with measurements made at 11 visible and IR wavelengths: of particular value are the 10.8 and 13.4 μm channels which can be used to infer dust aerosol optical depth (AOD) over land (Banks & Brindley, 2013; Brindley & Russell, 2009), using a method specifically designed for arid and semi-arid regions. The first step in the retrieval process is to flag pixels as dusty and/or cloudy (Derrien & Le Gléau, 2005; Ipe et al., 2004; MétéoFrance, 2012). In order for an AOD to be inferred for a given pixel, we require either that cloud is not flagged, or that dust is flagged. A 'pristine sky' value of the brightness temperature at 10.8 μm ($T_{B108dfe}$) is calculated for each timeslot in a 28-day rolling window period, accounting for variations in total column water vapour and skin temperature from European Centre for Medium-range Weather Forecasts (ECMWF) ERA-Interim reanalyses. The deviation of the instantaneous T_{B108} value from the pristine sky value, due to dust, is given by:

$$\Delta T_{B108} = T_{B108dfe} - T_{B108} \quad (1)$$

An analogous calculation is made for ΔT_{B134}, which can be used to convert to dust AOD at 550 nm from a simulated relationship between $\Delta T_{B108}/\Delta T_{B134}$ and AOD (Brindley & Russell, 2009). The 13.4 μm channel is used to mitigate the effect of variations in dust height on the brightness temperature difference. The transfer coefficients for this relationship have been derived from radiative transfer simulations using the dust model described by Brindley & Russell (2009). While the algorithm attempts to account for the impact of variations in total column water vapour and surface temperature in order to isolate the dust only IR signal (Brindley, 2007), subsequent studies have suggested that at low dust loadings the retrieved dust optical depths may retain a sensitivity to, in particular, water vapour amount (Banks & Brindley, 2013). Over a three-year period, the correlation between the SEVIRI retrieval and individual AERONET sites ranges from 0.52 to 0.73. The RMS differences range from 0.19 to 0.46 and the biases range from −0.12 to 0.14.

Another widely used and useful qualitative tool which can be derived from SEVIRI is the 'desert dust' RGB imagery (Lensky & Rosenfeld, 2008), which employs brightness temperature differences in the 8.7, 10.8, and 12.0 μm channels to discriminate the presence of dust in the atmosphere. Dust appears pink in this analysis, although in moist atmospheres the dust signal can be masked (Brindley et al., 2012).

The Infrared Atmospheric Sounding Interferometer (IASI) instrument is carried by the METOP series of satellites. The dust retrieval method used here for IASI (Klüser et al., 2012, 2011) is based on singular vector decomposition of binned IASI spectra between 830 and 1250 cm^{-1} (8–12 μm). The rationale behind the approach is to avoid radiative transfer forward simulations of IASI spectra over deserts as surface emissivity is highly variable and unknown (e.g. DeSouza-Machado et al., 2010). Moreover the retrieval is designed to minimise the necessary a priori information such as atmospheric state (temperature and humidity profiles). Mineral dust composed of silicate minerals can be detected in the thermal infrared (Ackerman, 1997) due to Si – O resonance absorption bands (Hudson et al., 2008a,b). Maximum value filtered brightness temperature spectra (in 42 bins) are converted to 'equivalent optical depth' spectra (Klüser et al., 2011):

$$L_{obs}(\nu) = \exp\left(-\tau_{eqv}/\cos\theta\right) B_{\nu}(T_{base}) \quad (2)$$

where $L_{obs}(\nu)$ is the radiance at wavenumber ν observed from space, θ is the viewing zenith angle and $B\nu(T_{base})$ is the spectral Planck-function evaluated for the baseline temperature defined as the maximum brightness temperature observed. The broad ozone absorption band around 1040 cm^{-1} is not used for dust retrieval. Singular vector decomposition has been performed for IASI spectra of equivalent optical depth covering North Africa, the Mediterranean and Arabia for a period of seven days. The singular vectors for the retrieval method, determined from this seven day period, are then used for dust retrieval for all 30 days in June 2011. The leading two singular vectors have been found to represent broad gas absorption and surface emissivity features, consequently dust optical depth is retrieved from the linear combination of higher order singular vectors. Extinction spectra of six mineral components of dust are projected onto the observed IASI spectra providing optical depth and weight for each component. Consequently, in contrast to most other dust retrieval methods, the singular-vector based approach is also able to account for variable mineralogy. In another iteration of the retrieval the thermal emission of the dust (Ackerman, 1997) is accounted for. After the IR optical depth (at 10 μm) of the dust has been determined the AOD is transferred to visible wavelengths (500 nm) by particle-size dependent transfer coefficients (Dufresne et al., 2002). Mathematical details of the method are presented by Klüser et al. (2011) and Klüser et al. (2012). The transfer coefficients are based on particle size, which is retrieved with great uncertainty, they are moreover the same for all mineralogical components (Klüser et al., 2012). The dust extinction models used in the current version neglect scattering by dust particles, which is only valid for small particles in the Rayleigh limit (e.g. Hudson et al.,

2008a,b). Surface temperature is underestimated at high thermal IR AOD, hence AOD would itself be underestimated. No hematite is contained in the dust models applied, which strongly absorbs solar radiation and is the main source of single-scattering-albedo reduction at solar wavelengths. Statistically, the correlation with AERONET is 0.76, the RMS difference is 0.17, the bias is 0.003, and the intrinsic retrieval uncertainty is about 20–30% (retrieved pixel-wise).

The Multi-angle Imaging SpectroRadiometer (MISR) was launched aboard the NASA Terra satellite into a sun-synchronous polar orbit in December 1999, and the data record currently extends over nearly 13 years. The instrument consists of nine cameras with view angles at the Earth's surface of ±70.5°, ±60.0°, ±45.6°, ±26.1°, and 0° (nadir), operating in four spectral bands centred at 446 nm (blue), 557 nm (green), 672 nm (red), and 866 nm (near infrared). The map-projected spatial resolution is 275 m at nadir and in the red band of all nine cameras. In the global observing mode, the remaining channels are spatially averaged and map-projected to 1.1 km resolution. The common swath width is ~400 km and global coverage is obtained every nine days at the equator and more frequently at higher latitudes (Diner et al., 2002).

The MISR standard aerosol retrieval algorithm reports AOD and aerosol type at 17.6 km × 17.6 km spatial resolution by analysing 1.1 km-resolution MISR top-of-atmosphere (TOA) radiances from 16 × 16 pixel regions (Kahn et al., 2009b). Coupled surface-atmosphere retrievals are performed using all four spectral bands over most land surface types, including bright desert surfaces (Martonchik et al., 2009). The retrieval algorithm used to generate Version 22 of the MISR Standard Aerosol Productused in this study utilises a lookup table containing 74 aerosol mixtures consisting of eight component particle types (Kahn et al., 2010). Two of these components are a medium mode, non-spherical dust optical analogue developed from aggregated angular shapes and a coarse mode dust analogue composed of ellipsoids (Kalashnikova et al., 2005). The MISR aerosol retrieval over land employs two different algorithms sequentially. The first algorithm applies the assumption that surface angular shapes are spectrally similar, as described by (Diner et al., 2005). Different aerosol models and AODs are tested, and those that fail this test are excluded from further consideration. The second algorithm performs an empirical orthogonal function (EOF) analysis of the angular shape of the TOA equivalent reflectances within the retrieval region after the atmospheric path radiance has been removed by subtracting the TOA measurements within a reference pixel. Aerosol properties are assumed to be the same for allpixels in the region. The AOD and aerosol model are determined by finding the combination of path radiance and linear sum of low-order EOFs that best fit the observations (Martonchik et al., 2009).

The performance of the operational MISR aerosol retrieval over bright desert sources and its sensitivity to near surface aerosols and surface properties have been validated and used in a number of studies (Christopher et al., 2008, 2009; Frank et al., 2007; Kahn et al., 2009a; Martonchik et al., 2004). A global comparison of coincident MISR and AERONET sunphotometer data showed that overall, about 70% to 75% of MISR AOD retrievals fall within the larger of 0.05 or 0.20 × AOD, and about 50% to 55% are within the larger of 0.03 or 0.10 × AOD, except for sites where dust or mixed dust and smoke are commonly found (Kahn et al., 2005, 2009b, 2010).

The MODerate resolution Imaging Spectroradiometer (MODIS) is located aboard the NASA Terra and Aqua satellites. Each of the MODIS instruments provides global aerosol information once a day at the spatial resolution of 10 km × 10 km at nadir. MODIS Deep Blue (Hsu et al., 2004, 2006) aerosol products use the blue wavelengths of the visible spectrum (412 and 470 nm referenced against 650 nm) to minimise the high surface signal in the visible wavelengths over bright surfaces such as the desert. Used here are the recently updated 'Collection 6' Deep Blue aerosol retrievals (the previous widely available product was 'Collection 5.1') from Aqua measurements: the similar method has been used for retrievals from the Sea-viewing Wide Field-of-view Sensor (SeaWIFS) satellite instrument, as described by Sayer et al. (2012). As compared to MODIS Collection 5.1, there are many improvements made in the Collection 6 Deep Blue algorithm. The most significant changes over desert regions include (1) the use of a newly developed Normalized Difference Vegetation Index (NDVI) dependent MODIS surface reflectance database to replace the previous static surface look-up tables; (2) a better dust aerosol model selection scheme using visible and thermal infrared bands simultaneously; (3) quality flag selection procedures; and (4) improved cloud flagging, decreasing the number of false detections. The resulting changes in monthly mean MODIS Aqua AODs for June 2011 from Collection 5.1 to Collection 6 are mapped in Fig. 1, indicating that Collection 6 retrieves more dust loading over the central Sahara, in contrast to Collection 5.1, which retrieves most dust on the desert margins, especially in the Sahel. These enhanced AOD values seen over the central Sahara are most likely due to the improvements in the dust model selection scheme made in the Collection 6 algorithm as mentioned above, which result in significant changes in retrieved AOD over regions where more absorbing dust aerosols prevail. The Deep Blue retrievals should be insensitive to both moisture and temperature, since the algorithm does not use channels with water vapour absorption. Similarly the retrieval should be insensitive to surface temperature, since only solar bands are used. The major assumptions in the Deep Blue algorithm are related to surface reflectance, aerosol microphysical properties, and aerosol height. The estimated uncertainty on an individual retrieval is 0.05 + 20% in Collection 5.

Note that throughout this paper the names of the satellite instruments are used to denote AOD results from the specific dust retrieval algorithms introduced above. Other aerosol retrieval products exist for most of these instruments, for example the 'DarkTarget' MODIS algorithm (Levy et al., 2007) which is unable to retrieve aerosol over bright desert surfaces and so is not used here.

2.2. Ground-based and aircraft data

Ground and in-situ data are invaluable for understanding and validating satellite product data. From the ground, the Aerosol Robotic Network (AERONET) of sun-photometers provides multi-year time-series of AOD measurements from numerous sites (Holben et al., 1998). The nine AERONET sites in west Africa with co-located satellite product data in June 2011 are mapped in Fig. 2, with further details provided in Table 1. Two of these, Bordj Badji Mokhtar (BBM) and Zouerat (Marsham et al., in press; Todd et al., in press), were established within the framework of the Fennec project, with the goal of contributing to a new data set of atmospheric observations from the central Sahara (Washington et al., 2012). There are three levels of AERONET data for data quality purposes (Smirnov et al., 2000): Level 1 data, the 'raw' AOD measurements; Level 1.5, which are 'cloud-screened'; and Level 2, which are individually inspected and have the final calibration applied. The difference between Level 1 and Level 1.5 can be used as a crude measure for determining the influence of cloud on the observations (e.g. Brindley & Russell, 2009). Following the procedure outlined by Banks & Brindley (2013), AERONET data is regarded as representative for grid cells within a 25 km radius of the AERONET site, and observations are regarded as dusty where the Ångström coefficient $\alpha \leq 0.6$ and the AOD $\tau_{1020\ \mathrm{nm}} \geq 0.2$ (Dubovik et al., 2002), where α is computed between 440 and 870 nm. Uncertainties in the AERONET measurements are of the order 0.01 to 0.02 (Holben et al., 1998).

During the Fennec campaign in June 2011, ground data were supplemented by aircraft data from flights across Mauritania and northern Mali (McQuaid et al., 2013), using the Service des Avions Français Instrumentés pour la Recherche en Environnement (SAFIRE) Falcon 20 aircraft. The Falcon 20 was equipped with the backscatter LIDAR Leandre New Generation (LNG, deVilliers et al., 2010) allowing the measurement of atmospheric reflectivity at three wavelengths (355, 532, and 1064 nm) to analyse the structure and radiative

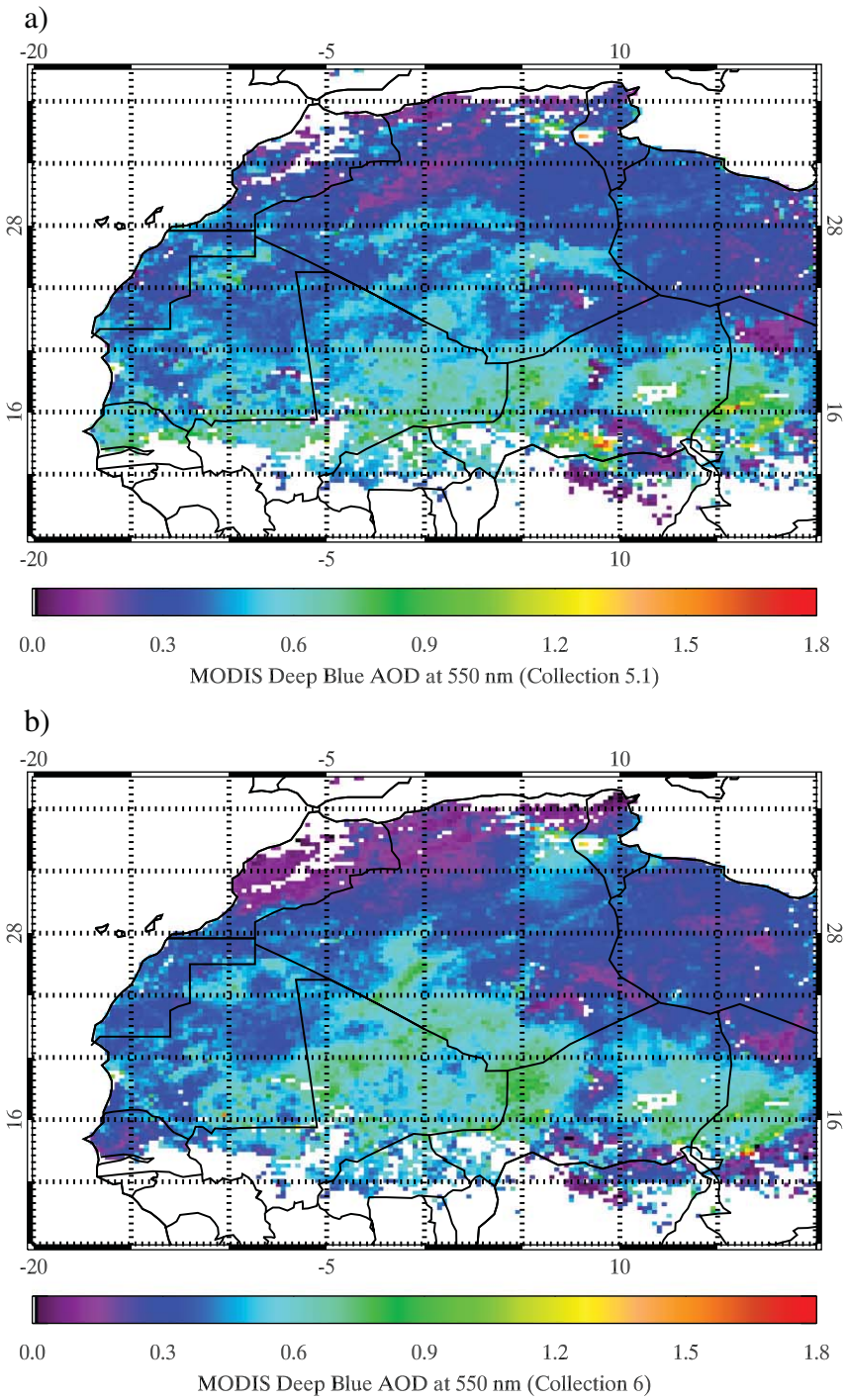

Fig. 1. Monthly mean MODIS Deep Blue retrieved AODs: (a) Collection 5.1, (b) Collection 6. One outlier in MODIS Collection 6 at 13.75°N, 16.75°E has a value of 2.07.

characteristics of desert dust plumes. The Falcon 20 was also equipped with a Vaisala AVAPS dropsonde launching device, radiometers (broad-band up- and down-looking Kipp and Zonen pyranometers and pyrgeometers), the CLIMAT radiometer (Legrand et al., 2000) as well as in situ PTU and wind sensors. The profiles of atmospheric extinction coefficient at 532 nm are retrieved using a standard LIDAR inversion technique (Cuesta et al., 2008; Fernald et al., 1972). The profiles of molecular extinction coefficient used in the inversion procedure are obtained from molecular density profiles computed using temperature and pressure data from dropsondes released during the flight (Bodhaine et al., 1999). The aerosol backscatter-to-extinction ratio used for the inversion is considered to be constant with altitude, set at 0.021 sr^{-1}. This value is intermediate between the value derived at 532 nm from space-borne, airborne, and ground-based LIDAR systems over northern Africa (i.e. 0.018 sr^{-1}, see Heintzenberg, 2009; Schuster et al., 2012) and those derived over Sahelian Africa (i.e. 0.024 sr^{-1}, see Omar et al., 2009; Schuster et al., 2012). Given the uncertainty on the backscatter-to-extinction ratio ($\pm$0.001 sr^{-1}), the uncertainty on the LIDAR-derived AODs is estimated to be of the order of 15%. For inversion, a backscatter ratio (the total backscatter coefficient divided by the molecular backscatter coefficient) of 1 is considered at 9.5 km above ground level (agl), i.e. above dust observed during the period of interest. In Section 4.2 we will show and discuss particulate extinction coefficient profiles (PEC) and AOD obtained from the PEC profiles

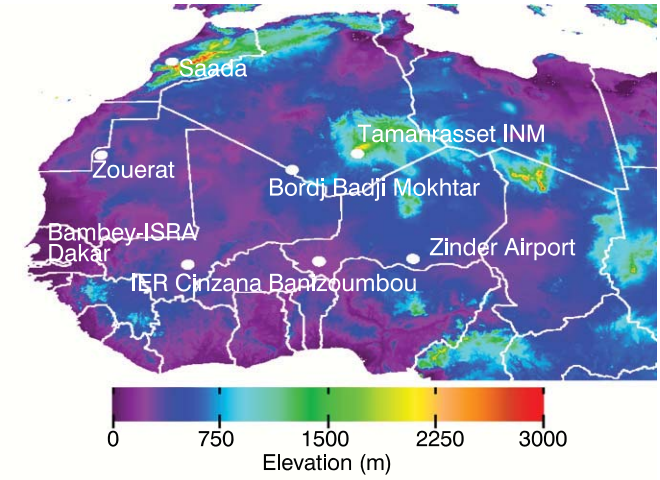

Fig. 2. Map of the nine AERONET sites with co-located data in June 2011, overplotted on the surface elevation (as developed by the Eumetsat Satellite Application Facility for Nowcasting (MétéoFrance, 2012)).

integrated between 0 and 9.5 km agl. Finally, the evolution of the integrated water vapour content in the lower atmosphere along the Falcon 20 flight track was derived from dropsonde-derived water vapour mixing ratio profiles integrated between 0 and 10 km agl.

3. Satellite product intercomparisons during June 2011

In order to compare the various satellite products, we have established a common grid onto which the satellite data are binned, at a latitude/longitude resolution of 0.25°. This resolution has been chosen so as to be coarser than the coarsest setof satellite data: in this case this is the MISR aerosol product, which has a resolution of 17.6 km (Kahn et al., 2010). Uncertainties are calculated by combining the pixel uncertainties that fall within each grid cell. The region chosen is the western half of the Sahara, 8–38°N, 20°W-20°E, a domain which covers all desert areas which may contribute substantially to the dust aerosol loading over west Africa. The local equator crossing times for the satellites are ~0930 UTC for METOP (IASI), 1030 UTC for Terra (MISR) and 1330 UTC for Aqua (MODIS), although AERONET observations suggest that the general diurnal variability of dust loading is quite small (Smirnov et al., 2002). Where all satellite products areincluded in the comparisons we choose MISR as our temporal reference point. For each day for a given grid cell observed by MISR, we retain the corresponding observation from SEVIRI which is closest in time (within ±15 min). If an IASI or a MODIS observation was made over the grid cell within five hours of the MISR observation, this is retained. Finally we impose the condition that all four satellite products must have made a valid AOD retrieval from these observations for the grid cell valuesto be included in the final intercomparison. Between the four satellite products, during June 2011 there are 11,516 co-located retrievals over 6716 grid cells. Because MISR has a very narrow swath this does place a relatively stringent limit on the number of intercomparison points available. Hence, to allow a greater range of conditions to be sampled and a greater number of AERONET/aircraft coincidences to be included, we relax these criteria for specific cases and retain SEVIRI, IASI, and MODIS co-locations only. In these cases IASI becomes the reference satellite track. For all products, the gridded uncertainties are derived from the standard deviation of the mean of the AOD retrievals within the grid cell.

Table 1
Locations of the relevant AERONET sites (latitudes in °N, longitudes in °E, and altitudes in m), surface emissivities (at 8.7 μm) and albedos, and averaged total column water vapour (TCWV, in mm) and skin temperature ($\overline{T_{skin}}$, in K) during June 2011.

Site, country	Lat.	Lon.	Alt.	ε	Alb.	$\overline{TCWV}$	$\overline{T_{skin}}$
Bambey-ISRA, Senegal	14.71	−16.48	30	0.91	0.25	45	311
Banizoumbou, Niger	13.54	2.67	250	0.85	0.29	44	310
BBM, Algeria	21.33	0.95	400	0.76	0.39	21	315
Dakar, Senegal	14.39	−16.96	0	0.93	0.21	39	308
IER Cinzana, Mali	13.28	−5.93	285	0.90	0.22	45	309
Saada, Morocco	31.63	−8.16	420	0.91	0.22	18	307
Tamanrasset INM, Algeria	22.79	5.53	1377	0.92	0.28	13	311
Zinder Airport, Niger	13.78	8.90	456	0.83	0.34	37	309
Zouerat, Mauritania	22.75	−12.48	343	0.77	0.33	16	315

For comparison with AERONET, all valid AERONET observations within three hours of the IASI overpass are included and averaged to find the co-located AERONET values. MODIS and SEVIRI also validated against the AERONET data taken from the IASI timeslot (±3 h). The uncertainties on the averaged observations are derived from the standard deviation of the mean of the AERONET measurements within this time period. Also mapped onto the intercomparison grid are co-located values of total column water vapour and skin temperature from ECMWF ERA-Interim re-analyses, re-gridded in time and space to the intercomparison grid. Emissivity at 8.7 μm (ϵ) as derived from MODIS data (Seemann et al., 2008) are also mapped alongside their co-located values, as are albedo values at 600 nm as derived from SEVIRI (Derrien & Le Gléau, 2005).

3.1. Intercomparisons across the west African Sahara

The distribution of mean co-located AODs for June 2011 for the four satellite products are mapped in Fig. 3. The four retrievals broadly agree on the dominance of the dust signal over eastern Mali and the central Sahara in general, although there are variations in the emphasis that they place on the strength of various dust events. For example, SEVIRI and MODIS, and to a lesser extent MISR, agree on the significance of a dust event in northern Algeria on the 1st June (which is the dominant contributor to the monthly mean in this area), a plume which does not appear as strongly in the IASI retrievals. It is clear that SEVIRI tends to report noticeably higher AODs than reported by the other retrievals, especially over a large area of the central Sahara: the values reported by the other retrievals are comparatively small, especially by IASI, as indicated by Table 2. High AODs appear to be an accurate representation of the dust loading in this area of the central Sahara, subject to the most frequent occurrence of haboob dust outbreaks (Marsham et al., 2008).

Due to the requirement for co-located data, there are many gaps in the spatial comparison. In some cases this is due to fewer occurrences of co-location, but more often the grid cells are excluded due to the prevalence of cloud, especially over the Sahel and sub-Saharan Africa, or due to other data quality issues. In the case of SEVIRI, observations are always available across the domain, but AOD retrievals may not be made due to the presence of cloud. Of the 53,918 points where and when all instruments made co-located observations, 39.6% of IASI points had valid AOD retrievals, as had 67.1% of MISR points, 52.8% of MODIS points, and 80.2% of SEVIRI points. Table 3 compares the product/product agreement on the presence of the valid retrievals, showing the highest agreement between SEVIRI and MISR. MODIS shows slightly less agreement with these two retrievals, although the bulk of the disagreement between these three products comes from unsuccessful MODIS retrievals. IASI has the lowest ratio of retrievals to observations, and so its agreement with the other products is markedly lower. IASI's low sensitivity to small amounts of airborne dust is due to the SVD technique and its application of dust spectra in the Rayleigh limit, which restricts the correct identification of the scattering signal of the dust. Moreover the dust vector in the IASI retrieval may not cover all components abundant in Saharan dust and may be insensitive to particle size and humidity effects (Klüser et al., 2011).

Turning to the successful retrievals only and looking at the mean value of all the co-located measurements, we find that, as suggested by Fig. 3, SEVIRI tends to retrieve the highest AODs compared to the

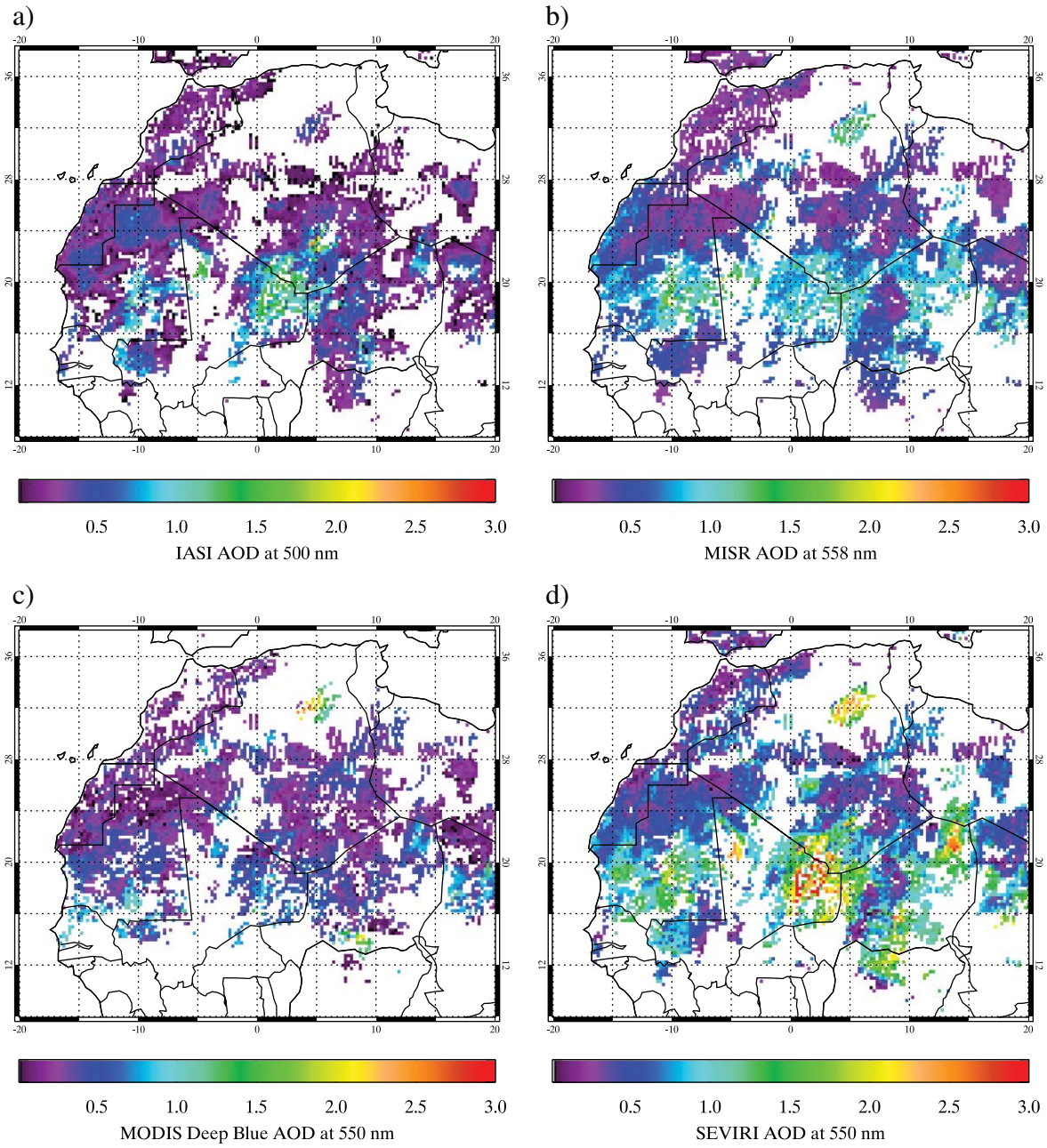

Fig. 3. Map of the June 2011 mean co-located satellite retrieved AODs: (a) IASI; (b) MISR; (c) MODIS; (d) SEVIRI. Regions in white did not have co-located data between all four satellite retrievals during the month. Co-located data are from points where all four products had a successful retrieval. Note that there are no more than 6 points in any grid cell. Eight grid cells in eastern Mali have SEVIRI AODs > 3, up to 3.40.

other products ($\overline{AOD} = 0.71$), followed by MISR (0.50) and MODIS (0.46), while IASI tends to retrieve the lowest AODs (0.30). Density plots of retrieval vs. retrieval AODs are shown in Fig. 4. Subdividing by meteorological conditions (Table 2), the differing sensitivity of the various products to column moisture and to skin temperature becomes more readily apparent. The threshold values have been chosen so as to be similar to the median values for column moisture and skin temperature. The chosen column moisture threshold is 20 mm as used by Brindley et al. (2012), slightly above the median value of 18 mm. For comparisons with MISR the median skin temperature of the co-located data is 317 K, while for comparisons with AERONET it is 312 K, so the skin temperature threshold is set at 315 K (42 °C). Using this simple subdivision, all products show a tendency to retrieve higher AODs in warmer and moister conditions. Fromthese data it would appear that SEVIRI and MISR are particularly sensitive to variations in column moisture, approximately doubling their $\overline{AOD}$ values between the dry and moist regimes in 'cool' conditions. In contrast, IASI shows a larger response to increases in skin temperature.

Table 2
Overall mean co-located satellite retrieved AODs and their standard deviations. Included are subdivided means by various regimes of column moisture and skin temperature. The boundary between column moisture regimes is 20 mm, and between skin temperature regimes the boundary is 315 K.

Instrument	Mean	σ	Cool/dry	Warm/dry	Cool/moist	Warm/moist
IASI	0.30	0.33	0.19	0.31	0.28	0.41
MISR	0.50	0.31	0.28	0.45	0.55	0.73
MODIS	0.46	0.30	0.32	0.45	0.48	0.60
SEVIRI	0.71	0.53	0.44	0.60	0.86	0.95

Table 3
Table of the percentages (out of all points where all four satellite instruments had co-located observations) of points where the two named satellite products agreed that the retrieval was either valid or invalid (due to, for example, cloud presence), or where the two satellite products disagreed on the validity of the retrieval.

	Agree	Disagree
SEVIRI/IASI	51.7	48.3
SEVIRI/MISR	83.5	16.5
SEVIRI/MODIS	69.4	30.6
IASI/MISR	54.3	45.7
IASI/MODIS	57.1	42.9
MISR/MODIS	72.3	27.7

MODIS appears to show a similar response to both factors. However, this kind of analysis does not take into account the potential for linkages between the meteorological conditions and dust activity. Warmer conditions are associated with the central desert where the dust sources are located, and where dust activity is at its strongest, which tends to have a higher skin temperature than the Sahel and the Mediterranean coast at this time of year. A complicating factor is that heavy dust loading may in fact cool the lower atmosphere and the surface of a hot desert. For example, Slingo et al. (2006) report a surface cooling of ~13 °C during a heavy dust event over Niger inMarch 2006. The relationship between column moisture and dust loading is also non-linear, since while high column moisture is associated with vegetated areas and heavy rainfall suppresses dust activation and transport, convective systems such as haboobs (Marsham et al., 2011), which bring moist 'cold-pool' outflows, are responsible for substantial dust uplift over west Africa and some of the thickest dust events. For example, LIDAR and radiosonde data from BBM show a clear association between moisture and dust at this location, and the highest AODs in haboobs (Marsham et al., in press). Furthermore, dust mobilisation by haboobs may be observable by satellite products only once the dust has travelled out from beneath the associated clouds.

This raises the question as to what extent the apparent relationships seen between meteorological conditions and AOD are a function of the sensitivity of the retrievals to these conditions? Or, more explicitly, to what extent is the dust activity itself related to these conditions? To address this question we recast the density plots of retrieval vs. retrieval AOD shown in Fig. 4 as a function of column moisture (Fig. 5), to which the majority of retrievals appear most

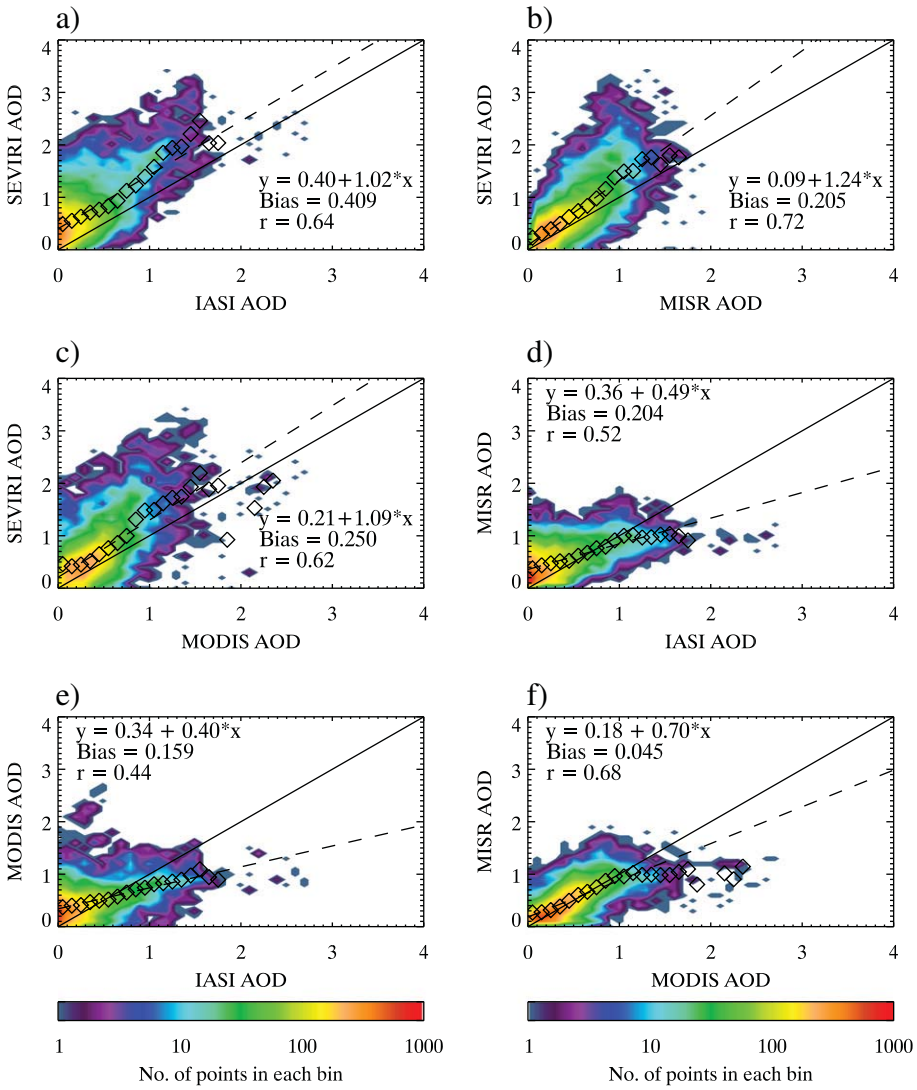

Fig. 4. Density plots of satellite product vs. satellite product AODs. (a) IASI/SEVIRI, (b) MISR/SEVIRI, (c) MODIS/SEVIRI, (d) IASI/MISR, (e) IASI/MODIS, (f) MODIS/MISR. The dashed lines indicate the lines of best fit for all points, while the diamonds represent the mean *y*-axis satellite AOD in each 0.1 *x*-axis AOD bin (for which there are ≥5 points). There are 11,451 points in each panel. The biases are *y*-*x*.

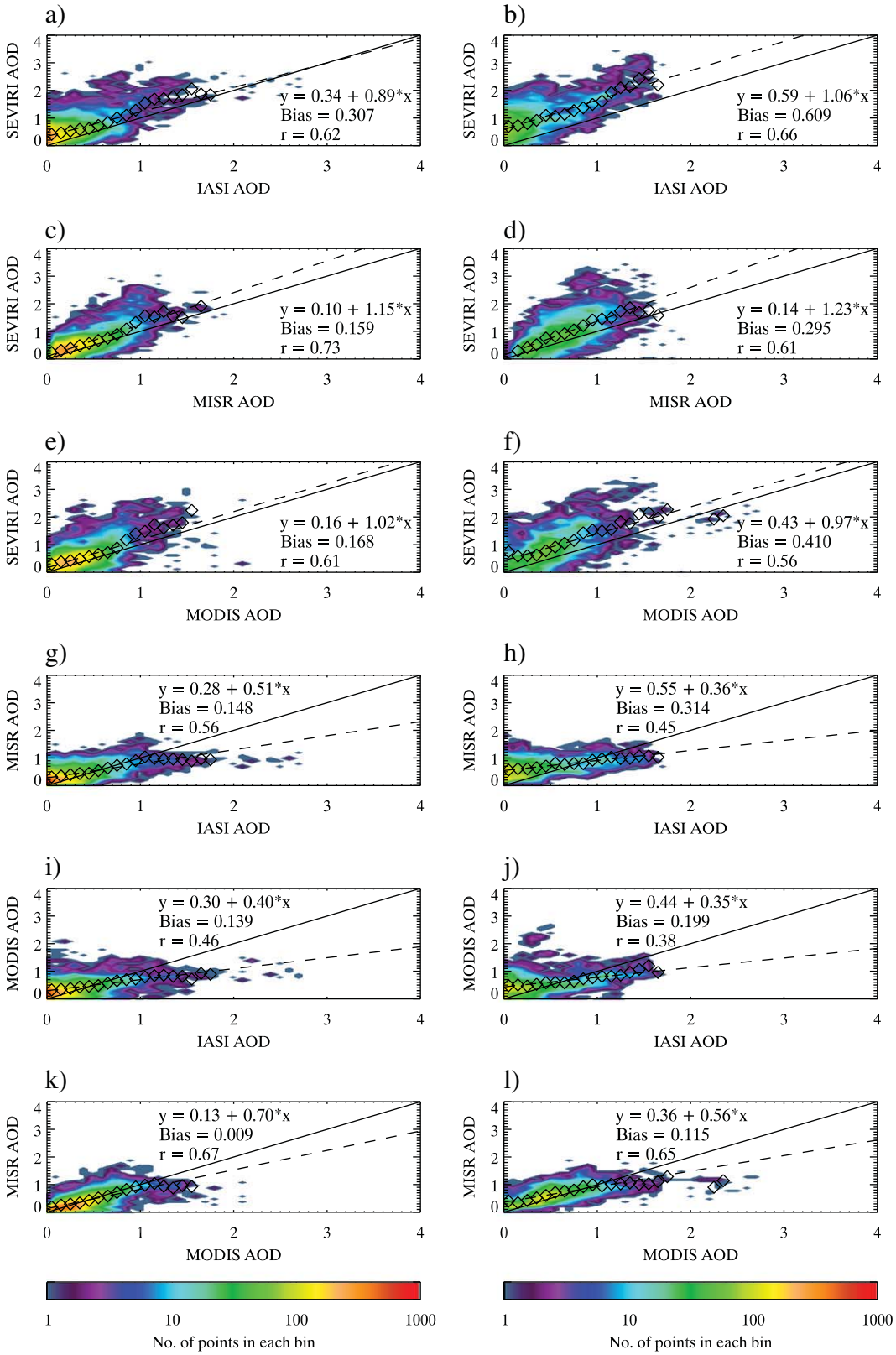

Fig. 5. Density plots of satellite product vs. satellite product AODs. (a) IASI/SEVIRI, (c) MISR/SEVIRI, (e) MODIS/SEVIRI, (g) IASI/MISR, (i) IASI/MODIS, (k) MODIS/MISR: 'dry' conditions. (b), (d), (f), (h), (j), (l): as for left-hand panels, but for 'moist' conditions. The boundary between moisture regimes is at 20 mm. The dashed lines indicate the lines of best fit for all points, while the diamonds represent the mean *y*-axis satellite AOD in each 0.1 *x*-axis AOD bin (for which there are ≥5 points). There are 7580 points in the left panels, 3871 points in the right panels. The biases are *y*-*x*.

sensitive overall. These indicate that the product biases between each other do vary according to the moisture regime in which the retrievals are made. SEVIRI's bias against all the other products increases when moving from dry to moist conditions by a factor of ~2. All products are biased high against IASI, especially in the moist regime, while MISR and MODIS show the smallest overall bias relative

to each other. Given the extent to which SEVIRI's bias against the other products increases with moisture, it is SEVIRI's retrieval that appears most likely affected by water vapour, beyond any association of the moisture content with the conditions which give rise to high dust loading. Briefly considering AERONET comparisons, the values of the mean AOD from the SEVIRI retrieval over all nine AERONET sites increases from 0.67 in dry conditions to 1.16 in moist conditions. By contrast, the mean AOD from AERONET increases from 0.70 to 0.84, indicating that SEVIRI is more sensitive to moisture than AERONET. Theoretically, given the direct sensitivity of the 10.8 μm channel used in the SEVIRI retrieval to column moisture this is perhaps not surprising, especially if variations in the atmospheric conditions are not adequately captured in the ERA-Interim analyses used in the retrieval process to account for this variability. Although we do not expect the visible channels used by the MISR and MODIS algorithms to be sensitive to the water vapour content, water vapour can have additional effects, such as causing aerosol swelling, that would indirectly affect the retrievals (e.g. Sullivan et al., 2009). In a similar manner, water vapour may indicate the presence of a different airmass with different aerosol content (e.g. Kahn et al., 2007).

Surface properties may also have a significant effect on the retrievals. Fig. 6 analyses the relationship between surface infrared emissivity, surface visible albedo, column moisture and retrieved AODs. Note that in general albedo is strongly anti-correlated with emissivity. Given the wavelength regimes that the different retrievals use we expect the MISR and MODIS results to be more susceptible to variations in surface albedo, while the SEVIRI and IASI retrievals might be expected to show sensitivity to surface emissivity. As noted earlier, except in a few specific locations, SEVIRI is biased high against the other products, and IASI is biased low. In the dry regime the pattern of AODs as a function of surface properties is consistent between all four satellite products, with the highest mean AODs to be found at high albedo and low emissivity, a combination which is most associated with sand seas, where the satellite products retrieve moderately high AODs(as in Fig. 3). In the moist regime there appear to be two contrasting patterns of AOD, one for the infrared IASI and SEVIRI retrievals, which we might expect to be most sensitive to moisture, and one for the MISR and MODIS retrievals made using the visible channels. The monthly mean IASI and SEVIRI retrievals tend to show stronger signals in the moist regime further up and left to the middle of the plots to lower albedo and higher emissivity, which is where eastern Mali, northern Niger and northern Algeria happen to lie on the albedo/emissivity grid. Meanwhile the retrievals from MISR and MODIS give peaks in AOD values towards high albedo and low emissivity, as in the dry regime, although there is a more homogeneous spread of AOD across the albedo/emissivity grid.

There are exceptions to this general pattern. Identifying specific geographical areas, in the moist regime at a relatively high albedo of 0.39 and a high emissivity of 0.91 is a bin where MISR and MODIS retrieve higher AODs than SEVIRI and IASI, corresponding to six grid cells in two regions: the dominant signal of high positive MISR and MODIS bias is at ~17.5°E, ~17°N, corresponding to an area of the Bodélé Depression in Chad (see Fig. 7). In this area the SEVIRI dust flagging may be filtered due to the high local emissivity (Ashpole & Washington, 2012; Banks & Brindley, 2013), which may be an overly stringent requirement in one of the world's biggest dust sources (Koren et al., 2006; Washington & Todd, 2005).

IASI has a positive bias against MISR and especially MODIS over specific mountainous regions such as the Hoggar mountains in southern Algeria and the Aïr mountains in Niger. These areas of high elevation have low skin temperature and column moisture, low albedo, and high emissivity with respect to the surrounding desert lowlands, and are found at an emissivity of ~0.91 and an albedo of ~0.2 predominantly in the dry regime. They are also areas identified by Shi et al. (2011) as having markedly lower MODIS Deep Blue Collection 5.1 AOD values compared to MISR. Low bias at high elevation has also been observed for Deep Blue retrievals from the SeaWiFS instrument (Sayer et al., 2012). The shallowness of the atmosphere may have varying effects on the retrievals. For IASI this reduces the absorption in the infrared due to water vapour and hence may increase the signal seen by the satellite retrieval and mean that the retrievals are higher in these regions than elsewhere. Moreover the high emissivity of the volcanic rock in the Hoggar where the AERONET site of Tamanrasset is based may also affect the IASI retrieval. Meanwhile for MODIS the reduced atmospheric column reduces the path length through which the blue channels of the visible spectrum may be scattered, and so the surface may appear brighter: this may reduce the contrast between the lofted dust and the surface on which the Deep Blue algorithm depends.

The frequency distributions of the retrieved AODs over the whole domain are plotted in Fig. 8(a). Overall, IASI is most weighted towards the lowest AODs, with a peak in distribution at 0–0.1, while the peaks for MISR (0.2–0.3), MODIS (0.3–0.4) and SEVIRI (0.4–0.5) are all shifted to higher values. SEVIRI has the longest and widest tail in its distribution while MISR has the smallest maximum values. A substantial component to SEVIRI's wide tail is revealed in Fig. 8(b), which covers the region (17–22°N, 0–5°E). Here, the dust loading is dominated by activity around the Malian/Algerian/Nigerien border (Fig. 3), an area which includes the BBM AERONET site. The frequency distribution of level 1.5 observations from this site seems to corroborate the occurrence of high dust loadings seen in this area by SEVIRI. A large fraction of the very high AODs retrieved by SEVIRI are solely from this region (Fig. 8(c)) although it is clear that the tendency for SEVIRI to show higher AODs compared to the other three satellite products is perpetuated across the domain. Further analysis of the observations and retrievals at a number of AERONET sites, including BBM, is presented in the following sections.

3.2. Intercomparisons over AERONET sites

To evaluate the accuracy of the satellite retrievals, we use AERONET data to provide 'ground-truth' of the aerosol loading. Scatterplots of AERONET/satellite retrieved AODs are presented in Fig. 9 for coincident IASI, MODIS, and SEVIRI data. MISR is not included in this analysis due to the scarcity of MISR overpasses of AERONET sites through the month. Since co-located Level 2 AERONET data are not available for a number of sites, Level 1.5 data are used. MODIS and SEVIRI AOD retrievals are provided at 550 nm, while IASI AOD retrievals are provided at 500 nm. AERONET measurements are not made at 550 nm, but we can use the AERONET AOD measurements at 675 nm and the Ångström coefficient (α, measured between 440 and 870 nm) to derive the AERONET AOD at 550 nm (Eck et al., 1999), using the relationship:

$$\tau_{550} = \tau_{675}(675/550)^{\alpha} \quad (3)$$

In terms of bias, the SEVIRI product shows the best overall agreement with AERONET, with a positive bias of 0.11. In contrast IASI and MODIS show negative biases of −0.21 and −0.32 respectively. The correlation coefficients are 0.78 for IASI and for MODIS, and 0.74 for SEVIRI. It is at the highest dust loadings that the biggest discrepancies are observed, where IASI and MODIS have substantially lower values than are observed by AERONET. Note that at high AOD the visible reflectance becomes less sensitive to changes in AOD, so for MISR and MODIS which retrieve dust using the visible channels there may be less AOD response to further increases in dust loading. There may also be a greater uncertainty at high dust loadings due to a greater sensitivity to other assumptions made in the retrievals such as those made for the aerosol properties, and similarly the uncertainty in the AERONET AOD also tends to be greater at high dust loading. By comparison SEVIRI is better able to retrieve such high values, although the retrieved AODs are still slightly lower than those observed

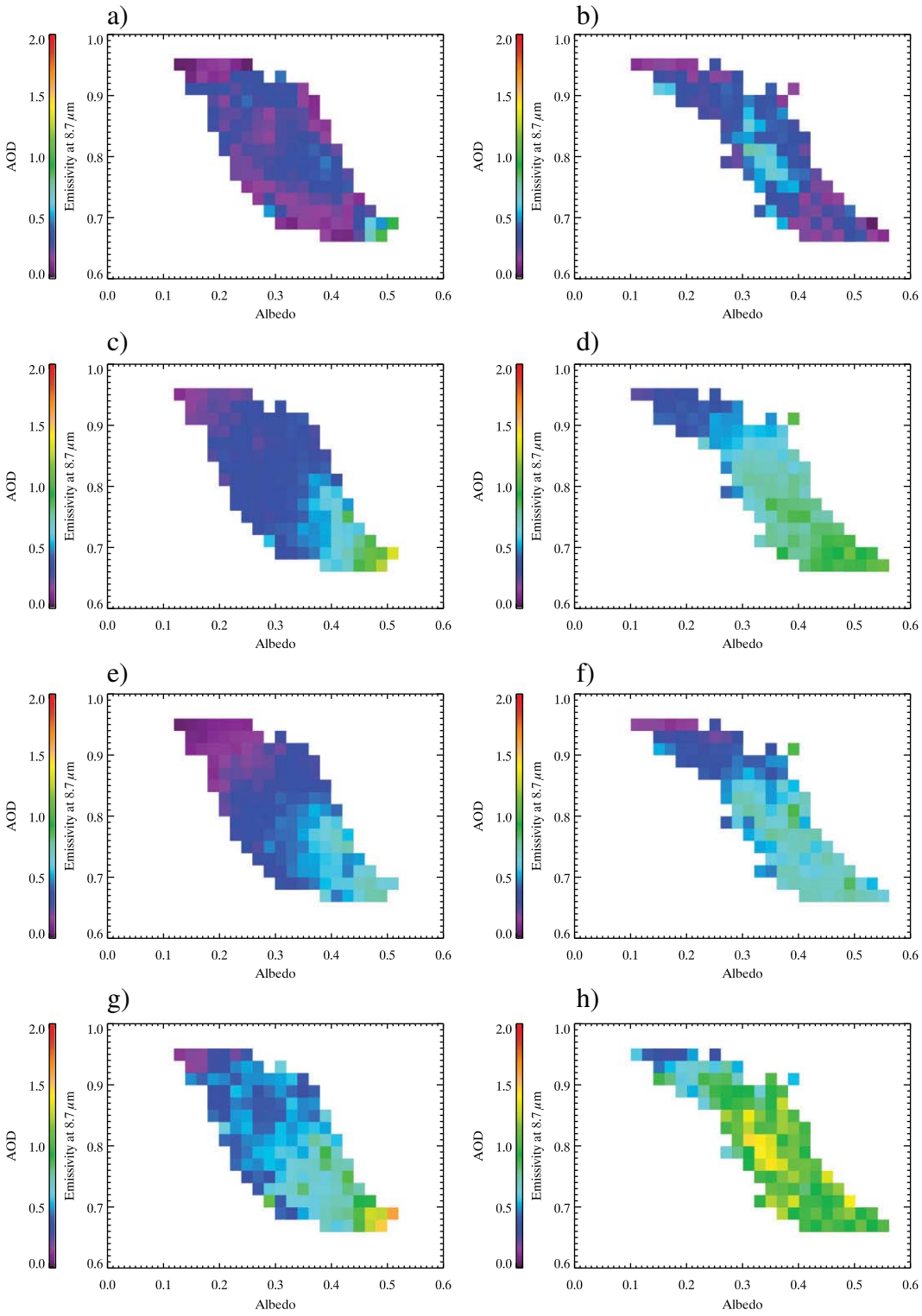

Fig. 6. Satellite retrieved mean AODs binned by albedo and emissivity at 8.7 μm, in the dry regime for left-hand panels, in the moist regime for right-hand panels. The albedo and emissivity bin widths are 0.02. (a,b): IASI; (c,d): MISR; (e,f) MODIS; (g,h) SEVIRI.

by AERONET. So for example, on 21st June at BBM, when AERONET observed an AOD of 3.08, IASI retrieved 1.57, MODIS retrieved 1.22 (0.62 in the Collection 5.1 retrievals, indicative of the improvement in the retrieval of heavy dust in Collection 6), and SEVIRI retrieved 2.22. Hence we see that at high AODs SEVIRI shows best agreement with AERONET. Where the AERONET AOD is in excess of 1, the retrieval RMS differences (biases) are: SEVIRI: 0.48 (−0.06); IASI: 0.68 (−0.51); MODIS: 0.89 (−0.76). At lower AODs IASI shows improved agreement with AERONET (bias = −0.15). SEVIRI has a tendency to over-estimate the AODs, with a positive bias against AERONET of 0.15, while MODIS under-estimates compared to the AERONET observations with a bias of −0.24.

The MODIS product shows little difference in its biases and RMS differences between the two regimes of column moisture, while IASI

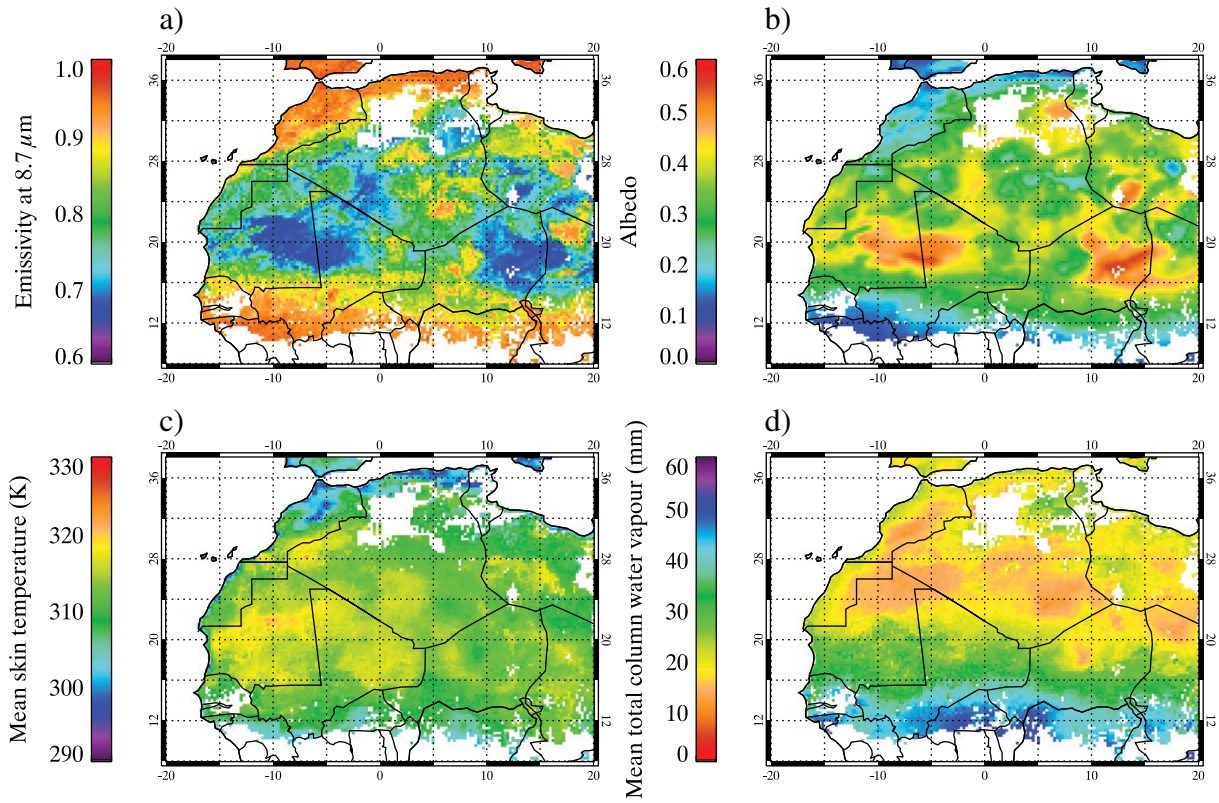

Fig. 7. Maps of surface properties and average meteorological conditions, for co-located IASI, MODIS, and SEVIRI points. (a) Emissivity at 8.7 μm, (b) albedo, (c) skin temperature, (d) total column water vapour.

does have a slightly more negative bias in moist compared to dry conditions. The sensitivity of the SEVIRI retrieval to column moisture is however quite pronounced: the bias jumps positively from dry to moist, from −0.03 to 0.31, as does the RMS which jumps from 0.29 to 0.51. That SEVIRI shows this positive bias even relative to AERONET again suggests that it is the retrieval itself which is being affected by the column moisture, beyond the possible relationship between moisture and dust activity. Moreover, we see that the divergence of the AODs between SEVIRI and AERONET is greatest at lower AERONET AODs and high moisture values, in particular at the Sahel sites (Banizoumbou, IER Cinzana, and Zinder Airport), under these conditions we suggest that the SEVIRI retrieval is less reliable.

Turning to surface properties, different patterns are clear among the three retrievals. Overall the SEVIRI product shows no significant difference in the quality of its retrievals between dark and bright albedo regimes, with bright RMS values most weighted by the highest AERONET AOD at BBM. However in the dark and dry regime, at Tamanrasset and Saada, there is a cluster of points which reveal a distinct subset in the aerosol retrieval from IASI and MODIS. Over these sites we see a slightly positive bias in the IASI retrievals and a substantially negative bias in the MODIS retrievals. Saada may be an anomaly since the site altitude of 420 m is not particularly high, however within the site's area of influence is a grid cell containing part of the Atlas mountains. At an altitude of 1377 m Tamanrasset is the most elevated site used in this study, with the shallowest atmospheric column above it as evidenced by its driest average column moisture. Hence IASI may have a positive bias and MODIS may have a negative bias as described in Section 3.1. It is thus not the albedo itself which is driving this pattern in the IASI and MODIS retrievals, rather it is the associated elevation.

Comparing the statistics between dark and bright points in the moist regime, we find that the SEVIRI product sees no variation with albedo, consistent with the overall picture. Meanwhile both IASI and MODIS have more negative biases in the bright regime where the dust loadings are highest. The trend in the points is not markedly different between dark and bright points for MODIS, so MODIS' decreased bias may just be a consequence of higher dust loading. For IASI the dark points are closer to and occasionally above the one-to-one line, whereas the bright points are markedly lower. Hence IASI appears to have a negative bias over the brighter surfaces at BBM and Zinder Airport, which also have some of the lowest emissivities (Table 1). IASI's low AODs over these surfaces are consistent with the results of Fig. 6(b). Taken together these results suggest that the general low bias in the IASI retrievals becomes more pronounced when the emissivity is low, as it is in parts of the west African Sahara.

4. Case studies in June 2011

4.1. A heavy dust case over Bordj Badji Mokhtar on 17th June

On 17th June, a large dust storm emanating from the Algeria/Mali/Niger tri-border area passed over the top of Bordj Badji Mokhtar (BBM). All four satellite products observed the area around BBM on this day, and the AERONET site was able to make some successful measurements, especially in the afternoon. Maps of co-located AODs and meterological conditions, a 'desert-dust' RGB image, and a time-series plot of AOD over BBM, are shown in Fig. 10. As subjective as the interpretation of the RGB rendering may be, it is clear that the surface underneath the dust storm cannot be seen. Hence we might expect that the signal seen by the satellite retrievals will be originating from the dust layer rather than from the underlying surface. Similarly, the AERONET site may have had difficulty seeing the Sun through the dust layer, and so several of the morning Level 1 data points were 'cloud-screened' and hence removed from the Level 1.5 and Level 2 data sets. The satellite retrievals do not detect cloud in

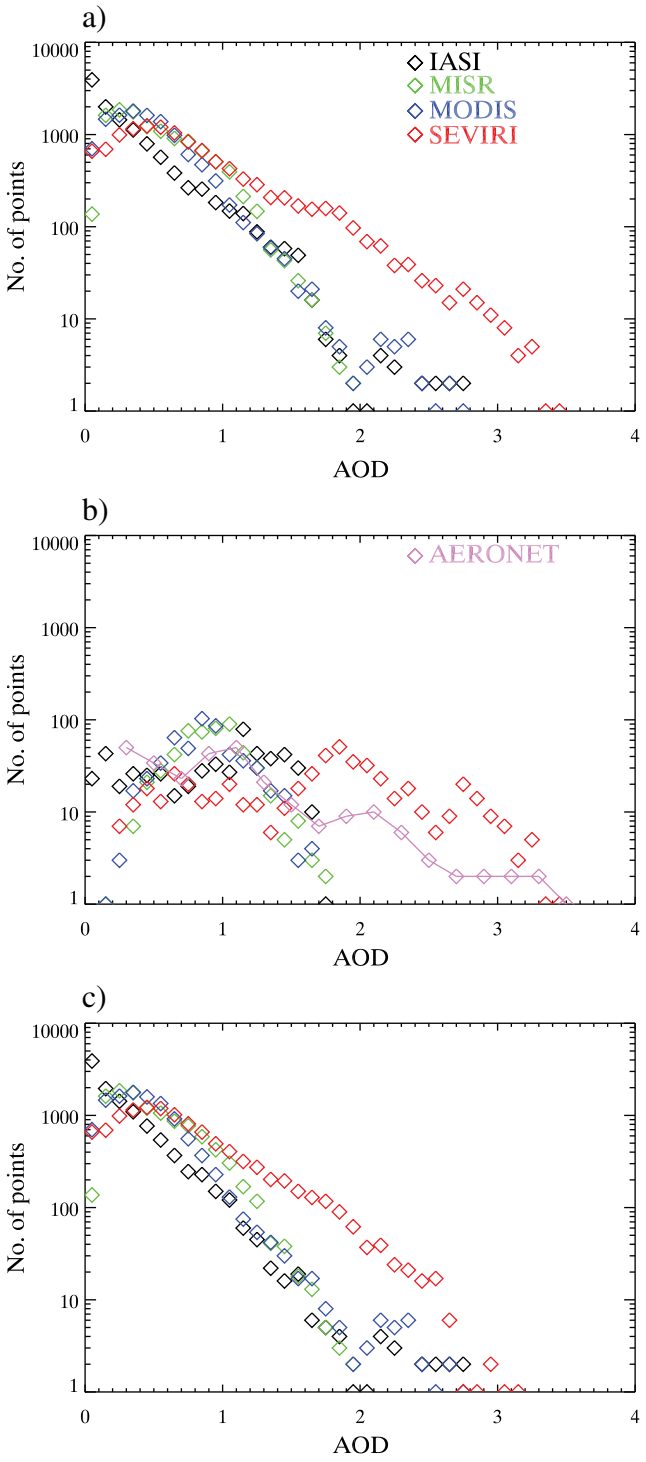

Fig. 8. Histograms of occurrences of AOD values for the four satellite retrievals, for three geographical regions. (a) full domain; (b) Mali/Algeria/Niger border, 17–22°N, 0–5°E; (c) all areas excluding the region plotted in (b). Overplotted in (b) is a histogram from all available half-hourly AERONET data from BBM. It is important to note that the AERONET data are not co-located with the satellite data.

this area until later in the afternoon, so we suggest that the 'cloud-screened' Level 1 data may give us appropriate measurements for the dust AOD in the morning.

The cause of this dust event was a convective system further to the south shown in red in the imagery, which formed a haboob that triggered dust emission overnight as it moved northwards. Haboobs are dense dust storms associated with squall lines (e.g. Farquharson, 1937). Haboobs appear to cause approximately half of the Saharan dust uplift in high-resolution models, and a similar fraction at BBM during June 2011, but are largely absent in global models (Marsham et al., 2011, in press). As a consequence of this formation, the dust event is strongly associated with areas of relatively high column moisture (Fig. 10(e)), with a gradient towards lower moisture values towards the leading edge of the dust front, andover BBM. The skin temperature is depressed underneath the dust (Fig. 10(f)). During the day from 0700 to 1600 UTC over BBM the mean column moisture is 17.5 $\pm$ 1.0 mm and the skin temperature is 318.9 $\pm$ 8.5 K. There is broad agreement between the satellite observations as to the dust spatial distribution and to the position of the leading edge of the dust front in the north. There is also agreement about the position of a smaller individual dust storm further north in central Algeria, at 26°N. However, SEVIRI is most able to capture the magnitude of this dust event, as shown by Fig. 10(g). Where there are simultaneous Level 1 AERONET and SEVIRI measurements, the mean AERONET AOD is 2.99, and the mean SEVIRI AOD is 2.62. For afternoon Level 2 measurements the mean AERONET AOD is 2.35 and the mean SEVIRI AOD is 2.60. By contrast, the IASI overpass gives an AOD of 1.50 while the simultaneous Level 1 AERONET AOD is 3.38, MISR gives 0.90 while the Level 1 AERONET AOD is 3.80, and MODIS gives 1.13 (MODIS Collection 5.1 gives just 0.19) while the Level 2 AERONET AOD is 3.32. The AOD values provided by SEVIRI are very large here (which might be regarded as suspect), however so are the AERONET values, which supports our earlier inference that of the four satellites products, SEVIRI's AOD retrievals are most reliable at high dust loading.

4.2. Falcon aircraft observations on 20th and 21st June

On 20th June, the Falcon 20 carried out a triangular flight across northern Mauritania and northern Mali to survey the Saharan atmospheric boundary layer as well as document the dust uplift in the region of the intertropical discontinuity to the southof the Saharan heat low over Mali (flight F21). F21 took place between 1322 and 1700 UTC, with the Falcon 20 flying at 11 km above mean sea level (amsl). Ten dropsondes were released along the flight track. On 21st June the Falcon 20 performed two flights (F22 and F23). On this day, convection over the Atlas Mountains had initiated a density current which moved southwestward over the northern Sahara during the morning. During the first Falcon 20 flight (F22), a dust front associated with the density current was observed over Mauritania, with older dust overlying it. During the afternoon flight (F23), airborne observations revealed that the dust layers were mixed together as a result of the developing Saharan convective boundary layer. F22 and F23took place between 0718 and 1035 UTC, and 1313 and 1630 UTC, respectively. Nine dropsondes were released during each flight.

Observations from the Falcon give us a greater spatial range of local AOD measurements than does AERONET, and these are taken over a greater range of surface types. We use the LIDAR as the 'best estimate' due to the LIDAR's insensitivity to moisture and surface albedo, such that it is only sensitive to the aerosol loading, a result of its active remote sensing technique. Located on an aircraft the LIDAR also has the highest intrinsic spatial resolution. Fig. 11 shows the dust activity and conditions along the Falcon flight tracks. MISR retrievals are not included in this analysis due to the lack of any spatial matching on any day during the Falcon's flight campaign. The start of the LIDAR measurements on both days is at the north-westernmost extremity of the flight tracks. On the 20th there is coincidence in the locations of high column moisture and albedo, with a particularly strong gradient in moisture as shown in Fig. 11(c); by contrast the atmosphere on the 21st is consistently dry, the aircraft traverses an area of generally lower, but spatially varying albedo.

For both flight F21 (20th) and flight F23 (21st) IASI and SEVIRI agree on the spatial distribution of dust with dominant dust presence in the

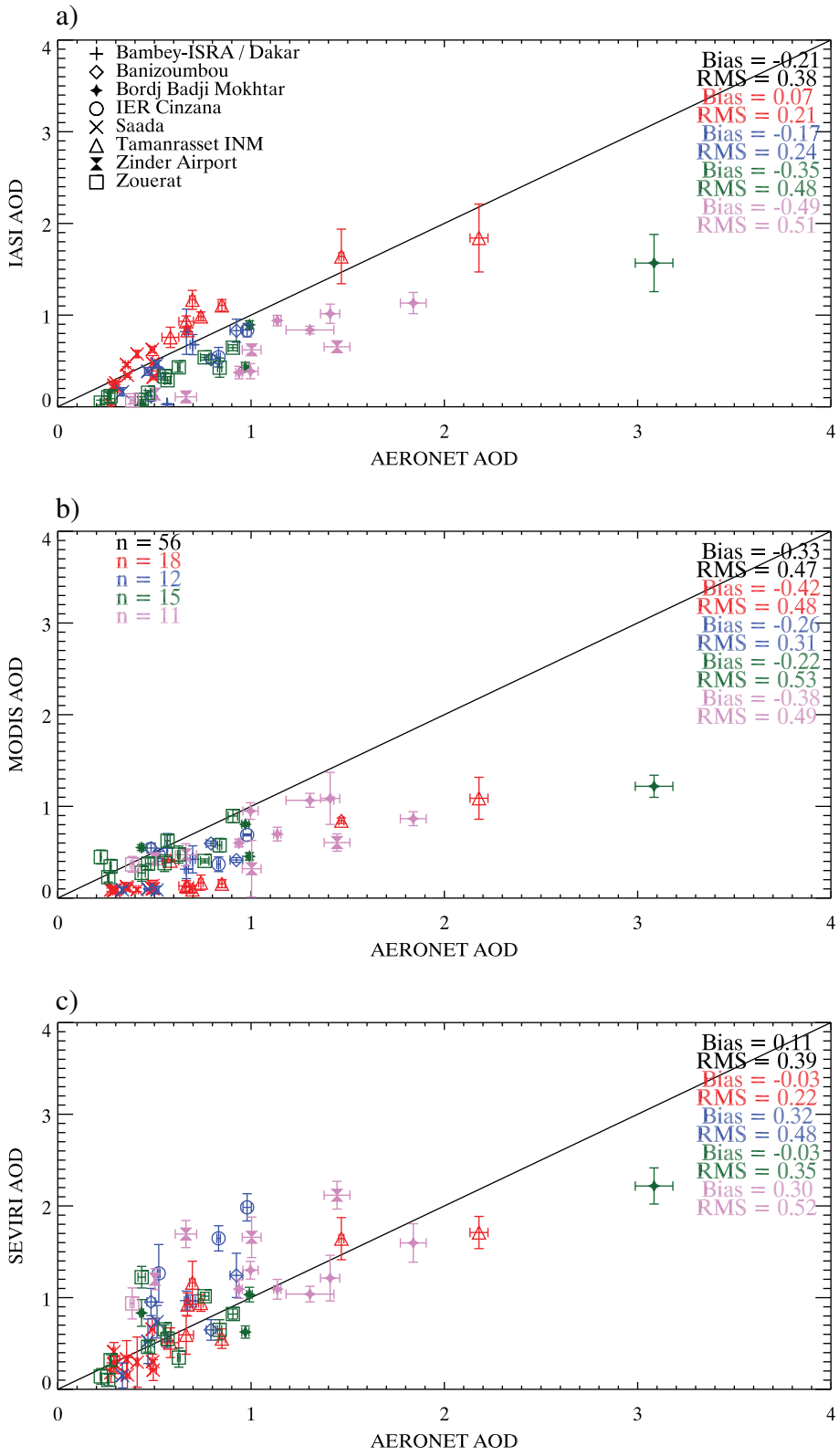

Fig. 9. Scatterplots of Level 1.5 AERONET against satellite retrieval data for June 2011: (a) IASI; (b) MODIS; (c) SEVIRI. Individual sites are marked by varying shapes, and the different moisture and albedo regimes are marked as red (dry/dark), blue(moist/dark), green (dry/bright) and purple (moist/bright). The albedo threshold is 0.3. The number of points (total and by regime) is identical for each panel, and is indicated in panel (b). For AERONET the error bars indicate the standard deviation of the mean of the measurements within three hours of the IASI overpass, while for the satellite products the error bars represent the spatial standard deviation of the mean of the measurements within 25 km of the AERONET sites for the relevant scene viewed.

north, as does MODIS on the 21st, in Figs. 11(e) and 11(f).MODIS does not see this high northern dust loading at the start of F21 (Fig. 11(e)): the reason for this is unclear but one possibility is that the retrieval has encountered a surface albedo regime over the bright desert surface where the TOA reflectance is not sensitive to AOD (e.g. Seidel & Popp, 2012). Looking more specifically at F21, from ~1430 UTC to ~1540

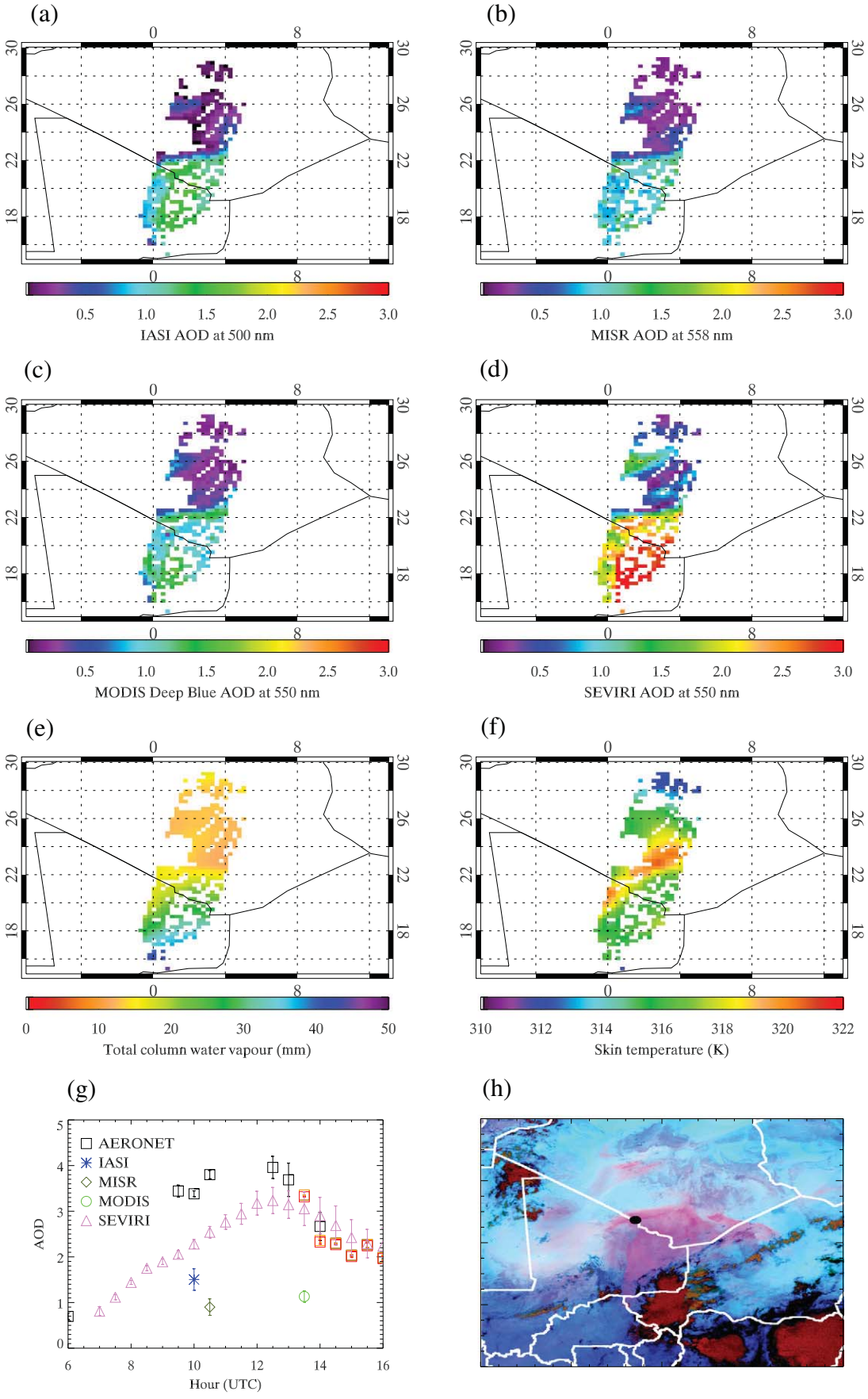
(a)
IASI AOD at 500 nm
(b)
MISR AOD at 558 nm
(c)
MODIS Deep Blue AOD at 550 nm
(d)
SEVIRI AOD at 550 nm
(e)
Total column water vapour (mm)
(f)
Skin temperature (K)
(g)
AERONET
IASI
MISR
MODIS
SEVIRI
AOD
Hour (UTC)
(h)

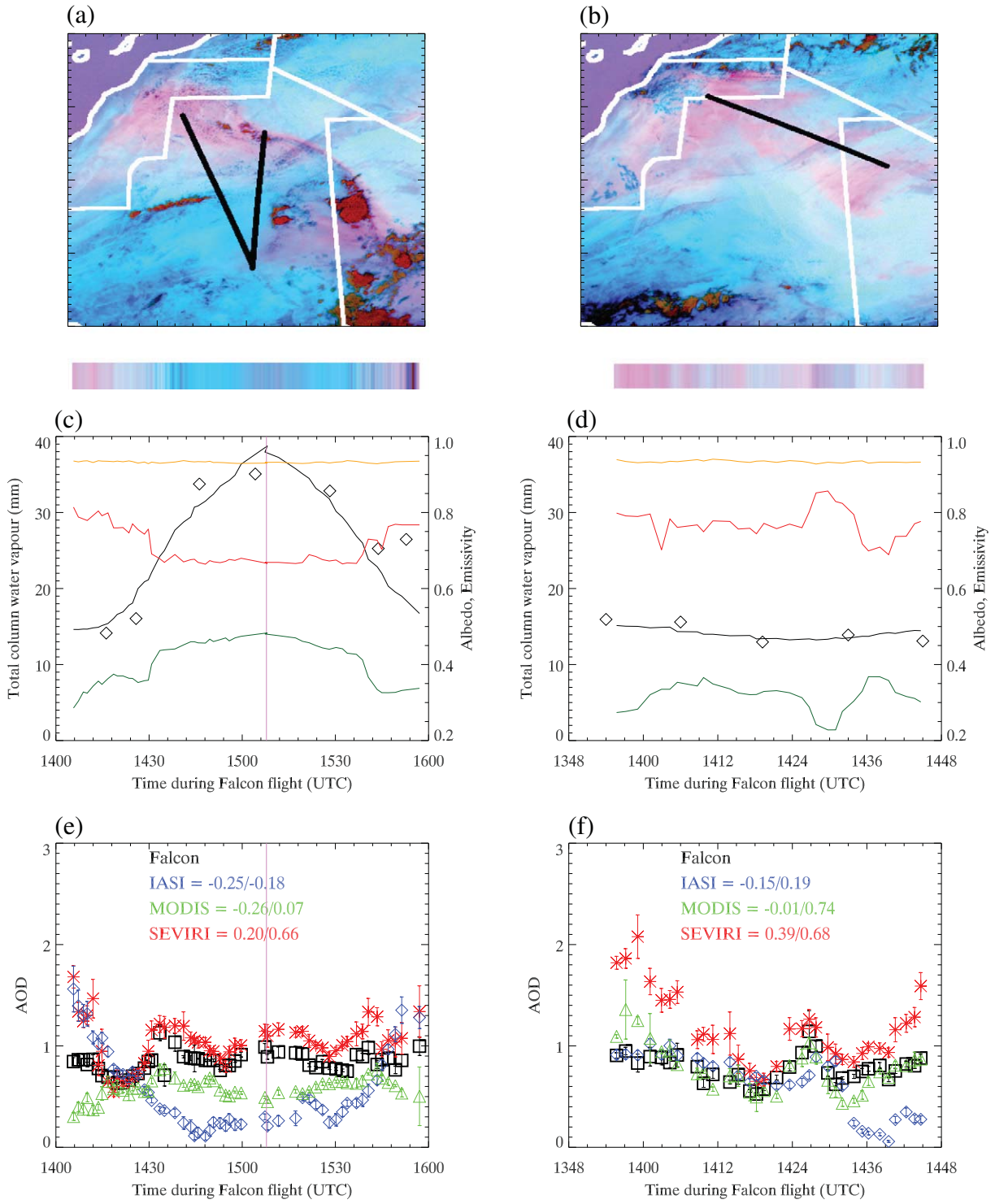

Fig. 11. Dust observations and conditions along the Falcon flight track, on the 20th, flight F21 (left), and the 21st, flight F23 (right). (a,b) SEVIRI RGB images on the 20th (1500 UTC) and the 21st (1415 UTC), included are the flight tracks in black, and below are the RGB colours along the tracks; (c,d) along-track column moisture from ERA-Interim (black line) and from the Falcon dropsondes (black diamonds), albedo (green line), emissivities at 8.7 and 10.8 μm (red and orange lines), and on the 20th the vertical purple line indicates the change in flight direction; (e,f) along-track AODs from the Falcon LIDAR, IASI, MODIS and SEVIRI, with biases/correlations with respect to the Falcon. The error bars indicate the standard deviation of the mean of the AOD measurements within the grid cells along the flight track.

Fig. 10. Dust activity and meteorological conditions over BBM on the 17th June. (a) IASI AOD; (b) MISR AOD; (c) MODIS AOD; (d) SEVIRI AOD; (e) total column water vapour; (f) skin temperature; (g) time-series of AERONET and satellite retrieved AODs during the day (black squares are Level 1 AERONET, orange are Level 1.5, and red are Level 2); (h) RGB 'desert-dust' image from SEVIRI at 1030 UTC (dust appears pink, thick cloud is red, and BBM is the black oval on the Algerian/Malian border). The AERONET error bars are derived from the standard deviation of the mean of the measurements made within ±15 min of each time slot, while the satellite product AODs are derived from the standard deviation of the mean of the retrievals made within 25 km of BBM. The error on the MISR retrieval is 0.2 × AOD as discussed in Section 2.1, since there is only one pixel with a successful retrieval.

UTC MODIS and especially IASI are negatively biased against, and weakly correlated with the LIDAR where the aircraft was overflying the region of high albedo and low emissivity. This is consistent with the findings of Fig. 9. IASI's more negative bias in moist conditions may also contribute to its very low values at the southern end of the flight track. Over darker and more emissive surfaces (at either end of flight F21, and along most of the flight F23) IASI is apparently better able to retrieve the AODs that the LIDAR observes. MODIS performs very well during flight F23 with the highest correlation with the LIDAR, under constant dry conditions and over moderately varying albedos. For this flight SEVIRI has a high positive bias against the LIDAR observations, even under dry conditions.

The conditions encountered on flight F23 and at the northern ends of flight F21 are analogous to the conditions generally found at Zouerat, i.e. a dry atmosphere over a semi-bright surface. Set in this context, SEVIRI's high bias against the LIDAR AODs during F23 is consistent with some of the dry/bright SEVIRI/AERONET comparisons at Zouerat seen in Fig. 9(c), at low AODs where SEVIRI is biased high. Hence, while moisture may be a significant driver of anomalously high SEVIRI AOD, this factor is not exclusive. IASI tends to be negatively biased against AERONET at Zouerat while MODIS retrieves AODs either side of the AERONET one-to-one line, consistent with what we see in the LIDAR/satellite product comparisons. Meanwhile no AERONET site is closely analogous to the conditions found at the southern end of flight F21 which has a moist atmosphere similar to that found over the Sahel, but has a very bright surface with an albedo peaking above 0.45. The most analogous sites would be BBM, which has the highest site albedo (0.39), and Zinder Airport, which also has a fairly bright surface (0.34) and a typically moist atmosphere. Both IASI and MODIS are biased somewhat lower over these sites than over Zouerat, especially IASI, which is also borne out by the LIDAR comparisons. SEVIRI is biased high against AERONET observations at Zinder Airport, but is biased slightly low against AERONET at BBM in moist conditions. Again, this is consistent with the LIDAR comparisons.

Correlating the AODs with the various conditions for the two flights, we find that the LIDAR AODs indicate no significant correlation. MODIS and SEVIRI to an even lesser extent have marginal anti-correlations with moisture and albedo/emissivity: for example, MODIS has a correlation with albedo of −0.30. In contrast, IASI shows a more marked relationship with both column moisture (correlation of −0.58) and 8.7 μm emissivity (correlation of 0.73). Especially at low emissivities, the infrared IASI retrieval may be less able to discriminate between the background sand and the lofted dust, and indeed it is at the lowest emissivities that IASI has the strongest negative bias. Moisture may amplify this effect over surfaces of low emissivity, as seen in Fig. 6(b). The RGB imagery extracted along the flight tracks tends to confirm this interpretation. Under dry conditions (Fig. 11(b)) there is a strong relationship in the degree of 'pinkness' to the retrieved SEVIRI AODs. Under more moist conditions (Fig. 11(a)) the pattern corresponds more closely to that seen in the IASI retrievals with enhanced moisture masking the dust signal as measured by the LIDAR. This behaviour is consistent with theoretical expectations (Brindley et al., 2012).

This analysis of the aircraft observations indicates that while broad judgements about the effectiveness of the satellite retrievals under various regimes of conditions can be made, the picture remains a complicated one, with subtle interconnections amongretrieved AODs, the meteorological conditions, and the underlying surface properties.

5. Conclusions

By comparing the dust aerosol retrievals of IASI, MISR, MODIS, and SEVIRI under varying conditions during the Fennec campaign period in June 2011 at the peak of the yearly cycle of dust activity in the Sahara, we can learn more about the conditions under which they are most reliable. Spatial agreement between the satellite products is good. Under heaviest dust loadings (AOD > 1) it appears that SEVIRI is most able to capture the best estimate of the AOD as measured by ground-based and aircraft instrumentation, whereas the other satellite products retrieve much lower values. Out of the mean AODs for each instrument, SEVIRI has the greatest fractional contribution of high AODs to the monthly mean, with values of 0.22 for IASI (from 5% of the number of points), 0.18 for MISR (8%), 0.13 for MODIS (5%), and 0.47 for SEVIRI (22%). Here the fractional contribution is defined as the sum of the high AODs divided by the sum of all AODs. On the other hand, SEVIRI does not perform so well at lower dust loadings where it can significantly overestimate the AOD, especially where the atmospheric water vapour content is also quite high (>20 mm). Under these conditions the other satellite products appear better able to capture the dust loading. Under moist conditions IASI retrievals also show a noticeably low bias with respect to the 'best estimate', so we may also have more confidence in the IASI retrievals made under drier conditions. MODIS has consistent statistics between dry and moist conditions and, while we have not evaluated MISR explicitly with the 'best estimate' because of a lack of coincident overpasses, satellite product inter-comparisons show that it has a similar response to MODIS. Hence as might be expected, MISR and MODIS seem to be least affected by the atmospheric water vapour content, and so would be the most trustworthy in sharply varying meteorological conditions given low dust loading and suitable surface conditions.

Surface type also plays a role in the effectiveness of the retrievals. Over elevated surfaces MODIS reports very low AODs, and is unable to retrieve the magnitude of the dust loading that the other satellite products and AERONET observe, while IASI appears to retrieve the most realistic AODs. On the other hand over brighter (albedo > 0.3), less emissive surfaces ($\epsilon < 0.84$) it is IASI which most underestimates the AOD with a negative bias of −0.41 with respect to the relevant AERONET sites. This behaviour is also seen in the comparisons with the Falcon LIDAR observations. As shown by Fig. 6, over these surfaces MISR retrieves higher AODs, although these tend to be smaller than those retrieved by SEVIRI, which has a positive bias against AERONET of 0.11. Hence over bright surfaces SEVIRI and MISR should be the preferred instruments, while over elevated surfaces IASI may instead be preferred.

Overall then, SEVIRI performs well at high dust loading, but at lower AODs it is biased high at high moisture content (>20 mm). These results suggest also a slightly high bias at low dust loadings under dry conditions. IASI performs well at high elevation but has a tendency to under-estimate the dust loading, and is negatively correlated with water vapour and positively correlated with surface infrared emissivity. The sensitivity of the SEVIRI and IASI retrievals due to moisture may arise from the (perhaps insufficiently constrained) corrections each of these infrared instruments must make in order to account for changes in brightness temperature due to water vapour. MODIS struggles particularly at high elevation, underestimating the AOD, but is generally unaffected by moisture. MISR has the most consistent retrievals, with no large variations in any moisture/albedo regime, but is unable to retrieve the magnitude of the largest dust events: at high dust loading with a homogeneous 'surface' of airborne dust, the advantages of MISR's multi-angle observations at minimising the radiance contribution from variable desert surfaces are reduced. These conclusions are summarised in Table 4.

These findings indicate the surface types, the meteorological conditions, and the dust loadings for which each of the satellite products is most capable of retrieving the appropriate values of the AOD, as assessed during the summer maximum in dust activity in June 2011. Observations made during the Fennec campaign have provided new information as to the dust size distributions (Ryder et al., 2013) and the dust layer distributions (McQuaid et al., 2013), for example. Such precise observations of the nature of the dust and of its activity may help to inform our understanding of the scenes that the satellite

Table 4
Conditions under which each product is most capable of retrieving accurate AOD values. Dashes indicate factors to which the specific retrieval algorithm appears relatively insensitive.

Instrument	Dust loading	Moisture	Emissivity	Elevation
IASI	Low	Low	High	High
MISR	Low	–	–	–
MODIS	Low	–	–	Low
SEVIRI	High	Low	–	–

products are trying to make retrievals of, and so it would be of benefit for subsequent studies to also make use of these new measurements when assessing and improving the capabilities of the satellite products for dust retrievals.

Acknowledgements

We thank the AERONET PIs and staff for establishing and maintaining the nine sites used in this study; the Fennec supersites at BBM and Zouerat were operated by the Offices Nationals de la Météorologie (ONM) of Algeria and Mauritania. The ERA-Interim meteorological data were produced by ECWMF, and access to the dataset was provided by the British Atmospheric Data Centre. Thanks also go to the Royal Meteorological Institute of Belgium for the provision of surface elevation and albedo dataand also 'GERBlike' data used in the SEVIRI AOD retrieval, as well as to researchers at the Cooperative Institute for Meteorological Satellite Studies at the University of Wisconsin for the emissivity data. This work has been carried out as part of the Fennec project. The Fennec-France project is funded by the Agence Nationale de la Recherche (ANR), the Institut National des Sciences de l'Univers (INSU/CNRS) through the LEFE program, by the Centre National d'Etudes Spatiales (CNES) through the TOSCA program and by Météo-France. Many thanks to the SAFIRE team for the radiation and dropsonde data from the Falcon 20 as well as to J. Pelon (LATMOS). The authors are grateful to D. Bruneau and P. Genau (LATMOS), F. Blouzon and A. Abchiche (DT/INSU) for operating the LNG system in the Falcon 20. The work of M. Garay and O. Kalashnikova was carried out at the Jet Propulsion Laboratory, California Institute of Technology under a contract with the National Aeronautics and Space Administration. Thanks also to John Marsham at the University of Leeds for his helpful comments during the preparation of this work, and to two anonymous reviewers whose valuable comments have also improved this work. J. R. Banks is supported under grant NE/G016283/1 by the UK Natural Environment Research Council.

References

Ackerman, S. A. (1997). Remote sensing of aerosol using satellite infrared observations. *Journal of Geophysical Research*, *102*, 17069–17079.
Ansmann, A., Petzold, A., Kandler, K., Tegen, I., Wendisch, M., Müller, D., et al. (2011). Saharan Mineral Dust Experiments SAMUM-1 and SAMUM-2: What have we learned? *Tellus*, *63B*, 403–429.
Ashpole, I., & Washington, R. (2012). An automated dust detection using SEVIRI: A multi-year climatology of summertime dustiness in the central and western Sahara. *Journal of Geophysical Research*, *117*.
Banks, J. R., & Brindley, H. E. (2013). Evaluation of MSG-SEVIRI mineral dust retrieval products over North Africa and the Middle East. *Remote Sensing of Environment*, *128*, 58–73.
Bodhaine, B. A., Wood, N. B., Dutton, E. G., & Slusser, J. R. (1999). On Rayleigh optical depth calculations. *Journal of Atmospheric and Oceanic Technology*, *16*, 1854–1861.
Brindley, H. E. (2007). Estimating the top-of-atmosphere longwave radiative forcing due to Saharan dust from satellite observations over a west African surface site. *Atmospheric Science Letters*, *8*, 74–79.
Brindley, H. E., Knippertz, P., Ryder, C., & Ashpole, I. (2012). A critical evaluation of the ability of the Spinning Enhanced Visible and InfraRed Imager (SEVIRI) thermal infrared red-green-blue rendering to identify dust events: Theoretical analysis. *Journal of Geophysical Research*, *117*.
Brindley, H. E., & Russell, J. E. (2009). An assessment of Saharan dust loading and the corresponding cloud-free longwave direct radiative effect from geostationary satellite observations. *Journal of Geophysical Research*, *114*.
Carboni, E., Thomas, G. E., Sayer, A. M., Siddans, R., Poulsen, C. A., Grainger, R. G., et al. (2012). Intercomparison of desert dust optical depth from satellite measurements. *Atmospheric Measurement Techniques*, *5*, 1973–2002.
Christopher, S. A., Gupta, P., & Haywood, J. (2008). Aerosol optical thicknesses over North Africa: 1. Development of a product for model validation using ozone monitoring instrument, multiangle imaging spectroradiometer, and aerosol robotic network. *Journal of Geophysical Research*, *113*.
Christopher, S. A., Gupta, P., Johnson, B., Ansell, C., Brindley, H., & Haywood, J. (2011). Multi-sensor satellite remote sensing of dust aerosols over North Africa during GERBILS. *Quarterly Journal of the Royal Meteorological Society*, *137*, 1168–1178.
Christopher, S. A., Johnson, B., Jones, T., & Haywood, J. (2009). Vertical and spatial distribution of dust from aircraft and satellite measurements during the GERBILS field campaign. *Geophysical Research Letters*, *36*.
Cuesta, J., Edouart, D., Mimouni, M., Flamant, P. H., Loth, C., Gilbert, F., et al. (2008). Multiplatform observations of the seasonal evolution of the Saharan atmospheric boundary layer in Tamanrasset, Algeria, in the framework of the African Monsoon Multidisciplinary Analysis field campaign conducted in 2006. *Journal of Geophysical Research*, *113*.
Cuesta, J., Marsham, J. H., Parker, D. J., & Flamant, C. (2009). Dynamical mechanisms controlling the vertical redistribution of dust and the thermodynamic structure of the West Saharan atmospheric boundary layer during summer. *Atmospheric Science Letters*, *10*, 34–42.
Derrien, M., & Le Gléau, H. (2005). MSG/SEVIRI cloud mask and type from SAFNWC. *International Journal of Remote Sensing*, *26*, 4707–4732.
DeSouza-Machado, S. G., Strow, L. L., Imbiriba, B., McCann, K., Hoff, R. M., Hannon, S. E., et al. (2010). Infrared retrievals of dust using AIRS: Comparisons of optical depths and heights derived for a North African dust storm to other collocated EOS A-train and surface observations. *Journal of Geophysical Research*, *115*.
deVilliers, R., Ancellet, G., Pelon, J., Quennehen, B., Schwarzenboeck, A., Gayet, J. F., et al. (2010). Airborne measurements of aerosol optical properties related to early spring transport of mid-latitude sources into the Arctic. *Atmospheric Chemistry and Physics*, *10*, 5011–5030.
Diner, D. J., Beckert, J. C., Bothwell, G., & Rodriguez, J. (2002). Performance of the MISR instrument during its first 20 months in Earth orbit. *IEEE Transactions on Geoscience and Remote Sensing*, *40*, 1449–1466.
Diner, D. J., Martonchik, J. V., Kahn, R. A., Pinty, B., Gobron, N., Nelson, D. L., et al. (2005). Using angular and spectral shape similarity constraints to improve MISR aerosol and surface retrievals over land. *Remote Sensing of Environment*, *94*, 155–171.
Dubovik, O., Holben, B., Eck, T. F., Smirnov, A., Kaufman, Y. J., King, M. D., et al. (2002). Variability of absorption and optical properties of key aerosol types observed in worldwide locations. *Journal of the Atmospheric Sciences*, *59*, 590–608.
Dufresne, J. -L., Gautier, C., Ricchiazzi, P., & Fouquart, Y. (2002). Longwave scattering effects of mineral aerosols. *Journal of the Atmospheric Sciences*, *53*, 1959–1966.
Eck, T. F., Holben, B. N., Reid, J. S., Dubovik, O., Smirnov, A., O'Neill, N. T., et al. (1999). Wavelength dependence of the optical depth of biomass burning, urban, and desert dust aerosols. *Journal of Geophysical Research*, *104*, 31,333–31,349.
Farquharson, J. S. (1937). Haboobs and instability in the Sudan. *Quarterly Journal of the Royal Meteorological Society*, *63*, 393–414.
Fernald, F. G., Herman, B. M., & Reagan, J. A. (1972). Determination of aerosol height distributions by Lidar. *Journal of Applied Meteorology*, *11*, 482–489.
Frank, T. D., Girolamo, L. D., & Geegan, S. (2007). The spatial and temporal variability of aerosol optical depths in the Mojave Desert of Southern California. *Remote Sensing of Environment*, *107*, 54–64.
Ginoux, P., Prospero, J. M., Gill, T. E., Hsu, N. C., & Zhao, M. (2012). Global-scale attribution of anthropogenic and natural dust sources and their emission rates based on MODIS Deep Blue aerosol products. *Reviews of Geophysics*, *50*.
Haywood, J. M., Johnson, B. T., Osborne, S. R., Baran, A. J., Brooks, M., Milton, S. F., et al. (2011). Motivation, rationale and key results from the GERBILS Saharan dust measurement campaign. *Quarterly Journal of the Royal Meteorological Society*, *137*, 1106–1116.
Heintzenberg, J. (2009). The SAMUM-1 experiment over Southern Morocco: Overview and introduction. *Tellus*, *61*, 2–11.
Holben, B. N., Eck, T. F., Slutsker, I., Tanré, D., Buis, J. P., Setzer, A., et al. (1998). AERONET—A federated instrument network and data archive for aerosol characterization. *Remote Sensing of Environment*, *66*, 1–16.
Hsu, N. C., Tsay, S. -C., King, M. D., & Herman, J. R. (2004). Aerosol properties over bright-reflecting source regions. *IEEE Transactions on Geoscience and Remote Sensing*, *42*, 557–569.
Hsu, N. C., Tsay, S. -C., King, M. D., & Herman, J. R. (2006). Deep blue retrievals of Asian aerosol properties during ACE-Asia. *IEEE Transactions on Geoscience and Remote Sensing*, *44*, 3180–3195.
Hudson, P. K., Gibson, E. R., Young, M. A., Kleiber, P. D., & Grassian, V. H. (2008a). Coupled infrared extinction spectra and size distribution measurements for several clay components of mineral dust aerosol. *Journal of Geophysical Research*, *113*.
Hudson, P. K., Young, M. A., Kleiber, P. D., & Grassian, V. H. (2008b). Coupled infrared extinction spectra and size distribution measurements for several non-clay components of mineral dust aerosol (quartz, calcite and dolomite). *Atmospheric Environment*, *42*, 5991–5999.
Ipe, A., Bertrand, C., Clerbaux, N., Dewitte, S., & Gonzalez, L. (2004). Validation and homogenization of cloud optical depth and cloud fraction retrievals for GERB/SEVIRI scene identification using Meteosat-7 data. *Atmospheric Research*, *72*, 17–37.
Kahn, R. A., Gaitley, B. J., Garay, M. J., Diner, D. J., Eck, T. F., Smirnov, A., et al. (2010). Multiangle Imaging SpectroRadiometer global aerosol product assessment by comparison with the Aerosol Robotic Network. *Journal of Geophysical Research*, *115*.

Kahn, R., Gaitley, B., Martonchik, J., Diner, D., Crean, K., & Holben, B. (2005). MISR global aerosol optical depth validation based on two years of coincident AERONET observations. *Journal of Geophysical Research*, *110*.

Kahn, R. A., Garay, M. J., Nelson, D. L., Yau, K. K., Bull, M. A., Gaitley, B. J., et al. (2007). Satellite-derived aerosol optical depth over dark water from MISR and MODIS: Comparisons with AERONET and implications for climatological studies. *Journal of Geophysical Research*, *112*.

Kahn, R., Petzold, A., Wendisch, M., Bierwirth, E., Dinter, T., Esselborn, M., et al. (2009a). Desert dust aerosol air mass mapping in the western Sahara, using particle properties derived from space-based multi-angle imaging. *Tellus B*, *61*, 239–251.

Kahn, R. A., Nelson, D. L., Garay, M. J., Levy, R. C., Bull, M. A., Diner, D. J., et al. (2009b). MISR aerosol product attributes and statistical comparisons with MODIS. *IEEE Transactions on Geoscience and Remote Sensing*, *47*, 4095–4114.

Kalashnikova, O. V., Kahn, R., Sokolik, I. N., & Li, W. -H. (2005). The ability of multi-angle remote sensing observations to identify and distinguish mineral dust types: Part 1. Optical models and retrievals of optically thick plumes. *Journal of Geophysical Research*, *110*.

Klüser, L., Kleiber, P., Holzer-Popp, T., & Grassian, V. (2012). Desert dust observation from space—Application of measured mineral component infrared extinction spectra. *Atmospheric Environment*, *54*, 419–427.

Klüser, L., Martynenko, D., & Holzer-Popp, T. (2011). Thermal infrared remote sensing of mineral dust over land and ocean: A spectral SVD based retrieval approach for IASI. *Atmospheric Measurement Techniques*, *4*, 757–773.

Koren, I., Kaufman, Y. J., Washington, R., Todd, M. C., Rudich, Y., Martins, J. V., et al. (2006). The Bodélé depression: A single spot in the Sahara that provides most of the dust to the Amazon forest. *Environmental Research Letters*, *1*.

Lee, S. S., & Penner, J. E. (2010). Aerosol effects on ice clouds: Can the traditional concept of aerosol indirect effects be applied to aerosol–cloud interactions in cirrus clouds? *Atmospheric Chemistry and Physics*, *10*, 10345–10358.

Legrand, M., Pietras, C., Brogniez, G., Haeffelin, M., Abuhassan, N. K., & Sicard, M. (2000). A high-accuracy multiwavelength radiometer for in situ measurements in the thermal infrared. Part I: Characterization of the instrument. *Journal of Atmospheric and Oceanic Technology*, *17*, 1203–1214.

Lensky, I. M., & Rosenfeld, D. (2008). Clouds–Aerosols–Precipitation Satellite Analysis Tool (CAPSAT). *Atmospheric Chemistry and Physics*, *8*, 6739–6753.

Levy, R. C., Remer, L. A., Mattoo, S., Vermote, E. F., & Kaufman, Y. J. (2007). Second-generation operational algorithm: Retrieval of aerosol properties over land from inversion of Moderate Resolution Imaging Spectroradiometer spectral reflectance. *Journal of Geophysical Research*, *112*.

Mahowald, N. M., Baker, A. R., Bergametti, G., Brooks, N., Duce, R. A., Jickells, T. D., et al. (2005). Atmospheric global dust cycle and iron inputs to the ocean. *Global Biogeochemical Cycles*, *19*.

Mahowald, N. M., & Kiehl, L. M. (2003). Mineral aerosol and cloud interactions. *Geophysical Research Letters*, *30*(9).

Marsham, J. H., Hobby, M., Allen, C. J. T., Banks, J. R., Bart, M., Brooks, B., et al. (2013). Meteorology and dust in the central Sahara: Observations from Fennec supersite-1 during the June 2011 Intensive Observation Period. *Journal of Geophysical Research* (in press) http://dx.doi.org/10.1002/jgrd.50211.

Marsham, J. H., Knippertz, P., Dixon, N. S., Parker, D. J., & Lister, G. M. S. (2011). The importance of the representation of deep convection for modeled dustgenerating winds over West Africa during summer. *Geophysical Research Letters*, *38*.

Marsham, J. H., Parker, D. J., Grams, C. M., Taylor, C. M., & Haywood, J. M. (2008). Uplift of Saharan dust south of the intertropical discontinuity. *Journal of Geophysical Research*, *113*.

Martonchik, J. V., Diner, D. J., Kahn, R., Gaitley, B., & Holben, B. N. (2004). Comparison of MISR and AERONET aerosol optical depths over desert sites. *Geophysical Research Letters*, *31*.

Martonchik, J. V., Kahn, R. A., & Diner, D. J. (2009). Retrieval of aerosol properties over land using MISR observations. In A. A. Kokhanovsky, & G. de Leeuw (Eds.), *Satellite Aerosol Remote Sensing Over Land chapter 9*. Chichester, UK: Springer- Praxis Publishing Ltd.

McConnell, C. L., Highwood, E. J., Coe, H., Formenti, P., Anderson, B., Osborne, S., et al. (2008). Seasonal variations of the physical and optical characteristics of Saharan dust: Results from the Dust Outflow and Deposition to the Ocean (DODO) experiment. *Journal of Geophysical Research*, *113*.

McQuaid, J., Ryder, C. L., Sodemann, H., Garcia-Carreras, L., Rosenberg, P., Banks, J. R., et al. (2013). Overview and insights gained by airborne observations over the Sahara during Fennec. *Presented at the European Geosciences Union, Vienna*.

MétéoFrance (2012). Algorithm theoretical basis document for cloud products (CMa-PGE01 v3.2, CT-PGE02 v2.2 & CTTH-PGE03 v2.2). *Technical Report SAF/NWC/CDOP/MFL/SCI/ATBD/01*. Paris: MétéoFrance.

Omar, A. H., Winker, D. M., Kittaka, C., Vaughan, M. A., Liu, Z. Y., Hu, Y. X., et al. (2009). The CALIPSO automated aerosol classification and Lidar ratio selection algorithm. *Journal of Atmospheric and Oceanic Technology*, *26*, 1994–2014.

Redelsperger, J. -L., Thorncroft, C. D., Diedhiou, A., Lebel, T., Parker, D. J., & Polcher, J. (2006). African monsoon multidisciplinary analysis: An international research project and field campaign. *Bulletin of the American Meteorological Society*, *87*, 1739–1746.

Ryder, C. L., Highwood, E. J., Rosenberg, P. D., Trembath, J., Brooke, J. K., Bart, M., et al. (2013). Optical properties of Saharan dust aerosol and contribution from the coarse mode as measured during the Fennec 2011 aircraft campaign. *Atmospheric Chemistry and Physics*, *13*, 303–325.

Sayer, A. M., Hsu, N. C., Bettenhausen, C., Jeong, M. -J., Holben, B. N., & Zhang, J. (2012). Global and regional evaluation of over-land spectral aerosol optical depth retrievals from SeaWiFS. *Atmospheric Measurement Techniques*, *5*, 1761–1778.

Schepanski, K., Tegen, I., Laurent, B., Heinold, B., & Macke, A. (2007). A new Saharan dust source activation frequency map derived from MSG-SEVIRI IR-channels. *Geophysical Research Letters*, *34*.

Schmetz, J., Pili, P., Tjemkes, S., Just, D., Kerkmann, J., Rota, S., et al. (2002). An introduction to Meteosat Second Generation (MSG). *Bulletin of the American Meteorological Society*, *83*, 977–992.

Schuster, G. L., Vaughan, M., MacDonnell, D., Su, W., Winker, D., Dubovik, O., et al. (2012). Comparison of CALIPSO aerosol optical depth retrievals to AERONET measurements, and a climatology for the lidar ratio of dust. *Atmospheric Chemistry and Physics*, *12*, 7431–7452.

Seemann, S. W., Borbas, E. E., Knuteson, R. O., Stephenson, G. R., & Huang, H. -L. (2008). Development of a global infrared land surface emissivity database for application to clear sky sounding retrievals from multispectral satellite radiance measurements. *Journal of Applied Meteorology and Climatology*, *47*, 108–123.

Seidel, F. C., & Popp, C. (2012). Critical surface albedo and its implications to aerosol remote sensing. *Atmospheric Measurement Techniques*, *5*, 1653–1665.

Shi, Y., Zhang, J., Reid, J. S., Hyer, E. J., Eck, T. F., Holben, B. N., et al. (2011). A critical examination of spatial biases between MODIS and MISR aerosol products—Application for potential AERONET deployment. *Atmospheric Measurement Techniques*, *4*, 2823–2836.

Slingo, A., Ackerman, T. P., Allan, R. P., Kassianov, E. I., McFarlane, S. A., Robinson, G. J., et al. (2006). Observations of the impact of a major Saharan dust storm on the atmospheric radiation balance. *Geophysical Research Letters*, *33*.

Smirnov, A., Holben, B. N., Eck, T. F., Dubovik, O., & Slutsker, I. (2000). Cloud-screening and quality control algorithms for the AERONET database. *Remote Sensing of Environment*, *73*, 337–349.

Smirnov, A., Holben, B. N., Eck, T. F., Slutsker, I., Chatenet, B., & Pinker, R. T. (2002). Diurnal variability of aerosol optical depth observed at AERONET (Aerosol Robotic Network) sites. *Geophysical Research Letters*, *29*(23).

Sullivan, R. C., Moore, M. J. K., Petters, M. D., Kreidenweis, S. M., Roberts, G. C., & Prather, K. A. (2009). Effect of chemical mixing state on the hygroscopicity and cloud nucleation properties of calcium mineral dust particles. *Atmospheric Chemistry and Physics*, *9*, 3303–3316.

Todd, M. C., Cavazos-Guerra, C., Wang, Y., Washington, R., Allen, C. J. T., Engelstaedter, S., et al. (2013). *Meteorological and dust aerosol conditions over the Western Saharan region observed at Fennec supersite-2 during the Intensive Observation Period in June 2011. Journal of Geophysical Research.* http://dx.doi.org/10.1002/jgrd.50470 (in press).

Washington, R., Flamant, C., Parker, D., Marsham, J., McQuaid, J., Brindley, H., et al. (2012). Fennec—The Saharan Climate System. *CLIVAR Exchanges*, *60*, 31–33.

Washington, R., & Todd, M. C. (2005). Atmospheric controls on mineral dust emission from the Bodélé Depression, Chad: The role of the low level jet. *Geophysical Research Letters*, *32*.

Washington, R., Todd, M., Middleton, N. J., & Goudie, A. S. (2003). Dust-storm source areas determined by the total ozone monitoring spectrometer and surface observations. *Annals of the Association of American Geographers*, *93*, 297–313.

Intercomparison of satellite dust retrieval products over the west African Sahara during the Fennec campaign in June 2011

J. R. Banks[a,*], H. E. Brindley[a], C. Flamant[b], M. J. Garay[c], N. C. Hsu[d], O. V. Kalashnikova[c], L. Klüser[e], A. M. Sayer[d,f]

[a] *Space and Atmospheric Physics Group, Imperial College, London, UK*
[b] *Laboratoire Atmosphères, Milieux, Observations Spatiales, CNRS, UMR 8190, Paris, France*
[c] *Jet Propulsion Laboratory, California Institute of Technology, Pasadena, California, USA*
[d] *NASA Goddard Space Flight Center, Greenbelt, Maryland, USA*
[e] *German Aerospace Center (DLR), German Remote Sensing Datacenter (DFD), 82334 Wessling, Germany*
[f] *Goddard Earth Sciences Technology And Research (GESTAR), Universities Space Research Association (USRA), Columbia, Maryland, USA*

Abstract

Dust retrievals over the Sahara Desert during June 2011 from the IASI, MISR, MODIS, and SEVIRI satellite instruments are compared against each other in order to understand the strengths and weaknesses of each retrieval approach. Particular attention is paid to the effects of meteorological conditions, land surface properties, and the magnitude of the dust loading. The period of study corresponds to the time of the first Fennec intensive measurement campaign, which provides new ground-based and aircraft measurements of the dust characteristics and loading. Validation using ground-based AERONET sunphotometer data indicate that of the satellite instruments, SEVIRI is most able to retrieve dust during optically thick dust events, whereas IASI and MODIS perform better at low dust loadings. This may significantly affect observations of dust emission and the mean dust climatology. MISR and MODIS are least sensitive to variations in meteorological conditions, while SEVIRI tends to overestimate the aerosol optical depth (AOD) under moist conditions (with a bias against

*Corresponding author. Space and Atmospheric Physics Group, The Blackett Laboratory, Imperial College London, Prince Consort Road, London, SW7 2BW, UK. Tel.: +44 207 5947677; fax: +44 207 7594 7772. *E-mail address*: j.banks@imperial.ac.uk (J. R. Banks).

AERONET of 0.31), especially at low dust loadings where the AOD < 1. Further comparisons are made with airborne LIDAR measurements taken during the Fennec campaign, which provide further evidence for the inferences made from the AERONET comparisons. The effect of surface properties on the retrievals is also investigated. Over elevated surfaces IASI retrieves AODs which are most consistent with AERONET observations, while the AODs retrieved by MODIS tend to be biased low. In contrast, over the least emissive surfaces IASI significantly underestimates the AOD (with a bias of -0.41), while MISR and SEVIRI show closest agreement.

Keywords: Remote sensing of dust, Satellite retrieval intercomparisons, Aerosol optical depth, Fennec

1. Introduction

The Sahara is the largest source of mineral dust aerosols in the world (e.g. Washington et al., 2003), and the atmosphere above it has some of the highest dust loadings. Large Saharan dust storms have been observed to increase the reflected shortwave radiation by as much as $100\,\mathrm{W\,m^{-2}}$ and to simultaneously significantly decrease the outgoing longwave radiation (Slingo et al., 2006). Dust may also have effects on ocean biogeochemistry through the transport of iron (e.g. Mahowald et al., 2005) and can affect fertility in the Amazon (Koren et al., 2006). Moreover, dust also interacts with the cloudy atmosphere and can change the occurence and microphysical properties of clouds (e.g. Mahowald & Kiehl, 2003; Lee & Penner, 2010). Dust loading over the Sahara peaks during the summer months when the Sahara has one of the deepest boundary layers on the planet (Cuesta et al., 2009).

Recent measurement campaigns have sought to deepen our understanding of climate and of dust activity in and near the Sahara. Such campaigns have included the African Monsoon Multidisciplinary Analyses (AMMA) project in 2006 (Redelsperger et al., 2006), which sought chiefly to understand the West African monsoon; Dust Outflow and Deposition (DODO) in 2006 (McConnell

et al., 2008), which sought to quantify dust deposition into the ocean; the Saharan Mineral Dust Experiment (SAMUM) in 2006 and 2008 (Heintzenberg, 2009; Ansmann et al., 2011), which sought to measure dust composition and optical properties; Geostationary Earth Radiation Budget experiment Intercomparison of Longwave and Shortwave radiation (GERBILS) in June 2007 (Haywood et al., 2011), which sought to understand dust properties and the atmospheric radiation balance over the western Sahara; and most recently Fennec in June 2011 and June 2012 (Washington et al., 2012), which aims to understand the climate system of the western Sahara in summer. The Fennec approach has used ground (Marsham et al., submitted 2012; Todd et al., submitted 2012), aircraft (McQuaid et al., in preparation; Ryder et al., 2012), and satellite (Banks & Brindley, 2013) observations, alongside numerical modelling.

The high dust loading in the turbulent Saharan summer atmosphere clearly has implications for the local climate. However, it is only relatively recently that multiple satellite retrieval algorithms have been developed which are able to quantify dust loadings over this region. Satellite observations are powerful tools which can also be used to study the distribution and intensity of dust sources (e.g. Schepanski et al., 2007; Ginoux et al., 2012). Depending on the methodology used, satellite instruments will be variously sensitive to the amount of dust, meteorological conditions, and surface properties (e.g. Shi et al., 2011). Previous studies have sought to quantify the differences between the satellite retrievals over the Sahara, e.g. during a large regional dust storm in March 2006 (Carboni et al., 2012), and during GERBILS in June 2007 (Christopher et al., 2011). New observations during Fennec in June 2011 provide a rich new set of local data to inform our knowledge of the atmospheric state that the satellites observe.

In this paper we present an analysis of co-located satellite aerosol retrieval products over the western half of the Sahara during the Fennec campaign in June 2011. We seek to quantify and understand the differences in the retrievals from the IASI, MISR, MODIS, and SEVIRI satellite instruments with respect to dust loading, meteorological conditions, and surface properties, before evaluating the

retrievals using data provided by AERONET (Holben et al., 1998) and aircraft observations made during the Fennec campaign.

2. Satellite, ground, and aircraft instrumentation

2.1. Satellite instruments

The Spinning Enhanced Visible and InfraRed Imager (SEVIRI) is located onboard the Meteosat Second Generation (MSG) series of satellites (Schmetz et al., 2002), which are in geostationary orbit above 0°N, 0°E, providing excellent coverage over Africa: these observations from SEVIRI have the advantage of a 15 minute temporal resolution, compared with the one or two observations over a given area per day provided by satellites in low Earth orbit. The nadir spatial sampling rate is 3 km (increasing to ∼4.5 km at higher SEVIRI viewing zenith angles within the west African field of interest), with measurements made at 11 visible and IR wavelengths: of particular value are the 10.8 and 13.4 μm channels which can be used to infer dust aerosol optical depth (AOD) over land (Brindley & Russell, 2009; Banks & Brindley, 2013), using a method specifically designed for arid and semi-arid regions. The first step in the retrieval process is to flag pixels as dusty and/or cloudy (MétéoFrance, 2012; Derrien & Le Gléau, 2005; Ipe et al., 2004). In order for an AOD to be inferred for a given pixel, we require either that cloud is not flagged, or that dust is flagged. A 'pristine sky' value of the brightness temperature at 10.8 μm (T_{B108dfe}) is calculated for each timeslot in a 28-day rolling window period, accounting for variations in total column water vapour and skin temperature from European Centre for Medium-range Weather Forecasts (ECMWF) ERA-Interim reanalyses. The deviation of the instantaneous T_{B108} value from the pristine sky value, due to dust, is given by:

$$\Delta T_{\mathrm{B108}} = T_{\mathrm{B108dfe}} - T_{\mathrm{B108}}. \quad (1)$$

An analogous calculation is made for ΔT_{B134}, which can be used to convert to dust AOD at 550 nm from a simulated relationship between $\Delta T_{\mathrm{B108}}/\Delta T_{\mathrm{B134}}$

and AOD (Brindley & Russell, 2009). The 13.4 μm channel is used to mitigate the effect of variations in dust height on the brightness temperature difference.

Another widely used and useful qualitative tool which can be derived from SEVIRI is the 'desert dust' RGB imagery (Lensky & Rosenfeld, 2008), which employs brightness temperature differences in the 8.7, 10.8, and 12.0 μm channels to discriminate the presence of dust in the atmosphere. Dust appears pink in this analysis, although in moist atmospheres the dust signal can be masked (Brindley et al., 2012).

The Infrared Atmospheric Sounding Interferometer (IASI) instrument is carried by the METOP series of satellites. The dust retrieval method for IASI (Klüser et al., 2011, 2012) is based on singular vector decomposition of binned IASI spectra between 830 and 1250 cm^{-1} (8-12 μm). The rationale behind the approach is to avoid radiative transfer forward simulations of IASI spectra over deserts as surface emissivity is highly variable and unknown (e.g. DeSouza-Machado et al., 2010). Moreover the retrieval is designed to minimise the necessary a priori information such as atmospheric state (temperature and humidity profiles). Mineral dust composed of silicate minerals can be detected in the thermal infrared (Ackerman, 1997) due to Si-O resonance absorption bands (Hudson et al., 2008b,a). Maximum value filtered brightness temperature spectra (in 42 bins) are converted to 'equivalent optical depth' spectra (Klüser et al., 2011):

$$L_{\mathrm{obs}}(\nu) = \exp(-\tau_{\mathrm{eq}}(\nu)/\cos\theta) B_\nu(T_{\mathrm{base}}), \tag{2}$$

where $L_{\mathrm{obs}}(\nu)$ is the radiance at wavenumber ν observed from space, θ is the viewing zenith angle and $B_\nu(T_{\mathrm{base}})$ is the spectral Planck-function evaluated for the baseline temperature defined as the maximum brightness temperature observed. The broad ozone absorption band around 1040 cm^{-1} is not used for dust retrieval. Singular vector decomposition has been performed for IASI spectra of equivalent optical depth covering North Africa, the Mediterranean and Arabia for a period of seven days. The leading two singular vectors have been found to represent broad gas absorption and surface emissivity features, con-

sequently dust optical depth is retrieved from the linear combination of higher order singular vectors. Extinction spectra of six mineral components of dust are projected onto the observed IASI spectra providing optical depth and weight for each component. Consequently, in contrast to most other dust retrieval methods, the singular-vector based approach is also able to account for variable mineralogy. In another iteration of the retrieval the thermal emission of the dust (Ackerman, 1997) is accounted for. After the IR optical depth of the dust has been determined the AOD is transferred to visible wavelengths by particle-size dependent transfer coefficients (Dufresne et al., 2002). Mathematical details of the method are presented by Klüser et al. (2011) and Klüser et al. (2012).

The Multi-angle Imaging SpectroRadiometer (MISR) was launched aboard the NASA Terra satellite into a sun-synchronous polar orbit in December 1999, and the data record currently extends over nearly 13 years. The instrument consists of nine cameras with view angles at the Earths surface of $\pm 70.5°$, $\pm 60.0°$, $\pm 45.6°$, $\pm 26.1°$, and $0°$ (nadir), operating in four spectral bands centred at 446 nm (blue), 559 nm (green), 672 nm (red), and 866 nm (near infrared). The map-projected spatial resolution is 275 m at nadir and in the red band of all nine cameras. In the global observing mode, the remaining channels are spatially averaged and map-projected to 1.1 km resolution. The common swath width is $\sim$400 km and global coverage is obtained every nine days at the equator and more frequently at higher latitudes (Diner et al., 2002).

The MISR standard aerosol retrieval algorithm reports AOD and aerosol type at 17.6 km$\times$17.6 km spatial resolution by analysing 1.1 km-resolution MISR top-of-atmosphere (TOA) radiances from 16$\times$16 pixel regions (Kahn et al., 2009b). Coupled surface-atmosphere retrievals are performed using all four spectral bands over most land surface types, including bright desert surfaces (Martonchik et al., 2009). The retrieval algorithm used to generate Version 22 of the MISR Standard Aerosol Product used in this study utilises a lookup table containing 74 aerosol mixtures consisting of eight component particle types (Kahn et al., 2010). Two of these components are a medium mode, non-spherical dust optical analogue developed from aggregated angular shapes and a coarse

mode dust analogue composed of ellipsoids (Kalashnikova et al., 2005). The MISR aerosol retrieval over land employs two different algorithms sequentially. The first algorithm applies the assumption that surface angular shapes are spectrally similar, as described by (Diner et al., 2005). Different aerosol models and AODs are tested, and those that fail this test are excluded from further consideration. The second algorithm performs an empirical orthogonal function (EOF) analysis of the angular shape of the TOA equivalent reflectances within the retrieval region after the atmospheric path radiance has been removed by subtracting the TOA measurements within a reference pixel. Aerosol properties are assumed to be the same for all pixels in the region. The AOD and aerosol model are determined by finding the combination of path radiance and linear sum of low-order EOFs that best fit the observations (Martonchik et al., 2009).

The performance of the operational MISR aerosol retrieval over bright desert sources and its sensitivity to near surface aerosols and surface properties have been validated and used in a number of studies (Christopher et al., 2008, 2009; Frank et al., 2007; Kahn et al., 2009a; Martonchik et al., 2004). A global comparison of coincident MISR and AERONET sunphotometer data showed that overall, about 70% to 75% of MISR AOD retrievals fall within the larger of 0.05 or 0.20×AOD, and about 50% to 55% are within the larger of 0.03 or 0.10×AOD, except for sites where dust or mixed dust and smoke are commonly found (Kahn et al., 2005, 2009b, 2010).

The MODerate resolution Imaging Spectroradiometer (MODIS) is located aboard the NASA Terra and Aqua satellites. MODIS Deep Blue (Hsu et al., 2004, 2006) aerosol products from Aqua use the blue wavelengths of the visible spectrum (412 and 490 nm referenced against 670 nm) to minimise the high surface signal in the visible wavelengths over bright surfaces such as the desert. Used here are the recently updated 'Collection 6' Deep Blue aerosol retrievals (the previous widely available product was 'Collection 5.1') from Aqua measurements: the same method has been used for retrievals from the Sea-viewing Wide Field-of-view Sensor (SeaWIFS) satellite instrument, as described by Sayer et al. (2012). The concept of the two versions of the Deep Blue algorithm is the

same, except Collection 6 has been updated for improved treatment of cloud-screening and of the aerosol model used, for example. The changes in monthly mean MODIS Deep Blue AODs from Collection 5.1 to Collection 6 are mapped in Figure 1, indicating that Collection 6 retrieves more dust loading over the central Sahara, in contrast to Collection 5.1, which retrieves most dust on the desert margins, especially in the Sahel.

Note that throughout this paper the names of the satellite instruments are used to denote AOD results from the specific dust retrieval algorithms introduced above. Other aerosol retrieval products exist for most of these instruments, for example the 'Dark Target' MODIS algorithm (Levy et al., 2007) which is unable to retrieve aerosol over bright desert surfaces and so is not used here.

2.2. Ground-based and aircraft data

Ground and in-situ data are invaluable for understanding and validating satellite data. From the ground, the Aerosol Robotic Network (AERONET) of sun-photometers provide multi-year time-series of AOD measurements from numerous sites (Holben et al., 1998). The nine AERONET sites in west Africa with co-located satellite data in June 2011 are mapped in Figure 2, with further details provided in Table 1. Two of these, Bordj Badji Mokhtar (BBM) and Zouerat (Marsham et al., submitted 2012; Todd et al., submitted 2012), were established within the framework of the Fennec project, with the goal of contributing to a new data set of atmospheric observations from the central Sahara (Washington et al., 2012). There are three levels of AERONET data for data quality purposes (Smirnov et al., 2000): Level 1 data, the 'raw' AOD measurements; Level 1.5, which are 'cloud-screened'; and Level 2, which are individually inspected and have the final calibration applied. The difference between Level 1 and Level 1.5 can be used as a crude measure for determining the influence of cloud on the observations (e.g. Brindley & Russell, 2009). Following the procedure outlined by Banks & Brindley (2013), AERONET data is regarded as representative for grid cells within a 25 km radius of the AERONET site, and

observations are regarded as dusty where the Ångström coefficient $\alpha \leq 0.6$ and the AOD $\tau_{1020\,\mathrm{nm}} \geq 0.2$ (Dubovik et al., 2002).

During the Fennec campaign in June 2011, ground data were supplemented by aircraft data from flights across Mauritania and northern Mali (McQuaid et al., in preparation; Ryder et al., 2012), using the UK Facility for Airborne Atmospheric Measurements (FAAM) BAe-146 and the Service des Avions Français Instrumentés pour la Recherche en Environnement (SAFIRE) Falcon 20 aircraft. The Falcon 20 was equipped with the backscatter LIDAR Leandre New Generation (LNG, deVilliers et al. (2010)) allowing the measurement of atmospheric reflectivity at three wavelengths (355, 532, and 1064 nm) to analyse the structure and radiative characteristics of desert dust plumes.The Falcon 20 was also equipped with a Vaisala AVAPS dropsonde launching device, radiometers (broad-band up- and down-looking Kipp and Zonen pyranometers and pyrgeometers), the CLIMAT radiometer (Legrand et al., 2000) as well as in situ PTU and wind sensors. The profiles of atmospheric extinction coefficient at 532 nm are retrieved using a standard LIDAR inversion technique (Fernald et al., 1972; Cuesta et al., 2008). The profiles of molecular extinction coefficient used in the inversion procedure are obtained from molecular density profiles computed using temperature and pressure data from dropsondes released during the flight (Bodhaine et al., 1999). The aerosol backscatter-to-extinction ratio used for the inversion is considered to be constant with altitude, set at $0.021\,\mathrm{sr}^{-1}$. This value is intermediate between the value derived at 532 nm from space-borne, airborne, and ground-based LIDAR systems over northern Africa (i.e. $0.018\,\mathrm{sr}^{-1}$, see Heintzenberg (2009); Schuster et al. (2012)) and those derived over Sahelian Africa (i.e. $0.024\,\mathrm{sr}^{-1}$, see Omar et al. (2009); Schuster et al. (2012)). Given the uncertainty on the backscatter-to-extinction ratio ($\pm 0.001\,\mathrm{sr}^{-1}$), the uncertainty on the LIDAR-derived AODs is estimated to be of the order of 15%. For inversion, a backscatter ratio (the total backscatter coefficient divided by the molecular backscatter coefficient) of 1 is considered at 9.5 km above ground level (agl), i.e. above dust observed during the period of interest. In Section 4.2 we will show and discuss particulate extinction coefficient profiles (PEC)

and AOD obtained from the PEC profiles integrated between 0 and 9.5 km agl. Finally, the evolution of the integrated water vapour content in the lower atmosphere along the Falcon 20 flight track was derived from dropsonde-derived water vapour mixing ratio profiles integrated between 0 and 10 km agl.

3. Satellite intercomparisons during June 2011

In order to compare the various satellite products, we have established a common grid onto which the satellite data are binned, at a latitude/longitude resolution of 0.25°. This resolution has been chosen so as to be coarser than the coarsest set of satellite data: in this case this is the MISR aerosol product, which has a resolution of 17.6 km (Kahn et al., 2010). Uncertainties are calculated by combining the pixel uncertainties that fall within each grid cell. The region chosen is the western half of the Sahara, 8-38°N, 20°W-20°E, a domain which covers all desert areas which may contribute substantially to the dust aerosol loading over west Africa. The local equator crossing times for the satellites are ∼0930 UTC for METOP (IASI), 1030 UTC for Terra (MISR) and 1330 UTC for Aqua (MODIS), although AERONET observations suggest that the general diurnal variability of dust loading is quite small (Smirnov et al., 2002). Where all satellites are included in the comparisons we choose MISR as our temporal reference point. For each day for a given grid cell observed by MISR, we retain the corresponding observation from SEVIRI which is closest in time (within ±15 minutes). If an IASI or a MODIS observation was made over the grid cell within five hours of the MISR observation, this is retained. Finally we impose the condition that all four satellites must have made a valid AOD retrieval from these observations for the grid cell values to be included in the final intercomparison. Because MISR has a very narrow swath this does place a relatively stringent limit on the number of intercomparison points available. Hence, to allow a greater range of conditions to be sampled and a greater number of AERONET/aircraft coincidences to be included, we relax these criteria for specific cases and retain SEVIRI, IASI, and MODIS co-locations only. In

these cases IASI becomes the reference satellite track.

For comparison with AERONET, all valid AERONET observations within three hours of the IASI overpass are included and averaged to find the co-located AERONET values. MODIS and SEVIRI also validated against the AERONET data taken from the IASI timeslot (± 3 hours). The uncertainties on the averaged observations are derived from the combination of the quoted uncertainties on each individual AERONET measurement. Also mapped onto the intercomparison grid are co-located values of total column water vapour and skin temperature from ECMWF ERA-Interim re-analyses, re-gridded in time and space to the intercomparison grid. Emissivity at 8.7 μm (ϵ) as derived from MODIS data (Seemann et al., 2008) are also mapped alongside their co-located values, as are albedo values at 600 nm as derived from SEVIRI (Derrien & Le Gléau, 2005).

3.1. Intercomparisons across the west African Sahara

The distribution of mean co-located AODs for June 2011 for the four satellite instruments are mapped in Figure 3. The four satellites broadly agree on the dominance of the dust signal over eastern Mali and the central Sahara in general, although there are variations in the emphasis that they place on the strength of various dust events. For example, SEVIRI and MODIS, and to a lesser extent MISR, agree on the significance of a dust event in northern Algeria on the 1st June (which is the dominant contributor to the monthly mean in this area), a plume which does not appear as strongly in the IASI retrievals. It is clear that SEVIRI tends to report noticeably higher AODs than reported by the other satellites, especially over a large area of the central Sahara: the values reported by the other satellites are comparatively small, especially by IASI, as indicated by Table 2. High AODs appear to be an accurate representation of the dust loading in this area of the central Sahara, subject to the most frequent occurrence of haboob dust outbreaks (Marsham et al., 2008), suggesting that SEVIRI is most capable of observing these dust events.

Due to the requirement for co-located data, there are many gaps in the spa-

tial comparison. In some cases this is due to fewer occurrences of co-location, but more often the grid cells are excluded due to the prevalence of cloud, especially over the Sahel and sub-Saharan Africa, or due to other data quality issues. In the case of SEVIRI, observations are always available across the domain, but AOD retrievals may not be made due to the presence of cloud. Of the 54,534 points where and when all satellites made co-located observations, 39.8% of IASI points had valid AOD retrievals, as had 67.0% of MISR points, 52.2% of MODIS points, and 76.6% of SEVIRI points. Table 3 compares the satellite/satellite agreement on the presence of the valid retrievals, showing the highest agreement between SEVIRI and MISR. MODIS shows slightly less agreement with these two satellites, although the bulk of the disagreement between these three satellites comes from unsuccessful MODIS retrievals. IASI has the lowest ratio of retrievals to observations, and so its agreement with the other satellites is markedly lower.

Turning to the successful retrievals only and looking at the mean value of all the co-located measurements, we find that, as suggested by Figure 3, SEVIRI tends to retrieve the highest AODs compared to the other satellites ($\overline{\mathrm{AOD}} = 0.71$), followed by MISR (0.50) and MODIS (0.46), while IASI tends to retrieve the lowest AODs (0.30). Density plots of satellite vs. satellite AODs are shown in Figure 4. Subdividing by meteorological conditions (Table 2), the differing sensitivity of the various satellites to column moisture and to skin temperature becomes more readily apparent. The threshold values have been chosen so as to be similar to the median values for column moisture and skin temperature. The chosen column moisture threshold is 20 mm as used by Brindley et al. (2012), slightly above the median value of 18 mm. For comparisons with MISR the median skin temperature of the co-located data is 317 K, while for comparisons with AERONET it is 312 K, so the skin temperature threshold is set at 315 K (42 °C). For all satellites there is a tendency to retrieve higher AODs in warmer and moister conditions; SEVIRI and MISR appear to be especially sensitive to variations in column moisture, approximately doubling their $\overline{\mathrm{AOD}}$ values between the dry and moist regimes in 'cool' conditions. In contrast, IASI

shows larger sensitivity to increases in skin temperature. MODIS appears to show a similar response to both factors. Warmer conditions are associated with the central desert where the dust sources are located, and where dust activity is at its strongest, which tends to have a higher skin temperature than the Sahel and the Mediterranean coast at this time of year. A complicating factor is that heavy dust loading may in fact cool the lower atmosphere and the surface of a hot desert. For example, Slingo et al. (2006) report a surface cooling of $\sim$13°C during a heavy dust event over Niger in March 2006. The relationship between column moisture and dust loading is also non-linear, since while high column moisture is associated with vegetated areas and heavy rainfall suppresses dust activation and transport, convective systems such as haboobs (Marsham et al., 2011), which bring moist 'cold-pool' outflows, are responsible for substantial dust uplift over west Africa and some of the thickest dust events. For example, LIDAR and radiosonde data from BBM show a clear association between moisture and dust at this location, and the highest AODs in haboobs (Marsham et al., submitted 2012). Furthermore, dust mobilisation by haboobs may be observable by satellites only once the dust has travelled out from beneath the associated clouds.

This raises the question: to what extent is this positive relationship between meteorological conditions and AOD a function of the sensitivity of the retrievals to these variables, and to what extent is it that the dust activity is itself related to these conditions? We recast the density plots of satellite vs. satellite AOD shown in Figure 4 as a function of column moisture (Figure 5), to which the majority of retrievals appear most sensitive overall. These indicate that the satellite biases between each other do vary according to the moisture regime in which the retrievals are made. SEVIRI's bias against all the other satellites increases between the dry and moist regimes (by a factor of $\sim$2), as to a lesser extent does MISR against both IASI and MODIS. All satellites are biased high against IASI, especially in the moist regime, while MISR and MODIS show the smallest overall bias relative to each other. Given the extent to which SEVIRI's bias against the other satellites increases with moisture, it is SEVIRI's retrieval

that appears most likely affected by water vapour, beyond any association of the moisture content with the conditions which give rise to high dust loading. Theoretically, given the direct sensitivity of the 10.8 μm channel used in the SEVIRI retrieval to column moisture this is perhaps not surprising, especially if variations in the atmospheric conditions are not adequately captured in the ERA-Interim analyses used in the retrieval process to account for this variability. By contrast we would not expect the visible channels used by the MISR and the MODIS algorithms to be sensitive to the water vapour content.

Surface properties may also have a significant effect on the retrievals. Figure 6 analyses the relationship between surface infrared emissivity, surface visible albedo, column moisture and satellite AODs. Note that in general albedo is strongly anti-correlated with emissivity. Given the wavelength regimes that the different retrievals use we expect the MISR and MODIS results to be more susceptible to variations in surface albedo, while the SEVIRI and IASI retrievals might be expected to show sensitivity to surface emissivity. As noted earlier, except in a few specific locations, SEVIRI is biased high against the other satellites, and IASI is biased low. In the dry regime the pattern of AODs as a function of surface properties is consistent between all four satellite instruments, with the highest mean AODs to be found at high albedo and low emissivity, a combination which is most associated with sand seas, where the satellites retrieve moderately high AODs (as in Figure 3). In the moist regime there appear to be two contrasting patterns of AOD, one for the infrared IASI and SEVIRI retrievals, which we might expect to be most sensitive to moisture, and one for the MISR and MODIS retrievals made using the visible channels. The monthly mean IASI and SEVIRI retrievals tend to show stronger signals in the moist regime further up and left to the middle of the plots to lower albedo and higher emissivity, which is where eastern Mali, northern Niger and northern Algeria happen to lie on the albedo/emissivity grid. Meanwhile the retrievals from MISR and MODIS give peaks in AOD values towards high albedo and low emissivity, as in the dry regime, although there is a more homogeneous spread of AOD across the albedo/emissivity grid.

There are exceptions to this general pattern. Identifying specific geographical areas, in the moist regime at a relatively high albedo of 0.39 and a high emissivity of 0.91 is a bin where MISR and MODIS retrieve higher AODs than SEVIRI and IASI, corresponding to six grid cells in two regions: the dominant signal of high positive MISR and MODIS bias is at ∼17.5°E, ∼17°N, corresponding to an area of the Bodélé Depression in Chad (see Figure 7). In this area the SEVIRI dust flagging may be filtered due to the high local emissivity (Banks & Brindley, 2013; Ashpole & Washington, 2012), which may be an overly stringent requirement in one of the world's biggest dust sources (Washington & Todd, 2005; Koren et al., 2006).

IASI has a positive bias against MISR and especially MODIS over specific mountainous regions such as the Hoggar mountains in southern Algeria and the Aïr mountains in Niger. These areas of high elevation have low skin temperature and column moisture, low albedo, and high emissivity with respect to the surrounding desert lowlands, and are found at an emissivity of ∼0.91 and an albedo of ∼0.2 predominantly in the dry regime. They are also areas identified by Shi et al. (2011) as having markedly lower MODIS Deep Blue Collection 5.1 AOD values compared to MISR. Low bias at high elevation has also been observed for Deep Blue retrievals from the SeaWiFS instrument (Sayer et al., 2012). The shallowness of the atmosphere may have varying effects on the retrievals. For IASI this reduces the absorption in the infrared due to water vapour and hence may increase the signal seen by the satellite and mean that the retrievals are higher in these regions than elsewhere. Moreover the high emissivity of the volcanic rock in the Hoggar where the AERONET site of Tamanrasset is based may also affect the IASI retrieval. Meanwhile for MODIS the reduced atmospheric column reduces the path length through which the blue channels of the visible spectrum may be scattered, and so the surface may appear brighter: this may reduce the contrast between the lofted dust and the surface on which the Deep Blue algorithm depends.

The frequency distributions of the satellite AODs over the whole domain are plotted in Figure 8(a). Overall, IASI is most weighted towards the lowest

AODs, with a peak in distribution at 0-0.1, while the peaks for MISR (0.2-0.3), MODIS (0.3-0.4) and SEVIRI (0.4-0.5) are all shifted to higher values. SEVIRI has the longest and widest tail in its distribution while MISR has the smallest maximum values. A substantial component to SEVIRI's wide tail is revealed in Figure 8(b), which covers the region (17-22°N, 0-5°E). Here, the dust loading is dominated by activity around the Malian/Algerian/Nigerien border (Figure 3), an area which includes the BBM AERONET site. The frequency distribution of level 1.5 observations from this site seems to corroborate the occurrence of high dust loadings seen in this area by SEVIRI. A large fraction of the very high AODs retrieved by SEVIRI are solely from this region (Figure 8(c)) although it is clear that the tendency for SEVIRI to show higher AODs compared to the other three satellite instruments is perpetuated across the domain. Further analysis of the observations and retrievals at a number of AERONET sites, including BBM, is presented in the following sections.

3.2. Intercomparisons over AERONET sites

To evaluate the accuracy of the satellite retrievals, we use AERONET data to provide 'ground-truth' of the aerosol loading. Scatterplots of AERONET/satellite AODs are presented in Figure 9 for coincident IASI, MODIS, and SEVIRI data. MISR is not included in this analysis due to the scarcity of MISR overpasses of AERONET sites through the month. Since co-located Level 2 AERONET data are not available for a number of sites, Level 1.5 data are used. MODIS and SEVIRI AOD retrievals are provided at 550 nm, while IASI AOD retrievals are provided at 500 nm. AERONET measurements are not made at 550 nm, but we can use the AERONET AOD measurements at 675 nm and the Ångström coefficient to derive the AERONET AOD at 550 nm (Eck et al., 1999).

In terms of bias, SEVIRI shows the best overall agreement with AERONET, with a positive bias of 0.11. In contrast IASI and MODIS show negative biases of -0.21 and -0.32 respectively. It is at the highest dust loadings that the biggest discrepancies are observed, where IASI and MODIS have substantially lower values than are observed by AERONET. Note that at high AOD the visible

reflectance becomes less sensitive to changes in AOD, so for MISR and MODIS which retrieve dust using the visible channels there may be less AOD response to further increases in dust loading. There may also be a greater uncertainty at high dust loadings due to a greater sensitivity to other assumptions made in the retrievals such as those made for the aerosol properties, and similarly the uncertainy in the AERONET AOD also tends to be greater at high dust loading. By comparison SEVIRI is better able to retrieve such high values, although the retrieved AODs are still slightly lower than those observed by AERONET. So for example, on 21st June at BBM, when AERONET observed an AOD of 3.08, IASI retrieved 1.57, MODIS retrieved 1.22 (0.62 in the Collection 5.1 retrievals, indicative of the improvement in the retrieval of heavy dust in Collection 6), and SEVIRI retrieved 2.23. Hence we see that at high AODs SEVIRI shows best agreement with AERONET. Where the AERONET AOD is in excess of 1, the retrieval RMS differences (biases) are: SEVIRI: 0.47 (-0.05); IASI: 0.68 (-0.51); MODIS: 0.89 (-0.76). At lower AODs IASI shows improved agreement with AERONET (bias = -0.15). SEVIRI has a tendency to over-estimate the AODs, with a positive bias against AERONET of 0.14, while MODIS under-estimates compared to the AERONET observations with a bias of -0.24.

MODIS shows little difference in its biases and RMS differences between the two regimes of column moisture, while IASI does have a slightly more negative bias in moist compared to dry conditions. The sensitivity of the SEVIRI retrieval to column moisture is however quite pronounced: the bias jumps positively from dry to moist, from -0.02 to 0.31, as does the RMS which jumps from 0.29 to 0.51. That SEVIRI shows this positive bias even relative to AERONET again suggests that it is the retrieval itself which is being affected by the column moisture, beyond the possible relationship between moisture and dust activity. Moreover, we see that the divergence of the AODs between SEVIRI and AERONET is greatest at lower AERONET AODs and high moisture values, in particular at the Sahel sites (Banizoumbou, IER Cinzana, and Zinder Airport), under these conditions we suggest that the SEVIRI retrieval is less reliable.

Turning to surface properties, different patterns are clear among the three

retrievals. Overall SEVIRI shows no significant difference in the quality of its retrievals between dark and bright albedo regimes, with bright RMS values most weighted by the highest AERONET AOD at BBM. However in the dark and dry regime, at Tamanrasset and Saada, there is a cluster of points which reveal a distinct subset in the aerosol retrieval from IASI and MODIS. Over these sites we see a slightly positive bias in the IASI retrievals and a substantially negative bias in the MODIS retrievals. Saada may be an anomaly since the site altitude of 420 m is not particularly high, however within the site's area of influence is a grid cell containing part of the Atlas mountains. At an altitude of 1377 m Tamanrasset is the most elevated site used in this study, with the shallowest atmospheric column above it as evidenced by its driest average column moisture. Hence IASI may have a positive bias and MODIS may have a negative bias as described in Section 3.1. It is thus not the albedo itself which is driving this pattern in the IASI and MODIS retrievals, rather it is the associated elevation.

Comparing the statistics between dark and bright points in the moist regime, we find that SEVIRI sees no variation with albedo, consistent with the overall picture. Meanwhile both IASI and MODIS have more negative biases in the bright regime where the dust loadings are highest. The trend in the points is not markedly different between dark and bright points for MODIS, so MODIS' decreased bias may just be a consequence of higher dust loading. For IASI the dark points are closer to and occasionally above the one-to-one line, whereas the bright points are markedly lower. Hence IASI appears to have a negative bias over the brighter surfaces at BBM and Zinder Airport, which also have some of the lowest emissivities (Table 1). IASI's low AODs over these surfaces are consistent with the results of Figure 6(b). Taken together these results suggest that the general low bias in the IASI retrievals becomes more pronounced when the emissivity is low, as it is in parts of the west African Sahara.

4. Case studies in June 2011

4.1. A heavy dust case over Bordj Badji Mokhtar on 17th June

On 17th June, a large dust storm emanating from the Algeria/Mali/Niger tri-border area passed over the top of Bordj Badji Mokhtar (BBM). All four satellites observed the area around BBM on this day, and the AERONET site was able to make some successful measurements, especially in the afternoon. Maps of co-located AODs and meterological conditions, a 'desert-dust' RGB image, and a time-series plot of AOD over BBM, are shown in Figure 10. As subjective as the interpretation of the RGB rendering may be, it is clear that the surface underneath the dust storm cannot be seen. Hence we might expect that the signal seen by the satellite instruments will be originating from the dust layer rather than from the underlying surface. Similarly, the AERONET site may have had difficulty seeing the Sun through the dust layer, and so several of the morning Level 1 data points were 'cloud-screened' and hence removed from the Level 1.5 and Level 2 data sets. The satellite instruments do not detect cloud in this area until later in the afternoon, so we suggest that the 'cloud-screened' Level 1 data may give us appropriate measurements for the dust AOD in the morning.

The cause of this dust event was a convective system further to the south shown in red in the imagery, which formed a haboob that triggered dust emission overnight as it moved northwards. Haboobs appear to cause approximately half of the Saharan dust uplift in high-resolution models, and a similar fraction at BBM during June 2011, but are largely absent in global models (Marsham et al., 2011, submitted 2012). As a consequence of this formation, the dust event is strongly associated with areas of relatively high column moisture (Figure 10(e)), with a gradient towards lower moisture values towards the leading edge of the dust front, and over BBM. The skin temperature is depressed underneath the dust (Figure 10(f)). During the day from 0700-1600 UTC over BBM the mean column moisture is 17.5±1.0 mm and the skin temperature is 318.9±8.5 K. There is broad agreement between the satellite observations as to the dust spatial

distribution and to the position of the leading edge of the dust front in the north. There is also agreement about the position of a smaller individual dust storm further north in central Algeria, at 26°N. However, SEVIRI is most able to capture the magnitude of this dust event, as shown by Figure 10(g). Where there are simultaneous Level 1 AERONET and SEVIRI measurements, the mean AERONET AOD is 2.99, and the mean SEVIRI AOD is 2.63. For afternoon Level 2 measurements the mean AERONET AOD is 2.35 and the mean SEVIRI AOD is 2.61. By contrast, the IASI overpass gives an AOD of 1.50 while the simultaneous Level 1 AERONET AOD is 3.38, MISR gives 0.90 while the Level 1 AERONET AOD is 3.80, and MODIS gives 1.13 (MODIS Collection 5.1 gives just 0.19) while the Level 2 AERONET AOD is 3.32. The AOD values provided by SEVIRI are very large here (which might be regarded as suspect), however so are the AERONET values, which supports our earlier inference that of the four satellites, SEVIRI's AOD retrievals are most reliable at high dust loading.

4.2. Falcon aircraft observations on 20th and 21st June

On 20th June, the Falcon 20 carried out a triangular flight across northern Mauritania and northern Mali to survey the Saharan atmospheric boundary layer as well as document the dust uplift in the region of the intertropical discontinuity to the south of the Saharan heat low over Mali (flight F21). F21 took place between 1322 and 1700 UTC, with the Falcon 20 flying at 11 km above mean sea level (amsl). Ten dropsondes were released along the flight track. On 21st June the Falcon 20 performed two flights (F22 and F23). On this day, convection over the Atlas Mountains had initiated a density current which moved southwestward over the northern Sahara during the morning. During the first Falcon 20 flight (F22), a dust front associated with the density current was observed over Mauritania, with older dust overlying it. During the afternoon flight (F23), airborne observations revealed that the dust layers were mixed together as a result of the developing Saharan convective boundary layer. F22 and F23 took place between 0718 and 1035 UTC, and 1313 and 1630 UTC, respectively. Nine dropsondes were released during each flight.

Observations from the Falcon give us a greater spatial range of local AOD measurements than does AERONET, and these are taken over a greater range of surface types. We use the LIDAR as the reference 'truth' due to the LIDAR's insensitivity to moisture and surface albedo, such that it is only sensitive to the aerosol loading. Figure 11 shows the dust activity and conditions along the Falcon flight tracks. MISR retrievals are not included in this analysis due to the lack of any spatial matching on any day during the Falcon's flight campaign. The start of the LIDAR measurements on both days is at the north-westernmost extremity of the flight tracks. On the 20th there is coincidence in the locations of high column moisture and albedo, with a particularly strong gradient in moisture as shown in Figure 11(c); by contrast the atmosphere on the 21st is consistently dry, the aircraft traverses an area of generally lower, but spatially varying albedo.

For both flight F21 (20th) and flight F23 (21st) IASI and SEVIRI agree on the spatial distribution of dust with dominant dust presence in the north, as does MODIS on the 21st, in Figures 11(e) and 11(f). MODIS does not see this high northern dust loading at the start of F21 (Figure 11(e)). Looking more specifically at F21, from ∼1430 UTC to ∼1540 UTC MODIS and especially IASI are negatively biased against the LIDAR where the aircraft was overflying the region of high albedo and low emissivity. This is consistent with the findings of Figure 9. IASI's more negative bias in moist conditions may also contribute to its very low values at the southern end of the flight track. Over darker and more emissive surfaces (at either end of flight F21, and along most of the flight F23) IASI is apparently better able to retrieve the AODs that the LIDAR observes. MODIS performs very well during flight F23, under constant dry conditions and over moderately varying albedos. For this flight SEVIRI has a high positive bias against the LIDAR observations, even under dry conditions.

The conditions encountered on flight F23 and at the northern ends of flight F21 are analogous to the conditions generally found at Zouerat, i.e. a dry atmosphere over a semi-bright surface. Set in this context, SEVIRI's high bias against the LIDAR AODs during F23 is consistent with some of the dry/bright

SEVIRI/AERONET comparisons at Zouerat seen in Figure 9(c), at low AODs where SEVIRI is biased high. Hence, while moisture may be a significant driver of anomalously high SEVIRI AOD, this factor is not exclusive. IASI tends to be negatively biased against AERONET at Zouerat while MODIS retrieves AODs either side of the AERONET one-to-one line, consistent with what we see in the LIDAR/satellite comparisons. Meanwhile no AERONET site is closely analogous to the conditions found at the southern end of flight F21 which has a moist atmosphere similar to that found over the Sahel, but has a very bright surface with an albedo peaking above 0.45. The most analogous sites would be BBM, which has the highest site albedo (0.39), and Zinder Airport, which also has a fairly bright surface (0.34) and a typically moist atmosphere. Both IASI and MODIS are biased somwehat lower over these sites than over Zouerat, especially IASI, which is also borne out by the LIDAR comparisons. SEVIRI is biased high against AERONET observations at Zinder Airport, but is biased slightly low against AERONET at BBM in moist conditions. Again, this is consistent with the LIDAR comparisons.

Correlating the AODs with the various conditions for the two flights, we find that the LIDAR AODs indicate no significant correlation. MODIS and SEVIRI to an even lesser extent have marginal anti-correlations with moisture and albedo/emissivity: for example, MODIS has a correlation with albedo of -0.31. In contrast, IASI shows a more marked relationship with both column moisture (correlation of -0.59) and 8.7 μm emissivity (correlation of 0.74). Especially at low emissivities, the infrared IASI retrieval may be less able to discriminate between the background sand and the lofted dust, and indeed it is at the lowest emissivities that IASI has the strongest negative bias. Moisture may amplify this effect over surfaces of low emissivity, as seen in Figure 6(b). The RGB imagery extracted along the flight tracks tends to confirm this interpretation. Under dry conditions (Figure 9(d)) there is a strong relationship in the degree of 'pinkness' to the retrieved SEVIRI AODs. Under more moist conditions (Figure 9(c)) the pattern corresponds more closely to that seen in the IASI retrievals with enhanced moisture masking the dust signal as measured by the LIDAR.

This behaviour is consistent with theoretical expectations (Brindley et al., 2012).

This analysis of the aircraft observations indicates that while broad judgements about the effectiveness of the satellite retrievals under various regimes of conditions can be made, the picture remains a complicated one, with subtle interconnections among retrieved AODs, the meteorological conditions, and the underlying surface properties.

5. Conclusions

By comparing the dust aerosol retrievals of IASI, MISR, MODIS, and SEVIRI under varying conditions during the Fennec campaign period in June 2011 at the peak of the yearly cycle of dust activity in the Sahara, we can learn more about the conditions under which they are most reliable. Spatial agreement between the satellite instruments is good. Under heaviest dust loadings ($\mathrm{AOD} > 1$) it appears that SEVIRI is most able to capture the true AOD as measured by ground-based and aircraft instrumentation, whereas the other satellite instruments retrieve much lower values. Out of the mean AODs for each instrument, SEVIRI has the greatest fractional contribution of high AODs to the monthly mean, with values of 0.22 for IASI (from 5% of points), 0.18 for MISR (8%), 0.13 for MODIS (5%), and 0.47 for SEVIRI (22%). On the other hand, SEVIRI does not perform so well at lower dust loadings where it can significantly overestimate the AOD, especially where the atmospheric water vapour content is also quite high ($> 20\,\mathrm{mm}$). Under these conditions the other satellite instruments appear better able to capture the dust loading. Under moist conditions IASI retrievals also show a noticeably low bias with respect to the 'truth', so we may also have more confidence in the IASI retrievals made under drier conditions. MODIS has consistent statistics between dry and moist conditions and, while we have not evaluated MISR explicitly with the 'truth' because of a lack of coincident overpasses, inter-satellite comparisons show that it has a similar response to MODIS. Hence as might be expected, MISR and MODIS seem to be least affected by the atmospheric water vapour content, and so would be the most

trustworthy in sharply varying meteorological conditions given low dust loading and suitable surface conditions.

Surface type also plays a role in the effectiveness of the retrievals. Over elevated surfaces MODIS reports very low AODs, and is unable to retrieve the magnitude of the dust loading that the other satellites and AERONET observe, while IASI appears to retrieve the most realistic AODs. On the other hand over brighter (albedo > 0.3), less emissive surfaces ($\epsilon < 0.84$) it is IASI which most underestimates the AOD with a negative bias of -0.41 with respect to relevant AERONET sites. This behaviour is also seen in the comparisons with the Falcon LIDAR observations. As shown by Figure 6, over these surfaces MISR retrieves higher AODs, although these tend to be smaller than those retrieved by SEVIRI, which has a positive bias against AERONET of 0.11. Hence over bright surfaces SEVIRI and MISR should be the preferred instruments, while over elevated surfaces IASI may instead be preferred.

Overall then, SEVIRI performs well at high dust loading, but at lower AODs it is biased high at high moisture content ($> 20\,\mathrm{mm}$). These results suggest also a slightly high bias at low dust loadings under dry conditions. IASI performs well at high elevation but has a tendency to under-estimate the dust loading, and is negatively correlated with water vapour and positively correlated with surface infrared emissivity. The sensitivity of the SEVIRI and IASI retrievals due to moisture may arise from the (perhaps insufficiently constrained) corrections each of these infrared instruments must make in order to account for changes in brightness temperature due to water vapour. MODIS struggles particularly at high elevation, underestimating the AOD, but is generally unaffected by moisture. MISR has the most consistent retrievals, with no large variations in any moisture/albedo regime, but is unable to retrieve the magnitude of the largest dust events: at high dust loading with a homogeneous 'surface' of airborne dust, the advantages of MISR's multi-angle observations at minimising the radiance contribution from variable desert surfaces are reduced. These conclusions are summarised in Table 4.

These findings indicate the surface types, the meteorological conditions, and

the dust loadings for which each of the satellite instruments is most capable of retrieving the appropriate values of the AOD, as assessed during the summer maximum in dust activity in June 2011. Observations made during the Fennec campaign have provided new information as to the dust size distributions (Ryder et al., 2012) and the dust layer distributions (McQuaid et al., in preparation), for example. Such precise observations of the nature of the dust and of its activity may help to inform our understanding of the scenes that the satellite instruments are trying to make retrievals of, and so it would be of benefit for subsequent studies to also make use of these new measurements when assessing and improving the capabilities of the satellite instruments for dust retrievals.

Acknowledgments

We thank the AERONET PIs and staff for establishing and maintaining the nine sites used in this study; the Fennec supersites at BBM and Zouerat were operated by the Offices Nationals de la Météorologie (ONM) of Algeria and Mauritania. The ERA-Interim meteorological data were produced by ECWMF, and access to the dataset was provided by the British Atmospheric Data Centre. Thanks also go to the Royal Meteorological Institute of Belgium for the provision of surface elevation and albedo data and also 'GERBlike' data used in the SEVIRI AOD retrieval, as well as to researchers at the Cooperative Institute for Meteorological Satellite Studies at the University of Wisconsin for the emissivity data. This work has been carried out as part of the Fennec project. The Fennec-France project is funded by the Agence Nationale de la Recherche (ANR), the Institut National des Sciences de l'Univers (INSU/CNRS) through the LEFE program, by the Centre National d'Etudes Spatiales (CNES) through the TOSCA program and by Météo-France. Many thanks to the SAFIRE team for the radiation and dropsonde data from the Falcon 20 as well as to J. Pelon (LATMOS). The authors are grateful to D. Bruneau and P. Genau (LATMOS), F. Blouzon and A. Abchiche (DT/INSU) for operating the LNG system in the Falcon 20. The work of M. Garay and O. Kalashnikova was carried out at the

Jet Propulsion Laboratory, California Institute of Technology under a contract with the National Aeronautics and Space Administration. Thanks also to John Marsham at the University of Leeds for his helpful comments during the preparation of this work. J. R. Banks is supported under grant NE/G016283/1 by the UK Natural Environment Research Council.

Ackerman, S. A. (1997). Remote sensing of aerosol using satellite infrared observations. *Journal of Geophysical Research*, *102*, 17069–17079.

Ansmann, A., Petzold, A., Kandler, K., Tegen, I., Wendisch, M., Müller, D., Weinzierl, B., Müller, T., & Heintzenberg, J. (2011). Saharan Mineral Dust Experiments SAMUM1 and SAMUM2: what have we learned? *Tellus*, *63B*, 403–429.

Ashpole, I., & Washington, R. (2012). An Automated dust detection using SEVIRI: A multi-year climatology of summertime dustiness in the central and western Sahara. *Journal of Geophysical Research*, *117*.

Banks, J. R., & Brindley, H. E. (2013). Evaluation of MSG-SEVIRI mineral dust retrieval products over North Africa and the Middle East. *Remote Sensing of the Environment*, *128*, 58–73.

Bodhaine, B. A., Wood, N. B., Dutton, E. G., & Slusser, J. R. (1999). On Rayleigh optical depth calculations. *Journal of Atmospheric and Oceanic Technology*, *16*, 1854–1861.

Brindley, H. E., Knippertz, P., Ryder, C., & Ashpole, I. (2012). A critical evaluation of the ability of the Spinning Enhanced Visible and InfraRed Imager (SEVIRI) thermal infrared red-green-blue rendering to identify dust events: Theoretical analysis. *Journal of Geophysical Research*, *117*.

Brindley, H. E., & Russell, J. E. (2009). An assessment of Saharan dust loading and the corresponding cloud-free longwave direct radiative effect from geostationary satellite observations. *Journal of Geophysical Research*, *114*.

737 Carboni, E., Thomas, G. E., Sayer, A. M., Siddans, R., Poulsen, C. A., Grainger,
738 R. G., Ahn, C., Antoine, D., Bevan, S., Braak, R., Brindley, H., DeSouza-
739 Machado, S., Deuzé, J. L., Diner, D., Ducos, F., Grey, W., Hsu, C., Kalash-
740 nikova, O. V., Kahn, R., North, P. R. J., Salustro, C., Smith, A., Tanré, D.,
741 Torres, O., & Veihelmann, B. (2012). Intercomparison of desert dust optical
742 depth from satellite measurements. *Atmospheric Measurement Techniques*,
743 *5*, 1973–2002.

744 Christopher, S. A., Gupta, P., & Haywood, J. (2008). Aerosol optical thick-
745 nesses over north africa: 1. development of a product for model validation
746 using ozone monitoring instrument, multiangle imaging spectroradiometer,
747 and aerosol robotic network. *Journal of Geophysical Research*, *113*.

748 Christopher, S. A., Gupta, P., Johnson, B., Ansell, C., Brindley, H., & Hay-
749 wood, J. (2011). Multi-sensor satellite remote sensing of dust aerosols over
750 North Africa during GERBILS. *Quarterly Journal of the Royal Meteorological*
751 *Society*, *137*, 1168–1178.

752 Christopher, S. A., Johnson, B., Jones, T., & Haywood, J. (2009). Vertical and
753 spatial distribution of dust from aircraft and satellite measurements during
754 the GERBILS field campaign. *Geophysical Research Letters*, *36*.

755 Cuesta, J., Edouart, D., Mimouni, M., Flamant, P. H., Loth, C., Gilbert, F.,
756 Marnas, F., Bouklila, A., Kharef, M., Ouchene, B., Kadi, M., & Flamant, C.
757 (2008). Multiplatform observations of the seasonal evolution of the Saharan
758 atmospheric boundary layer in Tamanrasset, Algeria, in the framework of
759 the African Monsoon Multidisciplinary Analysis field campaign conducted in
760 2006. *Journal of Geophysical Research*, *113*.

761 Cuesta, J., Marsham, J. H., Parker, D. J., & Flamant, C. (2009). Dynamical
762 mechanisms controlling the vertical redistribution of dust and the thermo-
763 dynamic structure of the West Saharan atmospheric boundary layer during
764 summer. *Atmospheric Science Letters*, *10*, 34–42.

765 Derrien, M., & Le Gléau, H. (2005). MSG/SEVIRI cloud mask and type from
766 SAFNWC. *International Journal of Remote Sensing*, *26*, 4707–4732.

767 DeSouza-Machado, S. G., Strow, L. L., Imbiriba, B., McCann, K., Hoff, R. M.,
768 Hannon, S. E., Martins, J. V., Tanré, D., Seuzé, J. L., Ducos, F., & Torres, O.
769 (2010). Infrared retrievals of dust using AIRS: comparisons of optical depths
770 and heights derived for a North African dust storm to other collocated EOS
771 A-train and surface observations. *Journal of Geophysical Research*, *115*.

772 deVilliers, R., G.Ancellet, J.Pelon, B.Quennehen, A.Schwarzenboeck,
773 J.F.Gayet, & K.S.Law (2010). Airborne measurements of aerosol optical prop-
774 erties related to early spring transport of mid-latitude sources into the Arctic.
775 *Atmospheric Chemistry and Physics*, *10*, 5011–5030.

776 Diner, D. J., Beckert, J. C., Bothwell, G., & Rodriguez, J. (2002). Performance
777 of the MISR instrument during its first 20 months in Earth orbit. *IEEE*
778 *Transactions on Geoscience and Remote Sensing*, *40*, 1449–1466.

779 Diner, D. J., Martonchik, J. V., Kahn, R. A., Pinty, B., Gobron, N., Nelson,
780 D. L., & Holben, B. N. (2005). Using angular and spectral shape similarity
781 constraints to improve MISR aerosol and surface retrievals over land. *Remote*
782 *Sensing of Environment*, *94*, 155–171.

783 Dubovik, O., Holben, B., Eck, T. F., Smirnov, A., Kaufman, Y. J., King, M. D.,
784 Tanré, D., & Slutsker, I. (2002). Variability of Absorption and Optical Prop-
785 erties of Key Aerosol Types Observed in Worldwide Locations. *Journal of the*
786 *Atmospheric Sciences*, *59*, 590–608.

787 Dufresne, J.-L., Gautier, C., Ricchiazzi, P., & Fouquart, Y. (2002). Longwave
788 scattering effects of mineral aerosols. *Journal of the Atmospheric Sciences*,
789 *59*, 1959–1966.

790 Eck, T. F., Holben, B. N., Reid, J. S., Dubovik, O., Smirnov, A., O'Neill, N. T.,
791 Slutsker, I., & Kinne, S. (1999). Wavelength dependence of the optical depth

of biomass burning, urban, and desert dust aerosols. *Journal of Geophysical Research*, *104*, 31,333–31,349.

Fernald, F. G., Herman, B. M., & Reagan, J. A. (1972). Determination of Aerosol Height Distributions by Lidar. *Journal of Applied Meteorology*, *11*, 482–489.

Frank, T. D., Girolamo, L. D., & Geegan, S. (2007). The spatial and temporal variability of aerosol optical depths in the Mojave Desert of Southern California. *Remote Sensing of Environment*, *107*, 54–64.

Ginoux, P., Prospero, J. M., Gill, T. E., Hsu, N. C., & Zhao, M. (2012). Global-scale attribution of anthropogenic and natural dust sources and their emission rates based on MODIS Deep Blue aerosol products. *Reviews of Geophysics*, *50*.

Haywood, J. M., Johnson, B. T., Osborne, S. R., Baran, A. J., Brooks, M., Milton, S. F., Mulcahy, J., Walters, D., Allan, R. P., Klaver, A., Formenti, P., Brindley, H. E., Christopher, S., & Gupta, P. (2011). Motivation, rationale and key results from the GERBILS Saharan dust measurement campaign. *Quarterly Journal of the Royal Meteorological Society*, *137*, 1106–1116.

Heintzenberg, J. (2009). The SAMUM-1 experiment over Southern Morocco: overview and introduction. *Tellus*, *61*, 2–11.

Holben, B. N., Eck, T. F., Slutsker, I., Tanré, D., Buis, J. P., Setzer, A., Vermote, E., Reagan, J. A., Kaufman, Y. J., Nakajima, T., Lavenu, F., Jankowiak, I., & Smirnov, A. (1998). AERONET- A Federated Instrument Network and Data Archive for Aerosol Characterization. *Remote Sensing of Environment*, *66*, 1–16.

Hsu, N. C., Tsay, S.-C., King, M. D., & Herman, J. R. (2004). Aerosol Properties Over Bright-Reflecting Source Regions. *IEEE Transactions on Geoscience and Remote Sensing*, *42*, 557–569.

819 Hsu, N. C., Tsay, S.-C., King, M. D., & Herman, J. R. (2006). Deep Blue
820 Retrievals of Asian Aerosol Properties During ACE-Asia. *IEEE Transactions*
821 *on Geoscience and Remote Sensing*, *44*, 3180–3195.

822 Hudson, P. K., Gibson, E. R., Young, M. A., Kleiber, P. D., & Grassian, V. H.
823 (2008a). Coupled infrared extinction spectra and size distribution measure-
824 ments for several clay components of mineral dust aerosol. *Journal of Geo-*
825 *physical Research*, *113*.

826 Hudson, P. K., Young, M. A., Kleiber, P. D., & Grassian, V. H. (2008b). Coupled
827 infrared extinction spectra and size distribution measurements for several
828 non-clay components of mineral dust aerosol (quartz, calcite and dolomite).
829 *Atmospheric Environment*, *42*, 5991–5999.

830 Ipe, A., Bertrand, C., Clerbaux, N., Dewitte, S., & Gonzalez, L. (2004). Valida-
831 tion and homogenization of cloud optical depth and cloud fraction retrievals
832 for GERB/SEVIRI scene identification using Meteosat-7 data. *Atmospheric*
833 *Research*, *72*, 17–37.

834 Kahn, R., Gaitley, B., Martonchik, J., Diner, D., Crean, K., & Holben, B.
835 (2005). MISR global aerosol optical depth validation based on two years of
836 coincident aeronet observations. *Journal of Geophysical Research*, *110*.

837 Kahn, R., Petzold, A., Wendisch, M., Bierwirth, E., Dinter, T., Esselborn,
838 M., Fiebig, M., Heese, B., Knippertz, P., Muller, D., Schladitz, A., & von
839 Hoyningen-Huene, W. (2009a). Desert dust aerosol air mass mapping in the
840 western Sahara, using particle properties derived from space-based multi-
841 angle imaging. *Tellus B*, *61*, 239–251.

842 Kahn, R. A., Gaitley, B. J., Garay, M. J., Diner, D. J., Eck, T. F., Smirnov,
843 A., & Holben, B. N. (2010). Multiangle Imaging SpectroRadiometer global
844 aerosol product assessment by comparison with the Aerosol Robotic Network.
845 *Journal of Geophysical Research*, *115*.

Kahn, R. A., Nelson, D. L., Garay, M. J., Levy, R. C., Bull, M. A., Diner, D. J., Martonchik, J. V., Paradise, S. R., Hansen, E. G., & Remer, L. A. (2009b). MISR Aerosol Product Attributes and Statistical Comparisons With MODIS. *IEEE Transactions on Geoscience and Remote Sensing*, *47*, 4095–4114.

Kalashnikova, O. V., Kahn, R., Sokolik, I. N., & Li, W.-H. (2005). The ability of multi-angle remote sensing observations to identify and distinguish mineral dust types: Part 1. Optical models and retrievals of optically thick plumes. *Journal of Geophysical Research*, *110*.

Klüser, L., Kleiber, P., Holzer-Popp, T., & Grassian, V. (2012). Desert dust observation from space- Application of measured mineral component infrared extinction spectra. *Atmospheric Environment*, *54*, 419–427.

Klüser, L., Martynenko, D., & Holzer-Popp, T. (2011). Thermal infrared remote sensing of mineral dust over land and ocean: a spectral SVD based retrieval approach for IASI. *Atmospheric Measurement Techniques*, *4*, 757–773.

Koren, I., Kaufman, Y. J., Washington, R., Todd, M. C., Rudich, Y., Martins, J. V., & Rosenfeld, D. (2006). The Bodélé depression: a single spot in the Sahara that provides most of the dust to the Amazon forest. *Environmental Research Letters*, *1*.

Lee, S. S., & Penner, J. E. (2010). Aerosol effects on ice clouds: can the traditional concept of aerosol indirect effects be applied to aerosol-cloud interactions in cirrus clouds? *Atmospheric Chemistry and Physics*, *10*, 10345–10358.

Legrand, M., Pietras, C., Brogniez, G., Haeffelin, M., Abuhassan, N. K., & Sicard, M. (2000). A High-Accuracy Multiwavelength Radiometer for In Situ Measurements in the Thermal Infrared. Part i: Characterization of the Instrument. *Journal of Atmospheric and Oceanic Technology*, *17*, 1203–1214.

Lensky, I. M., & Rosenfeld, D. (2008). Clouds-Aerosols-Precipitation Satellite Analysis Tool (CAPSAT). *Atmospheric Chemistry and Physics*, *8*, 6739–6753.

874 Levy, R. C., Remer, L. A., Mattoo, S., Vermote, E. F., & Kaufman, Y. J. (2007).
875 Second-generation operational algorithm: Retrieval of aerosol properties over
876 land from inversion of Moderate Resolution Imaging Spectroradiometer spec-
877 tral reflectance. *Journal of Geophysical Research*, *112*.

878 Mahowald, N. M., Baker, A. R., Bergametti, G., Brooks, N., Duce, R. A.,
879 Jickells, T. D., Kubilay, N., Prospero, J. M., & Tegen, I. (2005). Atmospheric
880 global dust cycle and iron inputs to the ocean. *Global Biogeochemical Cycles*,
881 *19*.

882 Mahowald, N. M., & Kiehl, L. M. (2003). Mineral aerosol and cloud interactions.
883 *Geophysical Research Letters*, *30(9)*.

884 Marsham, J. H., Hobby, M., Allen, C. J. T., Banks, J. R., Bart, M., Brooks,
885 B., Cavazos-Guerra, C., Engelstaedter, S., Gasgoyne, M., Lima, A., Martins,
886 V., McQuaid, J. B., O'Leary, A., Ouchene, B., Ouladichir, A., Parker, D. J.,
887 Saci, A., Salah-Ferroudj, M., Todd, M. C., & Washington, R. (submitted
888 2012). Meteorology and dust in the central Sahara: Observations from Fennec
889 supersite-1 during the June 2011 Intensive Observation Period.

890 Marsham, J. H., Knippertz, P., Dixon, N. S., Parker, D. J., & Lister, G. M. S.
891 (2011). The importance of the representation of deep convection for modeled
892 dustgenerating winds over West Africa during summer. *Geophysical Research*
893 *Letters*, *38*.

894 Marsham, J. H., Parker, D. J., Grams, C. M., Taylor, C. M., & Haywood, J. M.
895 (2008). Uplift of Saharan dust south of the intertropical discontinuity. *Journal*
896 *of Geophysical Research*, *113*.

897 Martonchik, J. V., Diner, D. J., Kahn, R., Gaitley, B., & Holben, B. N. (2004).
898 Comparison of MISR and AERONET aerosol optical depths over desert sites.
899 *Geophysical Research Letters*, *31*.

900 Martonchik, J. V., Kahn, R. A., & Diner, D. J. (2009). Retrieval of aerosol
901 properties over land using MISR observations. In A. A. Kokhanovsky, &

902 G. de Leeuw (Eds.), *Satellite Aerosol Remote Sensing Over Land* chapter 9.
903 Chichester, UK: Springer- Praxis Publishing Ltd.

904 McConnell, C. L., Highwood, E. J., Coe, H., Formenti, P., Anderson, B., Os-
905 borne, S., Nava, S., Desboeufs, K., Chen, G., & Harrison, M. A. J. (2008).
906 Seasonal variations of the physical and optical characteristics of Saharan dust:
907 Results from the Dust Outflow and Deposition to the Ocean (DODO) exper-
908 iment. *Journal of Geophysical Research*, *113*.

909 McQuaid, J., Ryder, C. L., Flamant, C., Washington, R., Brindley, H., High-
910 wood, E. J., Marsham, J., Parker, D. J., Todd, M., Allen, C., Banks, J. R.,
911 Bourdon, A., Brooke, J., Cavazos, C., Dorsey, J., Engelstaedter, S., Formenti,
912 P., Garcia-Carreras, L., Kocha, C., Marenco, F., Rosenberg, P., Sodemann,
913 H., Trembath, J., Turnbull, K., & Woolley, A. (in preparation). Overview
914 and Insights gained by Airborne Observations over the Sahara during Fennec
915 2011 and 2012.

916 MétéoFrance (2012). *Algorithm Theoretical Basis Document for Cloud Prod-*
917 *ucts (CMa-PGE01 v3.2, CT-PGE02 v2.2 & CTTH-PGE03 v2.2)*. Technical
918 Report SAF/NWC/CDOP/MFL/SCI/ATBD/01 MétéoFrance Paris.

919 Omar, A. H., Winker, D. M., Kittaka, C., Vaughan, M. A., Liu, Z. Y., Hu,
920 Y. X., Trepte, C. R., Rogers, R. R., Ferrare, R. A., Lee, K. P., Kuehn, R. E.,
921 & Hostetler, C. A. (2009). The CALIPSO Automated Aerosol Classification
922 and Lidar Ratio Selection Algorithm. *Journal of Atmospheric and Oceanic*
923 *Technology*, *26*, 1994–2014.

924 Redelsperger, J.-L., Thorncroft, C. D., Diedhiou, A., Lebel, T., Parker, D. J.,
925 & Polcher, J. (2006). African Monsoon Multidisciplinary Analysis: An In-
926 ternational Research Project and Field Campaign. *Bulletin of the American*
927 *Meteorological Society*, *87*, 1739–1746.

928 Ryder, C. L., Highwood, E. J., Rosenberg, P. D., Trembath, J., Brooke, J. K.,
929 Bart, M., Dean, A., Crosier, J., Dorsey, J., Brindley, H., Banks, J., Marsham,

930 J. H., McQuaid, J. B., Sodemann, H., & Washington, R. (2012). Optical
931 properties of Saharan dust aerosol and contribution from the coarse mode as
932 measured during the Fennec 2011 aircraft campaign. *Atmospheric Chemistry*
933 *and Physics Discussions*, *12*, 26783–26842.

934 Sayer, A. M., Hsu, N. C., Bettenhausen, C., Jeong, M.-J., Holben, B. N.,
935 & Zhang, J. (2012). Global and regional evaluation of over-land spectral
936 aerosol optical depth retrievals from SeaWiFS. *Atmospheric Measurement*
937 *Techniques*, *5*, 1761–1778.

938 Schepanski, K., Tegen, I., Laurent, B., Heinold, B., & Macke, A. (2007). A new
939 Saharan dust source activation frequency map derived from MSG-SEVIRI
940 IR-channels. *Geophysical Research Letters*, *34*.

941 Schmetz, J., Pili, P., Tjemkes, S., Just, D., Kerkmann, J., Rota, S., & Ratier,
942 A. (2002). An introduction to Meteosat Second Generation (MSG). *Bulletin*
943 *of the American Meteorological Society*, *83*, 977–992.

944 Schuster, G. L., Vaughan, M., MacDonnell, D., Su, W., Winker, D., Dubovik,
945 O., Lapyonok, T., & Trepte, C. (2012). Comparison of CALIPSO aerosol
946 optical depth retrievals to AERONET measurements, and a climatology for
947 the lidar ratio of dust. *Atmospheric Chemistry and Physics*, *12*, 7431–7452.

948 Seemann, S. W., Borbas, E. E., Knuteson, R. O., Stephenson, G. R., & Huang,
949 H.-L. (2008). Development of a Global Infrared Land Surface Emissivity
950 Database for Application to Clear Sky Sounding Retrievals from Multispec-
951 tral Satellite Radiance Measurements. *Journal of Applied Meteorology and*
952 *Climatology*, *47*, 108–123.

953 Shi, Y., Zhang, J., Reid, J. S., Hyer, E. J., Eck, T. F., Holben, B. N., & Kahn,
954 R. A. (2011). A critical examination of spatial biases between MODIS and
955 MISR aerosol products- application for potential AERONET deployment.
956 *Atmospheric Measurement Techniques*, *4*, 2823–2836.

Slingo, A., Ackerman, T. P., Allan, R. P., Kassianov, E. I., McFarlane, S. A., Robinson, G. J., Barnard, J. C., Miller, M. A., Harries, J. E., Russell, J. E., & Dewitte, S. (2006). Observations of the impact of a major Saharan dust storm on the atmospheric radiation balance. *Geophysical Research Letters*, *33*.

Smirnov, A., Holben, B. N., Eck, T. F., Dubovik, O., & Slutsker, I. (2000). Cloud-Screening and Quality Control Algorithms for the AERONET Database. *Remote Sensing of Environment*, *73*, 337–349.

Smirnov, A., Holben, B. N., Eck, T. F., Slutsker, I., Chatenet, B., & Pinker, R. T. (2002). Diurnal variability of aerosol optical depth observed at AERONET (Aerosol Robotic Network) sites. *Geophysical Research Letters*, *29 (23)*.

Todd, M. C., Cavazos-Guerra, C., Wang, Y., Washington, R., Allen, C. J. T., Engelstaedter, S., Marsham, J. H., Garcia-Carreras, L., Hobby, M., Bart, M., Parker, D. J., Brooks, B. J., Gascoyne, M., McQuaid, J. B., Bechir, J. M., Gandega, A., Dieh, M., Traore, S., Martins, J. V., Rocha-Lima, A., Flamant, C., Lavaysse, C., Kocha, C., Podvin, T., Bentefouet, J., Clovis, T., & Ngamini, J. B. (submitted 2012). Meteorological and dust aerosol conditions over the Western Saharan region observed at Fennec supersite-2 during the Intensive Observation Period in June 2011.

Washington, R., Parker, D. J., Flamant, C., Marsham, J. H., McQuaid, J., Brindley, H., Todd, M. C., Highwood, E. J., Chaboureau, J.-P., Kocha, C., Bechir, M., & Saci, A. (2012). Fennec- The Saharan Climate System (part of the AMMA legacy). In *4th International AMMA Conference*.

Washington, R., Todd, M., Middleton, N. J., & Goudie, A. S. (2003). Dust-Storm Source Areas Determined by the Total Ozone Monitoring Spectrometer and Surface Observations. *Annals of the Association of American Geographers*, *93*, 297–313.

Table 1: Locations of the relevant AERONET sites (latitudes in °N, longitudes in °E, and altitudes in m), surface emissivities (at 8.7 μm) and albedos, and averaged total column water vapour (TCWV, in mm) and skin temperature ($\overline{T_{\mathrm{skin}}}$, in K) during June 2011.

Site, country	Lat.	Lon.	Alt.	ϵ	Alb.	$\overline{\mathrm{TCWV}}$	$\overline{T_{\mathrm{skin}}}$
Bambey-ISRA, Senegal	14.71	-16.48	30	0.91	0.25	45	311
Banizoumbou, Niger	13.54	2.67	250	0.85	0.29	44	310
BBM, Algeria	21.33	0.95	400	0.76	0.39	21	315
Dakar, Senegal	14.39	-16.96	0	0.93	0.21	39	308
IER Cinzana, Mali	13.28	-5.93	285	0.90	0.22	45	309
Saada, Morocco	31.63	-8.16	420	0.91	0.22	18	307
Tamanrasset INM, Algeria	22.79	5.53	1377	0.92	0.28	13	311
Zinder Airport, Niger	13.78	8.90	456	0.83	0.34	37	309
Zouerat, Mauritania	22.75	-12.48	343	0.77	0.33	16	315

Table 2: Overall mean co-located satellite AODs and their standard deviations. Included are subdivided means by various regimes of column moisture and skin temperature. The boundary between column moisture regimes is 20 mm, and between skin temperature regimes the boundary is 315 K.

Instrument	Mean	σ	Cool/dry	Warm/dry	Cool/moist	Warm/moist
IASI	0.30	0.33	0.19	0.31	0.28	0.41
MISR	0.50	0.31	0.28	0.45	0.56	0.73
MODIS	0.46	0.30	0.31	0.45	0.48	0.60
SEVIRI	0.71	0.53	0.44	0.60	0.86	0.95

Table 3: Table of the percentages (out of all points where all four satellites had co-located observations) of points where the two named satellites agreed that the retrieval was either valid or invalid (due to, for example, cloud presence), or where the two satellites disagreed on the validity of the retrieval.

	Agree	Disagree
SEVIRI/IASI	53.3	46.8
SEVIRI/MISR	85.1	14.9
SEVIRI/MODIS	71.5	28.5
IASI/MISR	54.4	45.6
IASI/MODIS	57.1	42.9
MISR/MODIS	72.0	28.0

985 Washington, R., & Todd, M. C. (2005). Atmospheric controls on mineral dust
986 emission from the Bodélé Depression, Chad: The role of the low level jet.
987 *Geophysical Research Letters*, *32*.

Table 4: Conditions under which each instrument is most capable of retrieving accurate AOD values. Dashes indicate factors to which the specific retrieval algorithm appears relatively insensitive.

Instrument	Dust loading	Moisture	Emissivity	Elevation
IASI	Low	Low	High	High
MISR	Low	-	-	-
MODIS	Low	-	-	Low
SEVIRI	High	Low	-	-

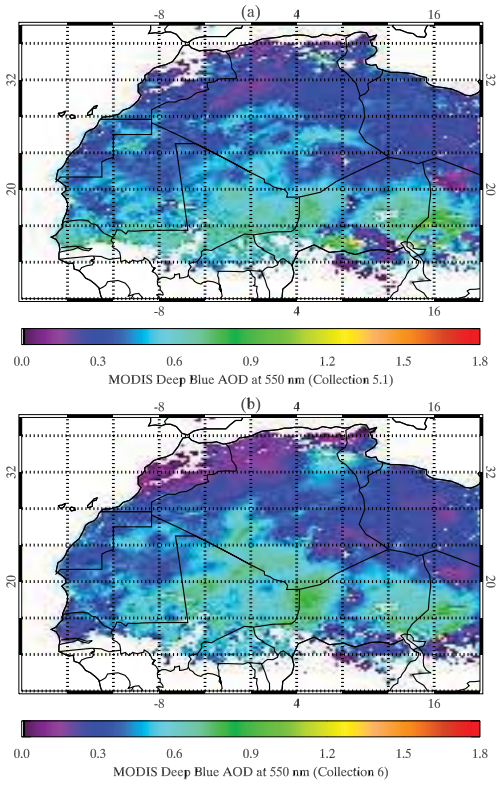

Figure 1: Monthly mean co-located successful MODIS Deep Blue retrieved AODs: (a) Collection 5.1, (b) Collection 6. One outlier in MODIS Collection 6 at 13.75°N, 16.75°E has a value of 2.07.

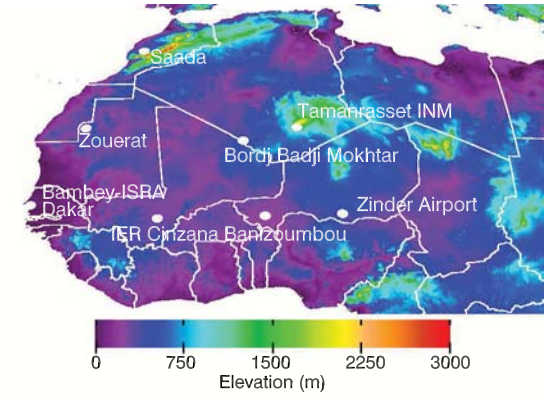

Figure 2: Map of the nine AERONET sites with co-located data in June 2011, overplotted on the surface elevation (as developed by the Eumetsat Satellite Application Facility for Nowcasting (MétéoFrance, 2012)).

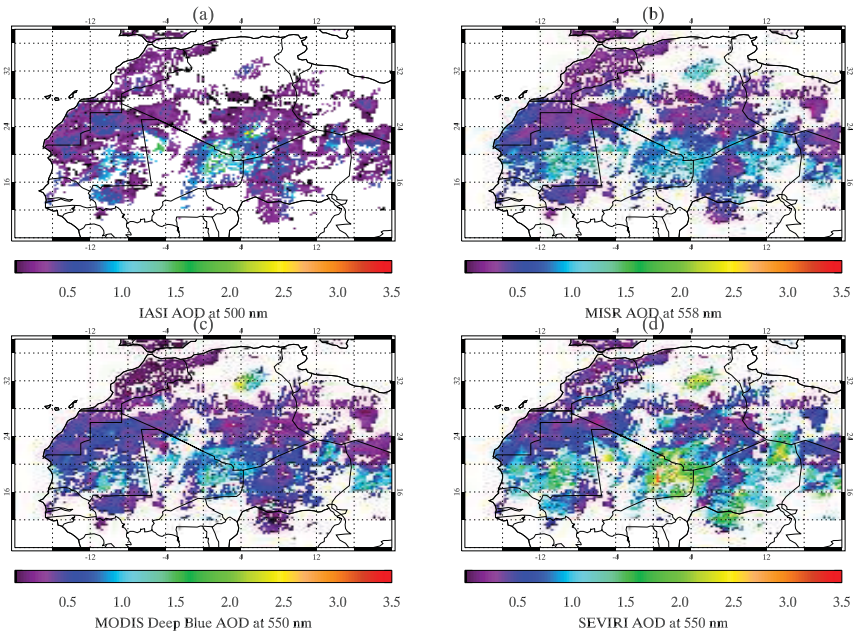

Figure 3: Map of the June 2011 mean co-located satellite AODs: (a) IASI; (b) MISR; (c) MODIS; (d) SEVIRI. Regions in white did not have co-located data between all four satellites during the month. Co-located data are from points where all four instruments had a successful retrieval. Note that there are no more than 6 points in any grid cell.

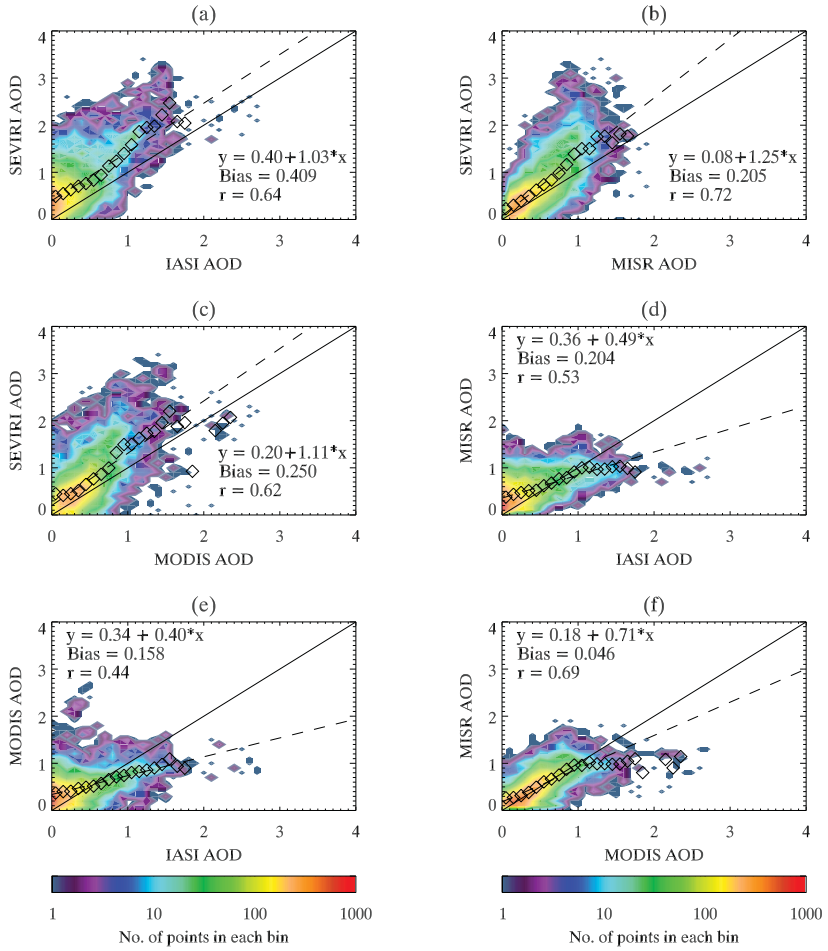

Figure 4: Density plots of satellite vs. satellite AODs. (a) IASI/SEVIRI, (b) MISR/SEVIRI, (c) MODIS/SEVIRI, (d) IASI/MISR, (e) IASI/MODIS, (f) MODIS/MISR. The dashed lines indicate the lines of best fit for all points, while the diamonds represent the mean y-axis satellite AOD in each 0.1 x-axis AOD bin (for which there are ≥ 5 points). There are 11451 points in each panel. The biases are y-x.

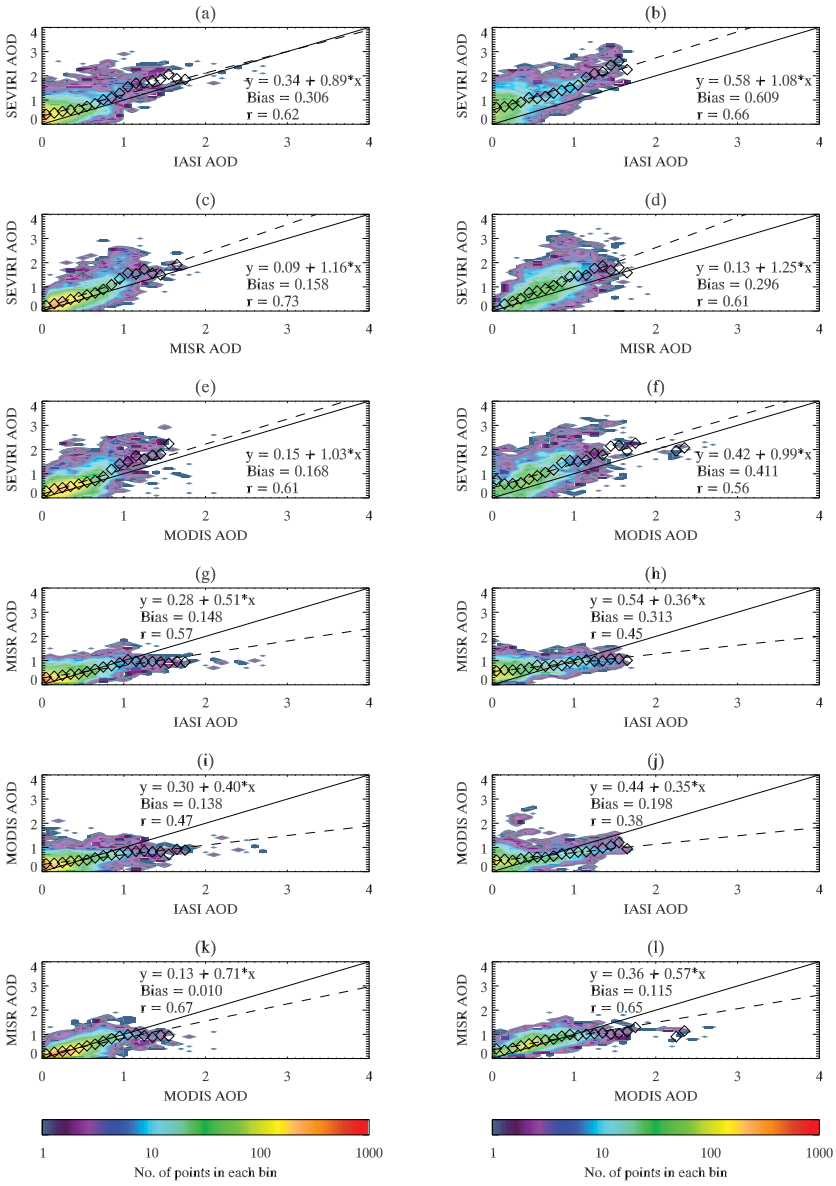

Figure 5: Density plots of satellite vs. satellite AODs. (a) IASI/SEVIRI, (c) MISR/SEVIRI, (e) MODIS/SEVIRI, (g) IASI/MISR, (i) IASI/MODIS, (k) MODIS/MISR: 'dry' conditions. (b), (d), (f), (h), (j), (l): as for left-hand panels, but for 'moist' conditions. The boundary between moisture regimes is at 20 mm. The dashed lines indicate the lines of best fit for all points, while the diamonds represent the mean y-axis satellite AOD in each 0.1 x-axis AOD bin (for which there are ≥ 5 points). There are 7580 points in the left panels, 3871 points in the right panels. The biases are y-x.

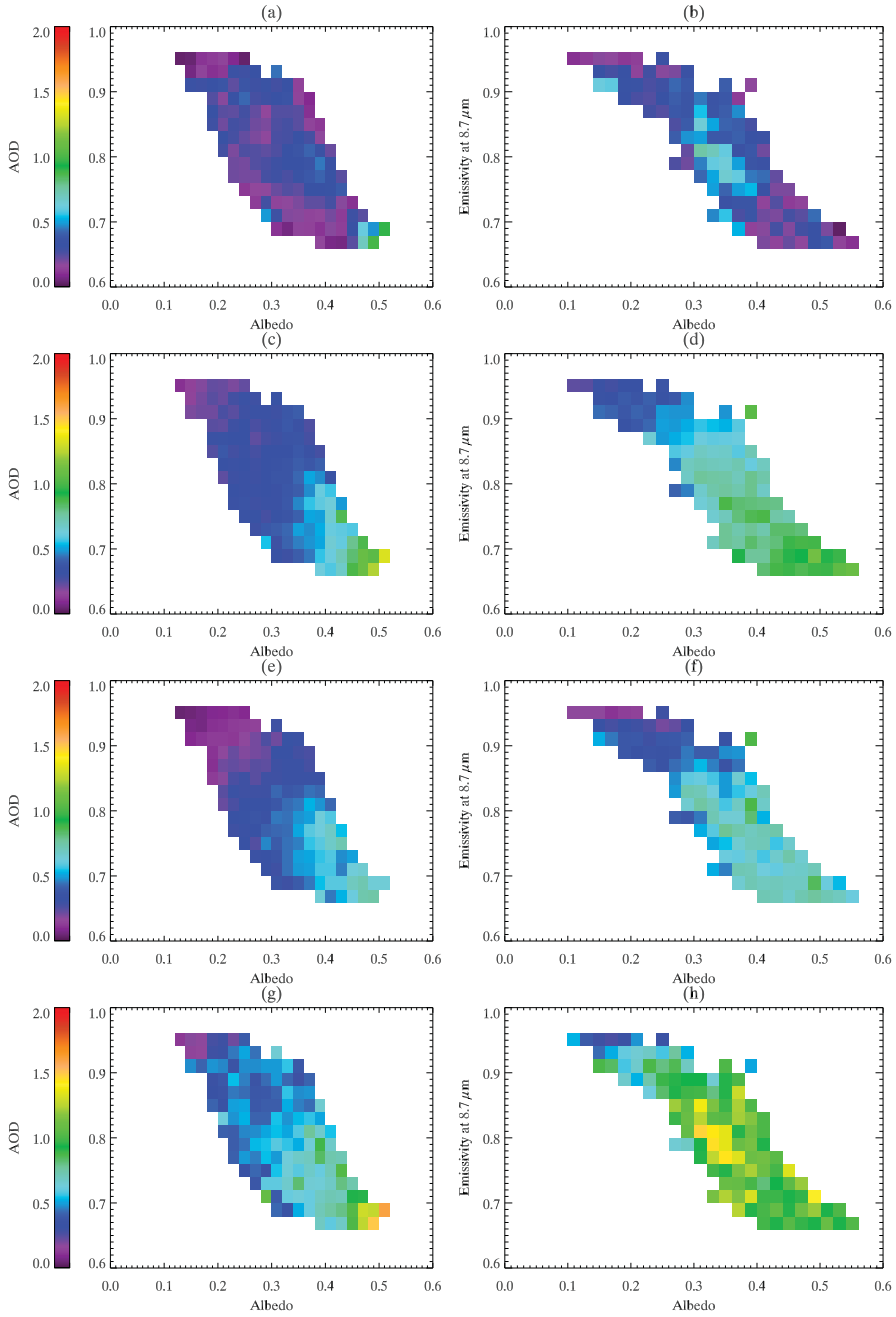

Figure 6: Satellite mean AODs binned by albedo and emissivity at 8.7 μm, in the dry regime for left-hand panels, in the moist regime for right-hand panels. The albedo and emissivity bin widths are 0.02. (a,b): IASI; (c,d): MISR; (e,f) MODIS; (g,h) SEVIRI.

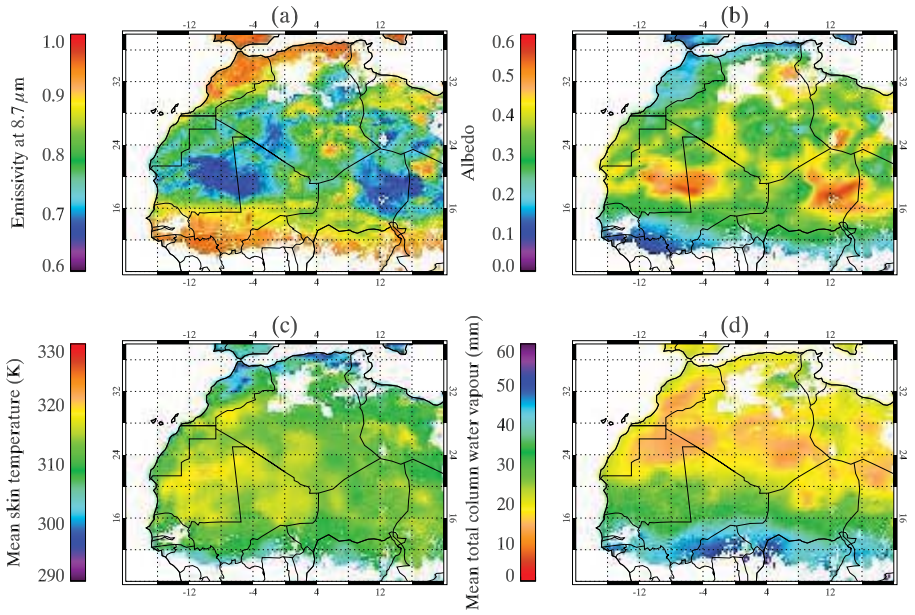

Figure 7: Maps of surface properties and average meteorological conditions, for co-located IASI, MODIS, and SEVIRI points. (a) Emissivity at 8.7 μm, (b) albedo, (c) skin temperature, (d) total column water vapour.

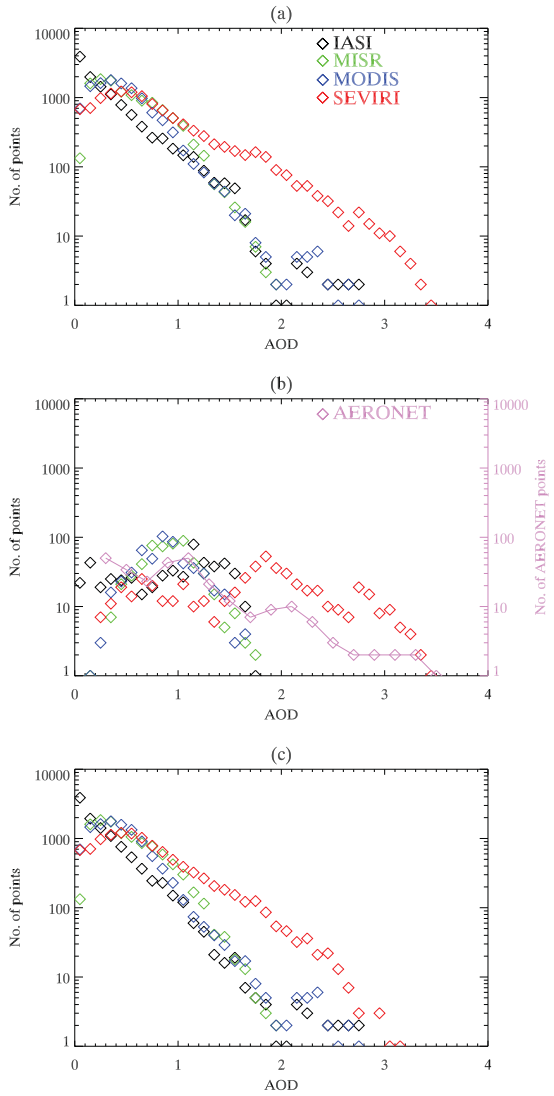

Figure 8: Histograms of occurrences of AOD values for the four satellites, for four gegraphical regions. (a) full domain; (b) Mali/Algeria/Niger border, 17-22°N, 0-5°E; (c) all areas excluding the region plotted in (b). Overplotted in (b) is a histogram from all available half-hourly AERONET data from BBM. It is important to note that the AERONET data are not co-located with the satellite data.

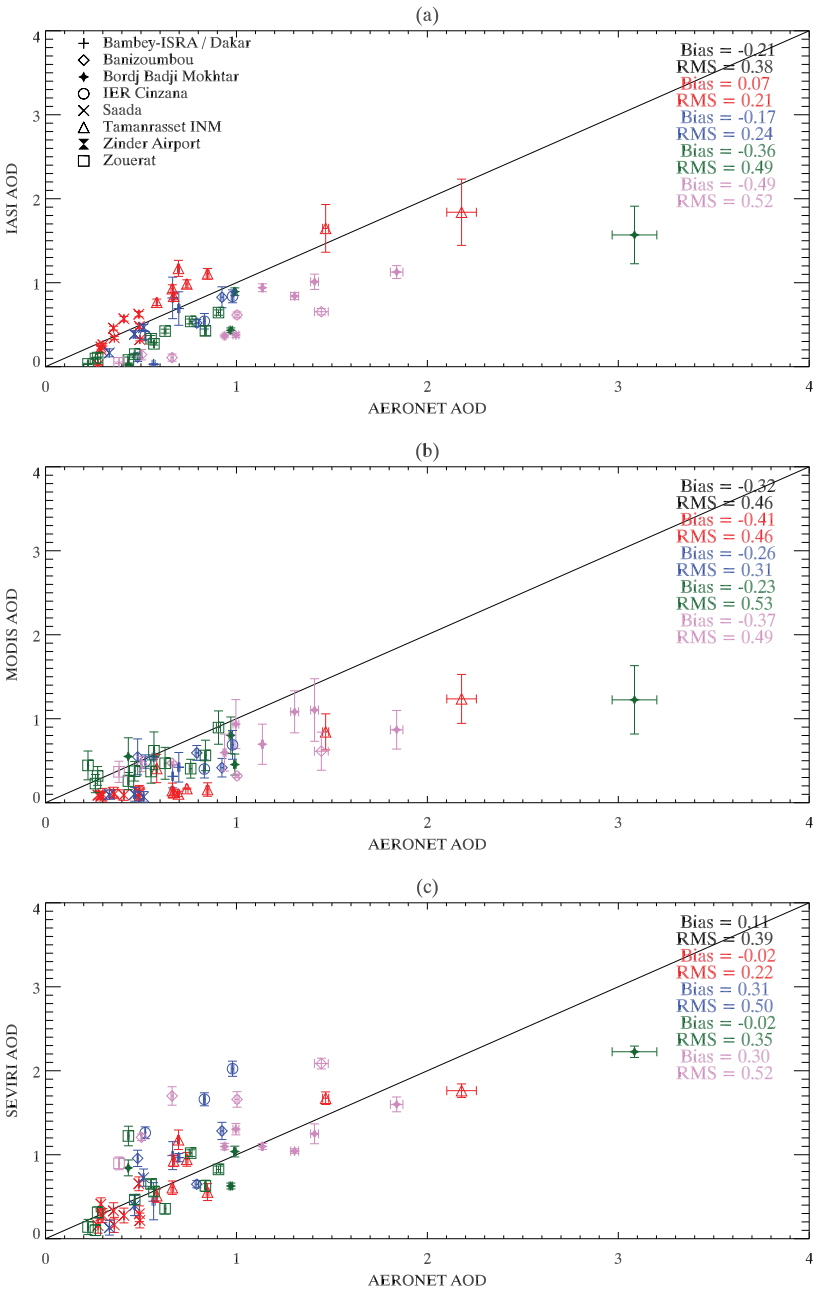

Figure 9: Scatterplots of Level 1.5 AERONET against satellite data for June 2011: (a) IASI; (b) MODIS; (c) SEVIRI. Individual sites are marked by varying shapes, and the different moisture and albedo regimes are marked as red (dry/dark), blue (moist/dark), green (dry/bright) and purple (moist/bright). The albedo threshold is 0.3.

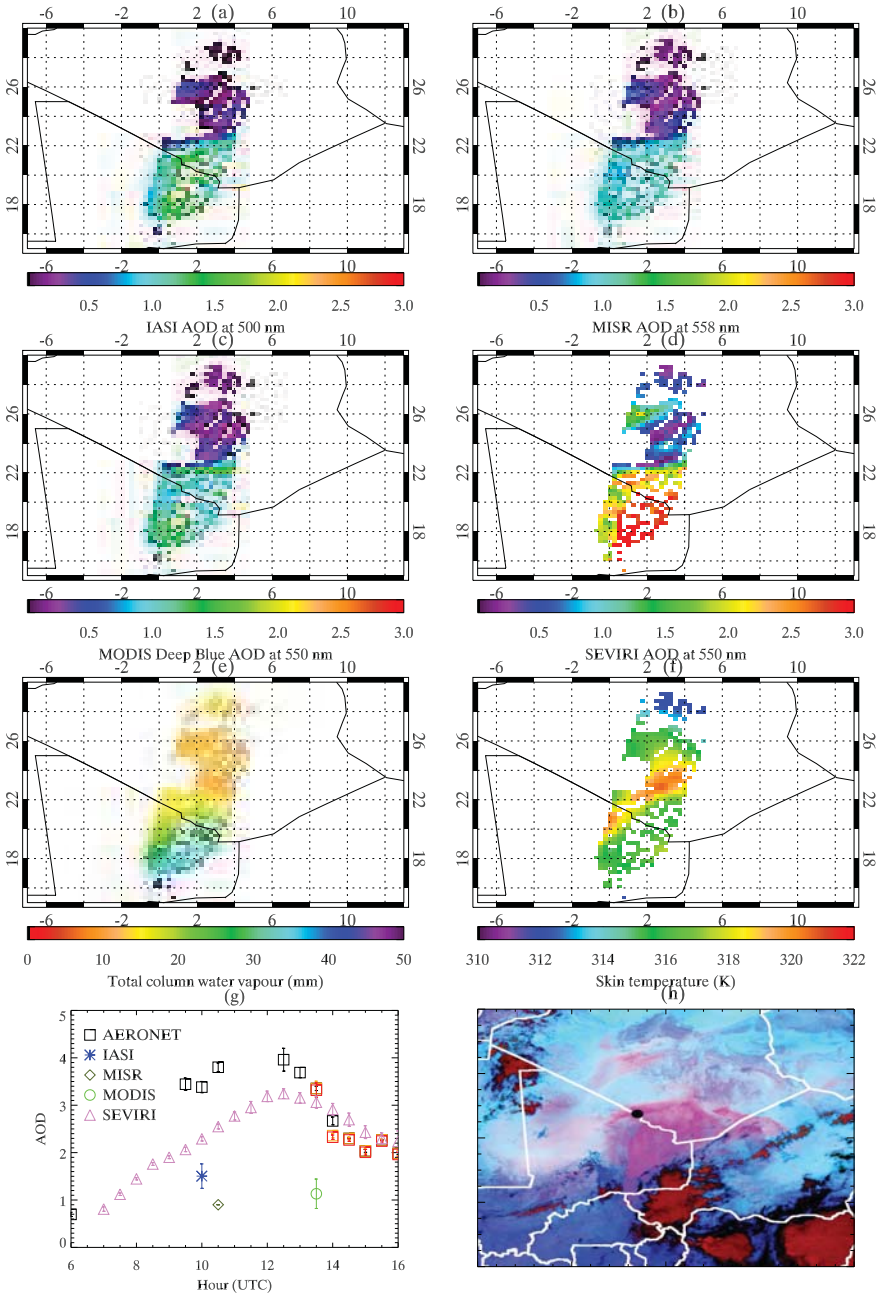

Figure 10: Dust activity and meteorological conditions over BBM on the 17th June. (a) IASI AOD; (b) MISR AOD; (c) MODIS AOD; (d) SEVIRI AOD; (e) total column water vapour; (f) skin temperature; (g) time-series of AERONET and satellite AODs during the day (black squares are Level 1 AERONET, orange are Level 1.5, and red are Level 2); (h) RGB 'desert-dust' image from SEVIRI at 1030 UTC (dust appears pink, thick cloud is red, and BBM is the black oval on the Algerian/Malian border).

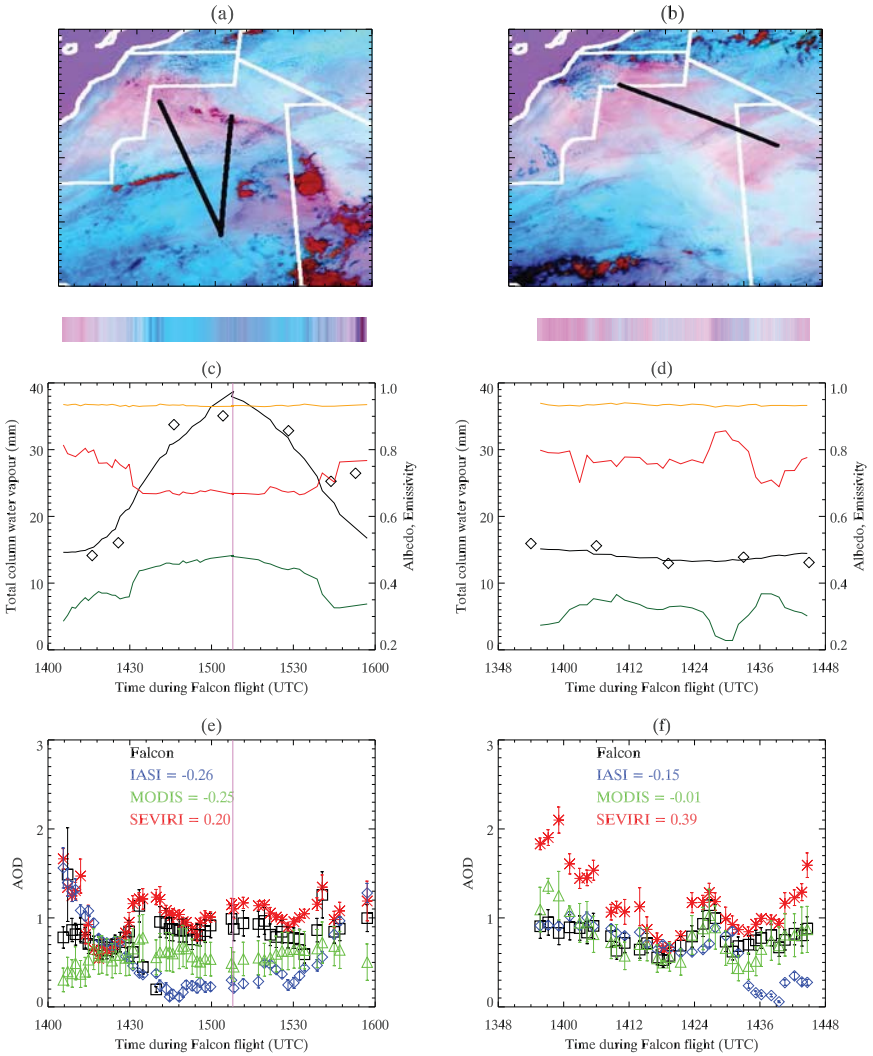

Figure 11: Dust observations and conditions along the Falcon flight track, on the 20th, flight F21 (left), and the 21st, flight F23 (right). (a,b) SEVIRI RGB images on the 20th (1500 UTC) and the 21st (1415 UTC), included are the flight tracks in black, and below are the RGB colours along the tracks; (c,d) along-track column moisture from ERA-Interim (black line) and from the Falcon dropsondes (black diamonds), albedo (green line), emissivities at 8.7 and 10.8 μm (red and orange lines), and on the 20th the vertical purple line indicates the change in flight direction; (e,f) along-track AODs from the Falcon LIDAR, IASI, MODIS and SEVIRI, with biases with respect to the Falcon.